Journal of Geophysical Research

VOLUME 64 APRIL 1959 NUMBER 4

THE SCIENTIFIC PUBLICATION
OF THE AMERICAN GEOPHYSICAL UNION

Journal of Geophysical Research

An International Scientific Publication

This Journal welcomes original scientific contributions on the physics of the earth and its environment.

Manuscripts should be transmitted to J. A. Peoples, Jr., Geology Department, University of Kansas, Lawrence, Kansas. Authors' institutions, if in the United States or Canada, are requested to pay a publication charge of $15 per page, which, if honored, entitles them to 100 free reprints.

Subscriptions to the *Journal of Geophysical Research* and *Transactions, AGU* are included in membership dues.

Non-member subscriptions, *Journal of Geophysical Research*.....$16 per calendar year, $2 per copy
Non-member subscriptions, *Transactions, AGU*.....$4 per calendar year, $1.25 per copy

Subscriptions, renewals, and orders for back numbers should be addressed to American Geophysical Union, 1515 Massachusetts Ave., Northwest, Washington 5, D. C. Suggestions to authors are available on request.

Advertising Representative: Howland and Howland, Inc., 114 East 32nd St., New York 16, N. Y.

Beginning with the January 1959 issue (Vol. 64, No. 1) the *Journal of Geophysical Research* is published monthly by the American Geophysical Union, 1515 Massachusetts Ave., Northwest, Washington 5, D. C., with the support of the Carnegie Institution of Washington and the National Science Foundation. The new monthly combines the type of scientific material formerly published in the bi-monthly *Transactions, American Geophysical Union*, and the quarterly *Journal of Geophysical Research*. The *Transactions, American Geophysical Union* will continue as a quarterly publication for Union business and items of interest to members of the Union.

Second-class postage paid at Richmond, Virginia

GEOPHYSICAL MONOGRAPH SERIES

AMERICAN GEOPHYSICAL UNION

1515 Massachusetts Avenue, N.W. Washington 5, D. C., U.S.A.

Antarctica in the International Geophysical Year—Geophysical Monograph No. 1 (Publication No. 462, National Academy of Sciences—National Research Council); Library of Congress Catalogue Card No. 56-60071; 133 pp. and large folded map of the Antarctic, 1956, 7″ x 10″

$6.00

Contains 16 separate papers by various American authorities on the Antarctic under the headings: General, Geographic and Meterological, Geological and Structural, Upper Atmospheric Physics, and Flora and Fauna. Map (41″ x 41″) compiled by the American Geographical Society. Introduction by L. M. Gould, President of Carleton College and internationally recognized authority on the Anarctic.

Geophysics and the IGY—Geophysical Monograph No. 2 (Publication No. 590, National Academy of Sciences—National Research Council); Library of Congress Catalogue Card No. 58-60035; 210 pp., 1958, 7″ x 10″

$8.00

Contains 30 separate papers by leading American authorities under the headings: Upper Atmospheric Physics, The Lower Atmosphere and the Earth, and The Polar Regions. Preface by Joseph Kaplan, Chairman of the U. S. National Committee for the IGY.

Atmospheric Chemistry of Chlorine and Sulfur Compounds—Geophysical Monograph No. 3 (Publication No. 652, National Academy of Sciences—National Research Council); Library of Congress Catalogue Card No. 59-60039; about 110 pp., 1959, 7″ x 10″

$5.50

Based on a symposium held jointly with the Robert A. Taft Sanitary Engineering Center of the U. S. Public Health Service in Cincinnati in November, 1957. Contains 23 papers (some as summaries) with discussion. Preface by James P. Lodge, Jr., of the Taft Sanitary Engineering Center and Chairman of AGU's Committee on Chemistry of the Atmosphere.

Prices plus postage, unless payment accompanies order. Quantity discounts: 5–19 copies, 10%; 20–49 copies, 15%; 50 or more copies, 20%.

It is anticipated that Geophysical Monographs 4 and 5 will be issued during 1959. Watch "Special Announcements" in the *Transactions* for word of these.

Purchase Order

To AMERICAN GEOPHYSICAL UNION

1515 Massachusetts Avenue, N.W., Washington 5, D. C., U.S.A.

Please enter our order for the following:

_____ copies of Geophysical Monograph No. 1, *Antarctica in the International Geophysical Year,* at $6.00* $_____

_____ copies of Geophysical Monograph No. 2, *Geophysics and the IGY,* at $8.00* $_____

_____ copies of Geophysical Monograph No. 3, *Atmospheric Chemistry of Chlorine and Sulfur Compounds,* at $5.50* $_____

☐ Payment of $_____ is enclosed.

☐ Please send invoice, adding postage charges.

☐ Enter our standing order for _____ copies of subsequent Geophysical Monographs at the special prepublication rates (e.g., prepublication rate for Monograph No. 3 for non-members was $4.00, payment in advance, or $4.75 on invoice).

* List price for quantities up to four; see advertisement above for discounts on quantity purchases. Special discounts to members.

Typed name _____ Signature _____

Address _____

_____

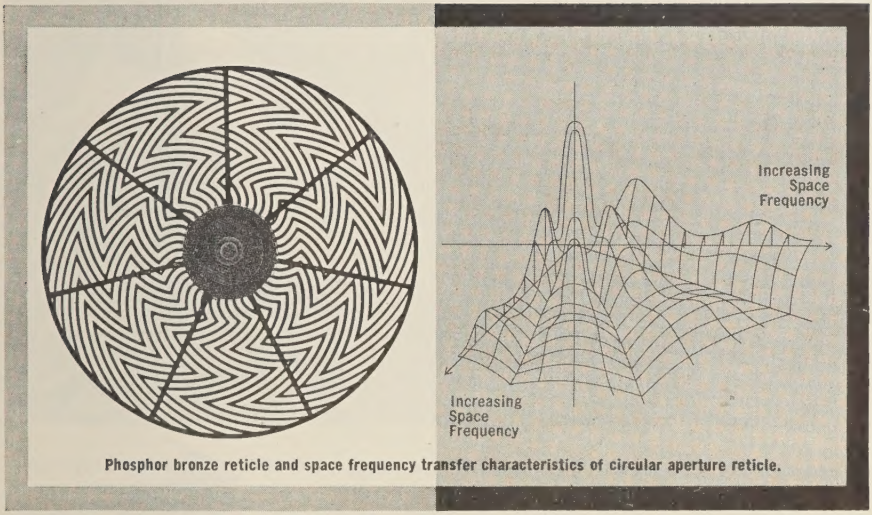

Phosphor bronze reticle and space frequency transfer characteristics of circular aperture reticle.

TARGET DISCRIMINATION IN INFRARED DETECTION SYSTEMS

The pioneering field of infrared detection offers many challenging opportunities to scientists and engineers at Ramo-Wooldridge for advanced studies in the solution of target discrimination problems. Research is continually under way at Ramo-Wooldridge in the integrating of infrared detection devices with the latest electronic systems techniques for enhanced target detection on the ground and in the air.

The phosphor bronze reticle, or image chopper, illustrated above, was developed by Ramo-Wooldridge. It indicates a marked stride in space filtering discrimination concepts, and is used for target signal enhancement in guided missiles, anti-aircraft fire control and air collision warning applications.

The reticle is used in the focal plane of an infrared optical system and is rotated to chop the target image for the desired space filtering. It is also employed in time-filtering, such as pulse length discrimination, or pulse bandwidth filtering.

Space filtering is critical to infrared systems, because of its ability to improve the detection of objects located in the midst of background interference. In a manner similar to that used in the modification of electronic waveforms by electrical filtering, space filtering enhances the two-dimensional space characteristics of a target. The size and features of the target are highlighted and the undesired background eliminated.

Scientists and engineers with backgrounds in infrared systems—or any of the other important areas of research and development listed below—are invited to inquire about current opportunities at Ramo-Wooldridge.

- Electronic reconnaissance and countermeasures systems
- Analog and digital computers
- Air navigation and traffic control
- Antisubmarine warfare
- Basic research
- Electronic language translation
- Information processing systems
- Advanced radio and wireline communications
- Missile electronics systems

RAMO-WOOLDRIDGE

P. O. BOX 90534 AIRPORT STATION • LOS ANGELES 45, CALIFORNIA

a division of ***Thompson Ramo Wooldridge Inc.***

Journal of
GEOPHYSICAL RESEARCH

VOLUME 64 APRIL, 1959 No. 4

Some Remarks on the Interaction of Solar Plasma and the Geomagnetic Field

JAMES W. WARWICK

High Altitude Observatory, University of Colorado, Boulder, Colorado

Abstract—A brief review of the magnetohydrodynamic and ion-cloud theories of magnetic storms and auroras suggests some difficulties, principally connected with the small scale of magnetic disturbances from point to point on the earth's surface. Currents flowing in ion clouds closer than one earth's radius from the surface of the earth appear to be necessary to explain the difficulties. The principal conclusion of this paper is that such currents will flow in plasma sheets moving along the curved magnetic lines of force as a condition of dynamic balance of centripetal forces. Furthermore, these currents produce perturbation fields of the size and direction required to explain storm-time geomagnetic variations.

The plasma involved is assumed to enter the region near the earth through 'horns' in incident ion clouds. The material flowing into the horns follows the lines of force to the auroral zone. Finally, these horns are supposed to develop into sheets, mathematically generated by the rotation of a line of force to the auroral zone about the earth's magnetic dipole axis. Plasma flowing along such sheets performs trajectories that concentrate in the midnight hemisphere. The high energies of auroral particles follows from the headlong collisions of such clouds in the night sky.

1. INTRODUCTION

Recent theories of geomagnetic storms and auroras generally begin with the assumption of a solar corona, permeating the entire earth-sun region. This corona is distended by its high kinetic temperature, maintained through thermal conduction of energy from the inner corona. This model, developed by *Chapman* [1957], allows the attractive possibility that the exosphere is heated by thermal conduction directly from the hot coronal gases. The coronal plasma contains some of the lines of force of the earth's field, particularly those lines of force intersecting the earth's surface in polar regions. Magnetohydrodynamic waves, originating in the boundary regions between the exosphere and the coronal gases, propagate down to the surface and create the phenomena of geomagnetic storms and auroras. The impact pressure of the solar wind [*Biermann*, 1957; *Parker*, in press; *Dessler*, 1958] equals the energy density in the earth's magnetic field at the outer boundary of the exosphere. Auroral particles accelerate to high energy as they move among irregularities in this boundary. The effect is the familiar Fermi mechanism generally believed to account for cosmic ray accelerations.

Older theories, outstandingly that of Chapman and Ferraro, took the point of view that corpuscular clouds, ejected by the sun at times of severe solar activity, pass through essentially empty space between the earth and the sun. The clouds impinge on the earth's magnetic field at the point where the impact pressure of the cloud is balanced by the magnetic pressure of the earth's field. In the Chapman and Ferraro theory a small disturbance to the geomagnetic field thus occurs whenever an ionized cloud of gas moves into the interplanetary space near the earth. The main phases of storms manifest a ring current flowing from east to west around the earth at a distance of a few earth's radii.

This current forms when ions bridge the hollow carved in the incident ion cloud by the pressure of the earth's field and complete an electrical circuit around the earth. *Martyn* [1951], in a further development of the theory, suggested that the potential gradient across the ring current, necessary for its stability, accelerates auroral particles to the observed high energies.

Obayashi and *Jacobs* [1957] indicated that the principal storm variations may involve the enhancement of an upper atmospheric current system. They showed that the same wind systems presumably responsible for normal diurnal variations in geomagnetism could account for storm variations through increased electrical conductivity arising from the entrance of corpuscular streams into the ionosphere. The strength of the theory is the fact that the same inferred wind system can account for both normal and storm effects. The weakness of the conclusions is that the winds are introduced *ad hoc* in a very complex pattern over the earth's surface. The question of the origin of the wind system is left unanswered, although it may also be closely related to the influx of corpuscular streams. Although these problems may receive satisfactory answers in future ionosperic studies, we shall disregard Obayashi and Jacobs' stimulating and thorough discussion in the remainder of the present work.

The distinction between the ideas of the Chapman and Ferraro theory and the present-day continuum theories essentially lies in the concept of a magnetohydrodynamic wave forming geomagnetic perturbations, which replaces the concept of perturbation currents flowing in ion clouds some few earth's radii from the surface of the earth. With the older or newer theories, it would seem that the scale of the perturbation field at the surface of the earth causes major difficulties. The observed perturbations, in sudden commencements or the main phases of storms, vary sharply over the earth's surface and are especially strong in the auroral regions 23 degrees from the geomagnetic poles. The sharp variations over the earth's surface appear to exclude the ring current as the source of more than part of the perturbation field during the main phase of storms. A magnetohydrodynamic wave must correspond, if it is to produce sharp local variations in the structure of the earth's field at the auroral zone, to small wavelengths at the boundary of the exosphere. It would appear that any solar-induced irregularities would likely have dimensions large compared with the scale of the earth's field even in the exosphere. As a test of the dimensions of the clouds, one might use simultaneous observations of auroras in the northern and southern hemispheres. If auroras occur simultaneously, certainly the irregularities must be as large as several earth's radii. Furthermore, any sharp localization of the wave at some arbitrary point on the boundary, supposing that it did exist, would appear to connect to a rather arbitrary point on the earth's surface, rather than to the statistically well-defined auroral zones. For example, disturbances might be expected with equal probability over the entire polar cap, or within a broad auroral zone.

Other objections can be made to the magnetohydrodynamic theory or to the distant-ion-cloud theory. The formation of an east-to-west current ring, according to *Parker* [1958], requires a time impossibly long in terms of geomagnetic storm development. The existence of the conduction corona, extending with very little decrease in temperature from sun to earth, depends on the detailed energetics of coronal gas. *Zirin's* [1957] conclusion that radiative losses for hydrogen are small appears to justify the importance of Chapman's conduction mechanism. However, near the sun, at least, the ultra-violet radiation field of the ionized metals plays an important, if not predominant, role in the energy losses. Since no evidence for coronal stratification according to atomic weight exists, all the solar energy fed into the corona from below may well be radiated, rather than conducted away. A further qualification to this problem has appeared with the observation of the Van Allen radiation [*National Academy of Sciences, IGY Bulletin*, 1958] as an almost universal phenomenon at sufficient elevations above the earth's surface. According to *Van Allen* and others [1958], the radiation may well play an important role in the energetics of the exosphere. If so, we deal with a highly non-thermal problem, the acceleration of particles, as the ultimate source of the observed downward energy flux in the exosphere, and we may not need to consider conduction effects in the corona.

The view adopted here will be the older idea that the interplanetary medium consists of solar

corpuscular clouds and streams, which impinge randomly in time and space on the magnetic environment of the earth. The major question to be answered is whether strong local variations in the surface magnetic field can exist without magnetohydrodynamic waves. Lacking a continuous medium for propagation of a magnetohydrodynamic wave, these local perturbations arise from the presence of corpuscular streams near the surface of the earth. We will assume that, during auroras and geomagnetic storms, corpuscular streams, restricted in the north-south direction to a thin sheet, flow in the direction of the earth's magnetic field near the auroral zone. As the streams move along the curved lines of force of the earth's dipole field, centrifugal acceleration results in magnetic pressures. These pressures represent geomagnetic perturbations, which agree in direction and magnitude with observed perturbation fields, as we seek to demonstrate in Section 2.

Any satisfactory discussion of auroras and geomagnetism should explain the location of the auroral zone. This point is discussed in Section 3. In Section 4, we discuss the maximum in frequency near midnight and the large energies necessary for penetration of auroras to 100-km levels.

2. Centrifugal Accelerations of Auroral Streams near the Earth's Surface

Regardless of their origin, we consider the experimental fact of the existence of corpuscular streams impinging on the earth's atmosphere along the magnetic lines of force. What is the centripetal pressure exerted at right angles to the lines of force by the motion of ionized hydrogen gas? At the auroral zone, the radius of curvature of a line of force is about $3r_0$, concave towards the equatorial plane. Where N is the particle density, m_H is the mass of the proton, v is the speed of the particles along the curved track, and h is the thickness of the corpuscular stream in the direction at right angles to the lines of force, the pressure is

$$P = N m_H \frac{v^2}{3r_0} h \qquad (1)$$

P compresses the lines of force on the high-latitude side of the stream and expands them on the low-latitude side. Equilibrium occurs when the difference in magnetic pressure between the high-and low-latitude sides equals the centripetal pressure. Where the field perturbation is ΔH

$$N m_H \frac{v^2}{3r_0} h = \frac{1}{8\pi}\left[(H + \Delta H)^2 - (H - \Delta H)^2\right] \qquad (2)$$

Taking $N = 10^6$ cm^{-3}, $v = 3 \times 10^3$ km sec^{-1}, and $h = 50$ km, we find $H\Delta H = 5 \times 10^{-3}$ gauss^2. The perturbation field, $\Delta H = 10^3\gamma$, if $H = 0.5$ gauss. Arcs, as they pass overhead, appear to have a minimum thickness of a few kilometers. In view of the uncertainties, ΔH is encouragingly similar to the magnitude of geomagnetic perturbations observed during storms. This perturbation field will have a scale roughly comparable to the earth's radius of curvature, in the directions parallel to the auroral sheet, and will change sign abruptly across the auroral zone, or, in any event, across the foot of an auroral arc 100 km above the surface of the earth.

Because the earth's field points downwards in the northern polar cap, the current flowing in the auroral arc flows parallel to the surface of the earth from east to west around the northern auroral zone. The current in the southern auroral stream also flows in the east-west direction, around the southern auroral zone. Suppose that a given auroral stream in the northern hemisphere occurs in exact time coincidence with a conjugate stream in the southern hemisphere. The total perturbation field is the sum of the fields produced by the two auroral zone currents. *Chapman* and *Bartels* [1940] derived a hypothetical atmospheric current system to represent conveniently the observed nature of storm-time geomagnetic variations. The effects of actual currents that must flow in the auroral plasma appear to be similar to those of the average Chapman distribution.

3. Latitude of the Auroral Zones

In discussing the shape of the advancing edge of an ion cloud moving towards the earth, *Chapman* and *Ferraro* [1931, 1932, 1933] noted long ago the existence of two points of zero magnetic field on the surface of the cloud. They assumed that the edge of the cloud, which is very large in comparison with the earth or the scale of its

magnetic field even at distances of tens of earth's radii, was equivalent to a conducting plane surface. In that event, the cloud sweeps together the lines of force of the earth's field, until the back pressure exerted by the field on the induced currents in the surface of the cloud just equals the forward pressure, $Nm_H v^2$, of the ionized material of the cloud. For a plane surface at any distance from the earth, the total field is represented by the sum of the fields produced by the earth's dipole and a parallel image dipole of equal strength, situated as far into the cloud as is the earth's dipole away from it. Since the surface of the cloud bisects the line joining the image and real dipoles, the field vanishes at two points, lying in the plane containing the dipoles and equidistant above and below the line joining them.

At these points, the back pressure of the magnetic field on the surface element of the cloud vanishes and therefore permits 'horns' of material to protrude into the space between the ion cloud and earth. Chapman and Ferraro concluded that these horns "are not likely to be significant for the theory of the auroras," since horns in a plane cloud will come towards only the sunlit side of the earth. Nevertheless, in this section, attention will be directed again to these structures as possible sources of auroral material.

The position of vanishing magnetic field on the surface of the cloud occurs where the earth's magnetic field is perpendicular to the cloud, at geomagnetic colatitude $\vartheta_1 = \text{arc cos } (1/\sqrt{3}) = 54.6$ degrees. At what position on the earth's surface does the line of force touch that just vanishes at the zero-field position on the cloud's surface? The total field between the earth and the cloud is accurately the sum of real and image fields. Since, however, each field falls away as the inverse cube of the distance, to a very good approximation the total field is given by the field of the real earth's dipole alone, which has lines of force given by

$$r = r_{\max} \sin^2 \vartheta \tag{3}$$

If r_1 is the distance from the center of the earth to the zero-field position on the surface of the cloud, and νr_0 is the distance from the earth of radius r_0 to the surface of the cloud, measured on a perpendicular,

$$r_1 = \frac{\nu r_0}{\sin^2 \vartheta_1} = r_{\max} \sin^2 \vartheta_1 \tag{4}$$

The line of force to the zero-field position therefore is approximately given by

$$r = \frac{\nu r_0}{\sin^3 \vartheta_1} \sin^2 \vartheta \tag{5}$$

This line of force intersects the surface of the earth at geomagnetic colatitude ϑ_0, satisfying

$$\sin^2 \vartheta_0 = \frac{(2/3)^{\frac{3}{2}}}{\nu} \tag{6}$$

For an ion cloud with a density of one hydrogen atom cm^{-3}, moving at a speed $v = 10^3$ km sec^{-1}, the equality of impact pressure and the energy density of the earth's magnetic field occurs at about $\nu = 4$. Then ϑ_0, which depends insensitively on the distance to the ion cloud, is 22 degrees.

This zone, at ϑ_0, represents the points at which material flowing from the ion cloud will touch the earth's surface. The zone is sharply defined for any single ion cloud, but will vary somewhat with the kinetic energy of the cloud. In other words, for a wide range of cloud velocities near 10^3 km sec^{-1}, material will impinge on the zone near 22 degrees. This represents the most striking feature of auroras and geomagnetic storms, their concentration towards the auroral zone. The conclusion is that whenever plasma is stopped by the earth's magnetic field, material must flow down to the auroral zone, defined by ϑ_0. That the value of ϑ_0 derived from the simple theory of a plane ion cloud agrees so well with the observed auroral zone may be coincidental. On the other hand, we shall take the point of view that even though they may not be the entire physical phenomenon in a geomagnetic storm, the horns must represent an important aspect.

This computation of the latitude of the auroral zone strictly holds only in the case of a plane ion cloud. Do these positions of vanishing field on the surface of the cloud disappear if the curvature of an actual cloud is taken into account? It is possible to solve simply the potential problem of a magnetic dipole within a hollow, if the hollow has the shape of a separable coordinate system. One such system is the paraboloidal coordinate system, in which the surface of the cloud is a paraboloid of revolution with the earth at the focus. It is easy to show that there are four points on the surface of the cloud where the field vanishes in this case, and these points tend to surround the earth. The same situation of

vanishing field at *points* holds for any separable system (for another example, the rectangular prism, which can also be solved by the method of images) but becomes, for the circular cylinder, a vanishing field along a *line*, which surrounds the earth completely.

The field of the earth's dipole, in any of these cases, represents the total field within the curved cloud surface to a good approximation. The point of intersection of the line of force from the zero-field point on the surface of the cloud to the surface of the earth tends to remain essentially at the same zone as that given by the value of ϑ_0, previously computed. This prediction of the auroral zone agrees formally with *Martyn's* [1951]. Martyn's argument is that the auroral particles originate at the ring current, and that most of the lines of force of the current ring cross the surface of the earth in polar regions. It is not clear in Martyn's theory why particles follow the line of force to the zone at, say, $\vartheta_0 = 22$ degrees rather than the line of force to, say, 20 degrees, or, even both of those lines of force. One of the striking features of the phenomenon is that particles follow a single line of force to a given zone, rather than to several parallel zones.

4. Three-Dimensional Trajectories of Auroral Plasma

The incidence of auroral particles on all sides of the earth represents a major difficulty for the direct interpretation of the horns as auroral phenomena, as pointed out by Chapman. One solution may be, as suggested above, the consideration of the curvature of the surface of Chapman's plane ion cloud. In that event several different zero-field points exist on the surface of the cloud, and even field-free lines may develop in the case that the earth is completely surrounded by the cloud. Visualize, for example, the curved sheet containing the lines of force touching the surface of the earth at the auroral zone and extending back to the surface of the ion cloud several earth's radii distant. Since the field is zero at the cloud's surface, plasma is free to move along the line of force into the space between the cloud and the earth. In this way a three-dimensional cut may develop in the magnetic field surrounding the earth and provide a path along which plasma material may reach the earth on all sides. Suppose that rapidly-moving concentrations of plasma move, without lateral constraints, along the surface of this auroral sheet. The trajectories followed depend critically on the point of injection into the sheet; they reach the surface of the earth at points mainly depending on the distance of the point of injection away from the plane containing the earth's dipole and the sun. The details of computations on such a model of auroral motions appear in the Appendix.

Regardless of their energy, plasma concentrations cannot curve farther around the earth than about 270 degrees for an ion cloud distant four earth's radii. The distributions of high-velocity plasma, moving around the earth from east to west, or west to east, respectively, therefore overlap only in the nighttime hemisphere. Plasma concentrates in the midnight hemisphere, if it is incident from the direction of the sun. The midnight hemisphere is further marked by the fact that fast-moving plasma clouds collide with relative velocities twice their velocity of approach to the earth. Since the mean-free-paths of protons in the clouds are short(of the order of tens of kilometers near the earth), the entire relative energy of motion of the two clouds is available for conversion of thermal particles into auroral particles.

The concept of an auroral sheet is motivated primarily by the Störmer problem of the motions of a single charged particle in the earth's magnetic field. In its application to auroral theory, the Störmer theory seems unrealistic insofar as clouds of neutral plasma, rather than individual separate particles, appear to be involved, at least in the exospheric regions well away from the earth's atmosphere. Nevertheless, the Störmer theory had one outstandingly successful feature, the precipitation of individual particles around a narrow zone, for particles at a single kinetic energy. The auroral sheet permits concentrations of plasma to follow similar trajectories as the individual particles in Störmer orbits.

5. Summary and Conclusions

The magnetic pressure exerted on corpuscular streams moving along dipole lines or force of the earth's magnetic field appears to account quantitatively for the magnitude of the disturbance vector during geomagnetic storms. Furthermore, the direction of the disturbance appears

to agree qualitatively with schematic representations of typical geomagnetic storms.

Motions of clouds along the auroral sheet defined by the dipole lines of force converge with high relative speeds in the nighttime hemisphere. Although the model remains hypothetical, the conclusions appear to explain immediately the nighttime occurrence of auroras, and the high energies of auroral particles.

In further work, special attention should be given to the details of formation of the hollow in the incident ion cloud. Current methods for computation of potential problems using high-speed computers should permit practical solutions.

In conclusion, I should like to acknowledge many discussions of auroral topics with Donald H. Menzel, of the Harvard College Observatory, and Robert S. Lawrence, of the Boulder Laboratories, the National Bureau of Standards, especially in the development of the ideas of Section 3. Sydney Chapman has provided much useful criticism of the manuscript. A substantial part of the numerical computations leading to Figures 1, 2, and 3 was done by George Bakalyar, of the staff of the High Altitude Observatory.

The Geophysics Research Directorate of the Air Force Cambridge Research Center supported the research reported in this paper.

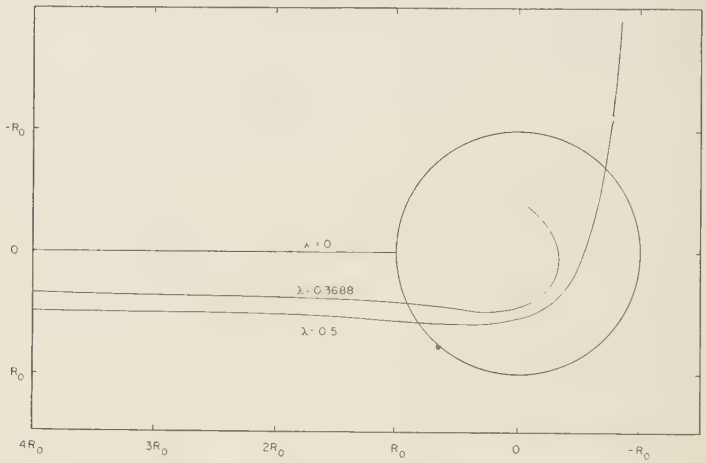

Fig. 1—Projection of trajectory on plane $\vartheta = 90°$

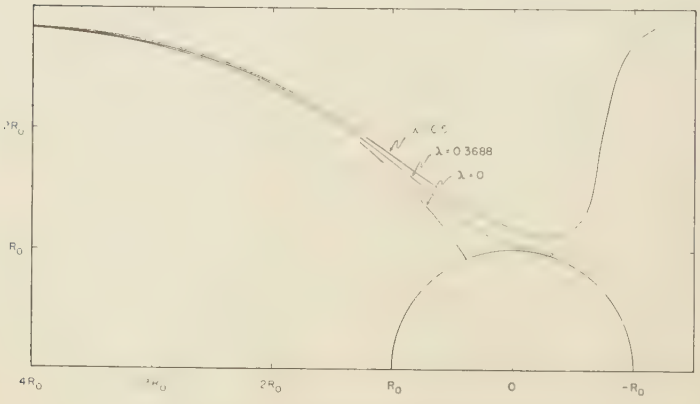

Fig. 2—Projection of trajectory on plane $\varphi = 0°$

Appendix

Motion of auroral Plasma—A frictionless blob of auroral plasma slides along the surface of revolution defined by the dipole line of force to the auroral zone. The speed of the blob is constant, and is given by

$$v^2 = \dot{r}^2 + r^2\dot{\vartheta}^2 + r^2 \sin^2 \vartheta \dot{\varphi}^2 \tag{7}$$

where azimuthal angle φ is measured to the east from the sunside of the plane containing the earth's dipole axis and the sun. Conservation of angular momentum states the constancy of

$$L = r^2 \sin^2 \vartheta \dot{\varphi} \tag{8}$$

The constraint of the plasma to the dipole sheet requires

$$\dot{r} = -2r_{\max} \sin \vartheta \cos \vartheta \dot{\vartheta} \tag{9}$$

according to equation (3).

Suppose that the plasma enters the sheet at coordinates $(r_1, \vartheta_1, \varphi_1)$. Introduce a non-dimensional parameter λ, representing the distance, in units of the earth's radius, of the initial point from the plane containing the earth's dipole and the sun. Then

$$[\dot{\varphi}]_1 = \frac{v \sin \varphi_1}{r_1 \sin \vartheta_1} = \frac{\lambda}{\nu^2} \frac{v}{r_0} \tag{10}$$

From equation (8),

$$L = \lambda v r_0 \tag{11}$$

Introduce the parameter

$$d\tau = \frac{v}{r_0} dt \tag{12}$$

representing the distance moved by the plasma in units of the earth's radius. Now rewrite (7) and (8), with the use of (9), in the form

$$1 - \frac{\lambda^2}{\nu^2} \frac{\sin^6 \vartheta_1}{\sin^6 \vartheta} = \frac{\lambda^2}{\sin^6 \vartheta_1} \sin^2 \vartheta (4 - 3 \sin^2 \vartheta) \left(\frac{d\vartheta}{dt}\right)^2 \tag{13}$$

and

$$\frac{\lambda}{\nu^2} \frac{\sin^6 \vartheta_1}{\sin^6 \vartheta} = \frac{d\varphi}{dt} \tag{14}$$

With the initial conditions

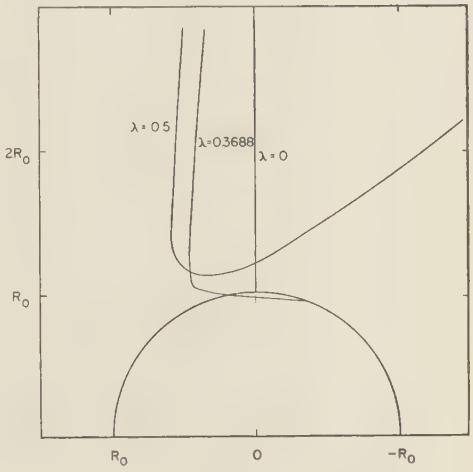

Fig. 3—Projection of trajectory on plane $\varphi = 90°$

$$\sin \vartheta_1 = (2/3)^{1/2} \tag{15}$$

$$\sin \varphi_1 = \frac{\lambda}{\nu} \tag{16}$$

equations (13) and (14) represent the trajectory of an auroral plasma. The speed of the plasma enters as a scaling factor and determines only when the plasma reaches the earth.

The left-hand member of (13) must satisfy

$$1 - \frac{\lambda^2}{\nu^2} \frac{\sin^6 \vartheta_1}{\sin^6 \vartheta} \geq 0 \tag{17}$$

The equality sign holds at the point where an auroral plasma approaches most closely to the surface of the earth, if that point lies above the earth's surface. Otherwise, the inequality always holds. For a fixed value of ν, consider the λ-value, $\lambda_{\max}$, corresponding to a trajectory that just grazes the surface of the earth. Substitute $\sin \vartheta_0$ from (3) for $\sin \vartheta$, in (16), and solve for $\lambda^2_{\max}$.

$$\lambda^2_{\max} = \frac{1}{\nu} \sin^3 \vartheta_1 \tag{18}$$

For $\nu = 4$, $\lambda_{\max} = 0.3688$. Note that $\lambda_{\max}$ depends insensitively on the distance from the cloud to the earth, and is independent of the speed of the plasma.

The azimuth at the grazing point, $\varphi_{\max}$, is the largest azimuth for any touching orbit with the given value of ν. To show this, integrate (14),

from the starting value $\tau = 0$, up to some fixed value, τ, not necessarily the final value when the plasma touches the earth.

$$\varphi = \arcsin\frac{\lambda}{\nu} + \frac{\lambda}{\nu^2}\sin^6\vartheta_1 \int_0^\tau \frac{d\tau}{\sin^6\vartheta} \qquad (15)$$

Substitute for $d\tau$ from the solution of (13). Then

$$\varphi = \arcsin\frac{\lambda}{\nu} + \left(\frac{\lambda}{\nu}\right)^2 \sin^3\vartheta_1 \cdot \int_0^\tau \sqrt{\frac{4 - 3\sin^2\vartheta}{1 - \left(\frac{\lambda}{\nu}\frac{\sin^3\vartheta_1}{\sin^3\vartheta}\right)^2}}\,\frac{d\vartheta}{\sin^5\vartheta} \qquad (20)$$

The derivative of (20) with respect to λ is positive. Therefore at any particular value of ϑ along a trajectory, the largest value of φ corresponds to the largest λ.

Figures 1, 2, and 3 show sample trajectories as projected on three coordinate planes. The computations have been made for $\nu = 4$, and for $\lambda = 0$, 0.3688, and 0.5.

References

Biermann, L., Solar corpuscular radiation and the interplanetary gas, *Observatory*, **77**, 109–110, 1957.

Chapman, S., Notes on the solar corona and the terrestrial ionosphere, *Smithsonian Contribs. to Astrophys.*, **2**, 1–12, 1957.

Chapman, S., and J. Bartels, The quantitative discussion of the first phase, *Geomagnetism*, Clarendon Press, Oxford, vol. 2, 859–866, 1940.

Chapman, S., and V. C. A. Ferraro, A new theory of magnetic storms, *Terrestrial Magnetism and Atmospheric Elec.*, **36**, 77–97, 171–186, 1931; **37**, 147–156, 421–429, 1932; **38**, 79–96, 1933.

Dessler, A. J., Large amplitude hydromagnetic waves above the ionosphere, *J. Geophys. Research*, **63**, 507–511, 1958.

Martyn, D. F., The theory of magnetic storms and auroras, *Nature*, **167**, 92–94, 1951.

National Academy of Sciences, Fourth US-IGY satellite, *IGY Bull. No. 15*, 8–9, September, 1958.

Obayashi, T., and J. A. Jacobs, Sudden commencements of magnetic storms and atmospheric dynamo action, *J. Geophys. Research*, **62**, 589–616, 1957.

Parker, E. N., To be published in the *Physics of Fluids*.

Parker, E. N., Electrical conductivity in the geomagnetic storm effect, *J. Geophys. Research*, **63**, 437–438, 1958.

Van Allen, J. A., G. H. Ludwig, E. C. Ray, and C. E. McIlwain, The observation of high intensity radiation by satellites 1958 Alpha and Gamma, *Rockets and Satellites, Rept. no. 3*, 73–92, 1958.

Zirin, H., Supplementary note, *Smithsonian Contribs. to Astrophys.*, **2**, 13–14, 1957.

(Manuscript received January 12, 1959.)

Ionospheric Heating by Hydromagnetic Waves

A. J. Dessler

Lockheed Aircraft Corporation
Missiles and Space Division
Palo Alto, California

Abstract—The rate of energy dissipation per unit volume is investigated for hydromagnetic waves traveling downward through the ionosphere. A calculation of the heating rate is made, based on assumptions as to the amplitude and Fourier spectrum of the hydromagnetic waves. It is argued in a general way that the peak heating rate due to hydromagnetic waves occurs near 175 kilometers. The results, which are strongly dependent on the assumed values for the amplitude and Fourier spectrum of the hydromagnetic waves, indicate that hydromagnetic heating is normally not important in determining the temperature of the F region. However, during a magnetic storm, the hydromagnetic heating may become the dominant source of heat in the F region. The suggestion is made that the observed lifting of the F region during a magnetic storm is due to an increased heating rate caused by the storm-generated hydromagnetic activity. It is shown that it is not possible to account for the main phase of a magnetic storm by ionospheric heating.

Introduction—It has been argued that large-amplitude hydromagnetic waves are present above the ionosphere [*Dessler*, 1958]. Such waves probably account for the transient fluctuations in magnetic field observed at the surface of the earth. In this paper, it will be assumed that hydromagnetic waves are present above the ionosphere. It will be necessary to make further assumptions regarding the amplitude and Fourier spectrum of these waves. At high altitudes the electrical conductivity of the ambient medium is high enough so that dissipation of hydromagnetic waves due to electron-ion and ion-atom collisions is negligible. However, at lower levels, collisions between ions and neutral atoms give rise to a new dissipation mechanism which can cause a significant amount of atmospheric heating. This dissipation mechanism was first pointed out by *Schluter* and *Biermann* [1950] and later by *Piddington* [1954] and *Cowling* [1957]. It is demonstrated in these papers that in the presence of magnetic field and when the neutral particle density is a sufficiently high fraction of the total density, a 'reduced conductivity' must be used to calculate dissipation. When the neutral particles can be neglected, the 'zero field conductivity' is used because the charged-particle collision frequency is not changed by the presence of a magnetic field (except in certain limiting cases where the collision frequency may be decreased). Particle collisions are the only agency for converting the electromagnetic energy into heat.

As explained in the previously mentioned references, the increased dissipation due to neutral atoms comes about in the following manner. When a hydromagnetic wave moves through a partially ionized gas, the ions and electrons follow the wave motion while the neutral atoms do not feel the wave's electrical forces. However, electromagnetic energy may be transferred to the neutral atoms by ion-atom collisions. These collisions are apt to be important, since there can be a large relative velocity between the ions and the neutral atoms. The opportunity is thus provided for a large rate of dissipation of energy from the wave. Therefore, an energy dissipation mechanism exists in a partially ionized gas which is not present in a completely ionized gas.

Calculation of heating rate—Let us calculate the rate of energy dissipation per unit volume due to a downward-traveling hydromagnetic wave. The calculation of the dissipation rate is essentially identical for either a longitudinal or a transverse wave. However, this calculation will be based on a longitudinal hydromagnetic wave since it gives a simpler physical model.

Consider a sinusoidal longitudinal hydromagnetic wave of magnetic amplitude b in a background magnetic field B. The current density j associated with the wave may be derived from

the Maxwell equation, $\nabla \times \bar{H} = \bar{j}$, in which the displacement current term is neglected (MKS units). The magnitude of the average current density may then be written as $j \approx 4b/\mu\lambda$, where λ is the wave length of the hydromagnetic wave and μ is the permeability. This current will flow perpendicularly to both the magnetic field and the direction of wave propagation. According to the formulation of Piddington and Cowling, the rate of energy dissipation per unit volume P is given by $P = j^2/\sigma_3$, where σ_3 will here be called the Cowling conductivity. This conductivity has been defined and discussed elsewhere [*Piddington*, 1954; *Cowling*, 1932, 1957; *Baker* and *Martyn*, 1954], and will not be elaborated on here.

Numerical values for the Cowling conductivity as a function of altitude are given by *Chapman* [1956] and will be used for the calculations in this paper. Chapman calculates σ_3 for two model atmospheres, one of which has a temperature of 850°K at 300 km while the other has a temperature of 1480°K at this altitude. The values of σ_3 calculated for the hotter atmosphere will be adopted, since satellite density data indicate that the hotter F region is more nearly correct. The values for the zero field conductivity σ_0 and the Cowling conductivity σ_3 are given in Table 1.

TABLE 1—*The zero field conductivity* σ_0, *Cowling conductivity* σ_3, *and ion-atom collision frequency* ν_{in} *vs. altitude (after Chapman)*

Altitude (km)	σ_0 (mho/m)	σ_3 (mho/m)	ν_{in} (collisions/sec)
100	1.7×10^{-2}	8.7×10^{-3}	8.6×10^{3}
125	2.9×10^{-1}	1.7×10^{-3}	6.2×10^{2}
150	1.6	3.9×10^{-4}	1.1×10^{2}
175	4.1	1.1×10^{-4}	3.2×10
200	7.7	3.9×10^{-5}	1.2×10
225	12.5	1.9×10^{-5}	5.5
250	18.	1.1×10^{-5}	2.9
275	23.	6.5×10^{-6}	1.7
300	28.	4.3×10^{-6}	1.1

The expression,

$$P = j^2/\sigma_3 = \frac{16b^2f^2}{\mu^2 V_{hm}^2 \sigma_3},$$

where V_{hm} is the hydromagnetic wave velocity and f is the frequency of the wave, does not apply unless the ion-atom collision frequency ν_{in} is much greater than the wave frequency f. When the ratio ν_{in}/f is of the order of one or less, it will be shown that P is much less than j^2/σ_3. The deviation from this formula is due to the fact that conductivity is not defined when $\nu_{in} \lesssim f$ because the definition of conductivity involves an equivalent drag force due to an average or steady-state momentum loss per unit time by collisions of the current carriers. When the current changes markedly in either magnitude or direction in a time of the order of or less than $1/\nu_{in}$, the drag force is not defined and hence the conductivity will differ from the steady-state value.

In the altitude range where the collision frequency is not much greater than the wave frequency, P can be calculated directly from the rate of transfer of kinetic energy from the ions to the neutral atoms, rather than from the more indirect formula, $P = j^2/\sigma_3$, which involves the steady-state drag term. Within the wave crest of a longitudinal hydromagnetic wave, the ions and electrons move together in the direction of propagation with an average velocity $v_{av} = \frac{1}{2} V_{hm}\,(b/B)$. (The current density j, which is associated with the hydromagnetic wave, always flows perpendicular to v_{av} and is made up of oppositely moving electrons and ions.) If it is assumed that on the average for ion-atom collisions, one half of the ion's kinetic energy is transferred to the neutral atom, the rate of energy loss is

$$P_1 = \tfrac{1}{4}\rho_i v_{av}^2 \nu_{in} = (1/16)\nu_{in}\rho_i V_{hm}^2 (b/B)^2,$$

where ρ_i is the mass density of ions. Since $V_{hm} = B/(\mu\rho)^{\frac{1}{2}}$, we have

$$P_1 = (1/16)\nu_{in}(b^2/\mu).$$

This result states that ν_{in} times per second, 1/16 of total energy in the hydromagnetic wave (b^2/μ) is transferred to the neutral atoms and converted into heat energy. The energy dissipated due to the current density j is negligible since the more mobile electrons carry all the current and they cannot transfer much energy to the neutral gas. Also, the velocity of charged particles necessary to produce the current density j is generally much less than v_{av}. Hence, the dissipation due to j would generally be negligible even if ions carried the total current.

In order to use the formulas for P and P_1 for an accurate calculation of the power dissipated

per unit volume, the Fourier spectrum of the hydromagnetic waves above the ionosphere must be known. In the absence of such knowledge, we will assume that the major portion of the Fourier spectrum is in the region near one cycle per second. This assumption is based on *Parker's* 1958] calculation of the flutter frequency of the edge of the earth's dipole magnetic field in the solar wind. It will be further assumed that on magnetically quiet days, the hydromagnetic wave amplitude b is of the order of 30γ (3×10^{-8} weber/m^2) above the ionosphere [*Dessler*, 1958]. On magnetically disturbed days, the high frequency end of the spectrum will probably become more important because of the formation of hydromagnetic shocks by the large amplitude waves.

On the basis of the above assumptions regarding the Fourier spectrum and hydromagnetic wave amplitude, the power dissipated per unit volume as given by

$$P = \frac{16 b^2 f^2}{\mu^2 V_{hm}{}^2 \sigma_3} \qquad \text{and} \qquad P_1 = \frac{\nu_{in} b^2}{16 \mu}$$

are shown in Figure 1. For simplicity in the calculation of P, the entire wave amplitude was taken to be at a frequency of one cycle per second.

At altitudes lower than about 150 to 175 km, the heating rate calculated from P_1 is an overestimate since it does not allow for the ions slipping relative to the motion of the magnetic field which would occur when $\nu_{in} \gg f$. For example, if we adopt the criterion of 30 ion-atom collisions per cycle as the limit for applying the P_1 formula for a 1-cps wave, then we see from Table 1 that $\nu_{in} = 30$ collisions/second at an altitude of about 175 km. The dissipation will be less than that given by P_1 below this altitude.

The heating rate calculated from P is an overestimate at altitudes above 200 to 225 km because σ_3 is smaller than the actual effective conductivity when $\nu_{in} \lesssim f$; that is, when current can flow for at least a large fraction of a cycle between ion-atom collisions. In this region, where there are only two or three collisions in a quarter cycle, the effective conductivity lies between σ_3 and σ_0, and the dissipation is much less than the value given by P. However, there is an even more definitive limitation on the hydromagnetic heating at high levels in that the dissipation can never exceed the values given by P_1. These general arguments place the peak heating rate

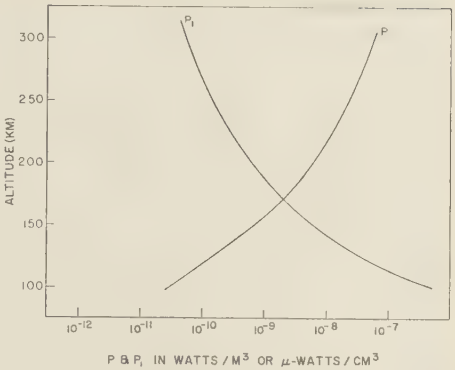

FIG. 1—Power dissipation per unit volume $P = j^2/\sigma_3$ and $P_1 = (1/16)\nu_{in}(b^2/\mu)$

between about 175 and 200 km. Figure 2 shows a possible heating rate versus altitude curve based on the heating rates calculated from P and P_1 in their respective regions of applicability.

Lifting of the F region during geomagnetic storms—It is observed that during the intense phase of a geomagnetic storm, the height of the F region increases and the critical frequency decreases [*Kirby* and others, 1935; *Lewis* and *McIntosh*, 1953; *Tandberg-Hanssen*, 1958]. This phenomenon may be interpreted in terms of a heating and a corresponding expansion of the F region. During a moderate or weak magnetic storm, the F region generally only lifts near

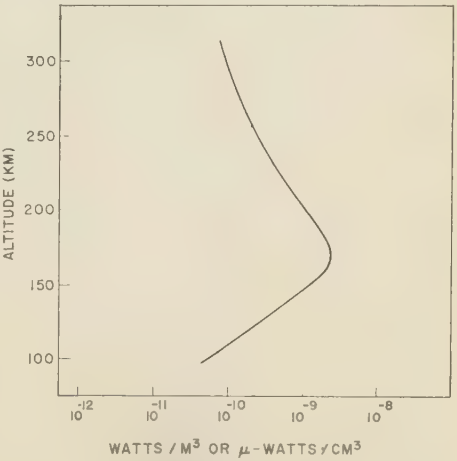

FIG. 2—Power dissipation per unit volume based on a combination of P and P_1; in drawing this curve, use is made of the fact that the power dissipation can never exceed P_1

auroral latitudes [*Appleton* and *Piggott*, 1950; *Berkner* and *Seaton*, 1940].

The above observations may be explained if we assume that the F region is normally heated by some source other than hydromagnetic waves. The F region will lift only when the root-mean-square amplitude of the hydromagnetic waves rises above some critical value so that the hydromagnetic heating rate exceeds that of the normal heat source. During a magnetic storm, the increase in the amplitude of the geomagnetic fluctuation is large enough so that it implies that the heating rate will increase by at least two orders of magnitude. Since magnetic activity is always more severe in the auroral zone than at lower latitudes, a moderate magnetic storm may contain hydromagnetic waves of sufficient amplitude to lift the F region only in the auroral latitudes. A severe magnetic storm may cause world-wide lifting of the F region.

The increase in F-region ionization usually observed at low and middle latitudes during moderate magnetic storms is not explained.

The main phase of a geomagnetic storm—The main phase of a geomagnetic storm is characterized by a world-wide decrease in H, the horizontal component of the magnetic field. It has been suggested that, as an alternative to the ring current hypothesis, the main phase may be explained by heating at some level where the expansion of the ions will push out the geomagnetic field and therefore decrease H at the earth's surface [*Parker*, 1956]. It will be shown in this section that it is not possible to account for the main phase of a magnetic storm by ionospheric heating due to hydromagnetic waves or any other form of ionospheric heating.

In order for an ion gas to push out the geomagnetic field so as to produce a decrease ΔB in the field strength at the ground, the ion gas pressure must be greater than the differential magnetic pressure, that is, $n_i kT > B\Delta B/\mu$, where n_i is the number of ions per unit volume. Note that it is only the ion pressure which must be compared with the magnetic pressure, since the neutral atoms cannot push on the magnetic field directly. Neither can the neutral atoms exert any sustained force on the magnetic field by pushing on the ions, because the dissipation which occurs in ion-atom collisions will allow the magnetic field to slip through the ions. For a numerical example take

$$B = 3 \times 10^{-5} w/m^2, \quad \Delta B = 5 \times 10^{-8} w/m^2,$$

$$n_i = 10^{12}/m^3, \quad T = 2000°\mathrm{K}$$

Then the magnetic differential pressure $B\Delta B/\mu$ is about 10^{-6} newtons/m^2, while the ion gas pressure $n_i kT$ is about 3×10^{-8} newtons/m^2. Thus, we see that the pressure the ionosphere is able to exert on the magnetic field is about two orders of magnitude too small to produce a sustained world-wide decrease in magnetic field strength of 50 γ on the ground. A comparison between $B\Delta B/\mu$ and $n_i kT$ at altitudes up to about 10 earth radii yields similar results.

Another difficulty arises from the speed with which a magnetic field can diffuse through the ionosphere. A stress in a magnetic field over a distance l will be relieved by diffusion in a characteristic time $\tau = (1/10)\mu\sigma_3 l^2$. For example, a value of less than one second is obtained for τ when l is 50 km and σ_3 is 1.1×10^{-4} mho/m (conductivity at 175 km). This result states that if the magnetic field were lifted by an ionospheric expansion near an altitude of 175 km, the field would diffuse through a layer 50 km deep and return to its equilibrium position in about one second. This time is to be compared with the main phase of a magnetic storm which lasts for several days. Above about 1500 km where the neutral atom density becomes negligibly small compared with the ion density, σ_3 will approach σ_0 and the diffusion time will become very long; therefore the objection of rapid diffusion does not apply at very high altitudes. However, here especially, the gas pressure is much less than the magnetic field pressure.

Conclusion—An examination of the dissipation of hydromagnetic waves in the ionosphere leads to the conclusion that the power dissipation per unit volume reaches a maximum between about 150 km and 200 km altitude. The magnitude of this power dissipation is uncertain because of the lack of knowledge concerning the amplitude and Fourier spectrum of the hydromagnetic waves. However, it is probable that the hydromagnetic heating is unimportant except during a magnetic storm.

It is suggested that the observed lifting of the F region and the reduction of the F-region critical frequency during a magnetic storm is due to hydromagnetic heating. Since this heating occurs in the lower F region, the D and *E*

regions will remain essentially unaffected by the magnetic storm heating, in agreement with observation [*Tandberg-Hanssen,* 1958]. Although there is dissipation of the hydromagnetic waves below 100 km, it is not apt to be physically important in regard to atmospheric heating, as the effect is overshadowed by the absorption of solar energy.

Expansion of the F region due to hydromagnetic heating cannot account for the decrease in the horizontal component of the earth's magnetic field during the main phase of a magnetic storm. This conclusion is reached by considering the pressure the ions may exert on the magnetic field. The ion pressure is about two orders of magnitude too small to account for the observed decrease in H. Also, if the magnetic stress were set up in the ionosphere, diffusion of the magnetic field through the ions would restore the magnetic field to its equilibrium position in a very short time. These arguments may be extended to exclude any explanation of the main phase of a magnetic storm which relies on ionospheric heating.

Acknowledgments—I wish to thank F. S. Johnson and E. N. Parker for their help in the preparation of this paper.

References

Appleton, E., and W. R. Piggott, World morphology of ionospheric storms, *Nature,* **165**, 130–131, 1950.

Baker, W. G., and D. F. Martyn, Electric currents in the ionosphere, I, The conductivity, *Phil. Trans. Roy. Soc. London, A,* **246**, 281–294, 1954.

Berkner, L. V., and S. L. Seaton, Ionospheric changes associated with the magnetic storm of March 24, 1940, *Terrestrial Magnetism and Atmospheric Elec.,* **45**, 393–418, 1940.

Chapman, S., The electrical conductivity of the ionosphere: A review, *Nuovo cimento, Suppl. 4,* **4**, 1385–1412, 1956.

Cowling, T. G., The electrical conductivity of an ionized gas in the presence of a magnetic field, *Monthly Notices Roy. Astron. Soc.,* **93**, 90–98, 1932.

Cowling, T. G., The dissipation of magnetic energy in an ionized gas, *Monthly Notices Roy. Astron. Soc.,* **116**, 114–124, 1956; and *Magnetohydrodynamics,* ch. 6, Interscience Publishers, Inc., New York, 1957.

Dessler, A. J., Large amplitude hydromagnetic waves above the ionosphere, *J. Geophys. Research,* **63**, 507–511, 1958; and *Phys. Rev. Letters,* **1**, 68–69, 1958.

Kirby, S. S., T. R. Gilliland, E. B. Judson, and N. Smith, The ionosphere, sunspots, and magnetic storms, *Phys. Rev.,* **48**, p. 849, 1935.

Lewis, R. P. W., and D. H. McIntosh, Geomagnetic and ionospheric relationships, *J. Atmospheric and Terrestrial Phys.,* **4**, 44–52, 1953.

Parker, E. N., On the geomagnetic storm effect, *J. Geophys. Research,* **61**, 625–637, 1956.

Parker, E. N., Interaction of the solar wind with the geomagnetic field, *Phys. Fluids,* **1**, 171–187, 1958.

Piddington, J. H., Electromagnetic field equations for a moving medium with Hall conductivity, *Monthly Notices Roy. Astron. Soc.,* **114**, 638–650, 1954.

Schluter, V. A., and L. Bierman, Interstellare Magnetfelder, *Z. Naturforsch.,* **5a**, 237–251, 1950.

Tandberg-Hanssen, E., Variations in the height of ionospheric layers during magnetic storms, *J. Geophys. Research,* **63**, 157–160, 1958.

(Manuscript received December 12, 1958.)

IGY Observations of F-Layer Scatter in the Far East

R. Bateman

Page Communications Engineers, Inc.
Washington, D. C.

J. W. Finney, E. K. Smith, L. H. Tveten, and J. M. Watts

Central Radio Propagation Laboratory
National Bureau of Standards
Boulder, Colorado

Abstract—Peculiar signal enhancements observed during transmissions at 36 to 50 Mc/s between the Philippines and Okinawa appear to represent F-layer scatter. These signals are observed nightly for periods of several hours during the months of September and October. Pulse tests indicate F-layer heights for these signals. Considerable pulse broadening is observed and the signals generally arrive from somewhat off the great circle path.

Transmission at VHF over several ionospheric-scatter propagation paths between the Philippines and Okinawa has been characterized by an anomalous signal enhancement during the evening hours. Normally on such paths propagation takes place by scatter in the lower ionosphere [*Bailey* and others, 1952, 1955], or occasionally sporadic E. In the evening hours, however, on these particular paths the signal often rises 30 to 40 db above the normal scatter signal level at 50 Mc/s and 40 to 50 db above the normal level at a frequency of 36 Mc/s. The frequency of occurrence of the enhancements appears to maximize during the months of September and October. The enhancements usually last several hours, beginning at about 1900 path midpoint time (GMT + 8). The signal intensity usually increases rapidly, then levels off, and finally drops back below the scatter level around midnight.

The first measurements of this anomaly were made over an experimental circuit operating at 36.4 Mc/s between Poro Point, Philippine Islands, and Sobe, Okinawa. This circuit operated from May 1956 to May 1957. A second circuit designed to measure sporadic E as part of the United States program for the IGY commenced operating at 49.84 Mc/s over an almost identical path (Poro, P. I., to Onna, Okinawa) in September 1957. During the year of operation at 36.4 Mc/s, the frequency of occurrence of the evening enhancement reached a peak during each equinoctial period. However, during the following year, at 49.84 Mc/s, only the fall peak could be observed. At the vernal equinox there appeared, if anything, to be a minimum. Curves showing a high month for the anomaly (October) and a low month (November) for each of the two circuits are seen in Figure 1. Signal levels are indicated as open-circuit antenna voltages referred to a 50 ohm line. The values shown are monthly medians of hourly medians. The details of these paths are shown in Table 1.

No simultaneous data for different frequencies are available for the same path using scaled antennas. However, a rough estimate of a decrease of one decibel per Mc/s relative to the normal ionospheric-scatter signal levels can be made for the anomaly from measurements at 50 Mc/s and below. If this estimate holds for frequencies above 50 Mc/s, then one would ex-

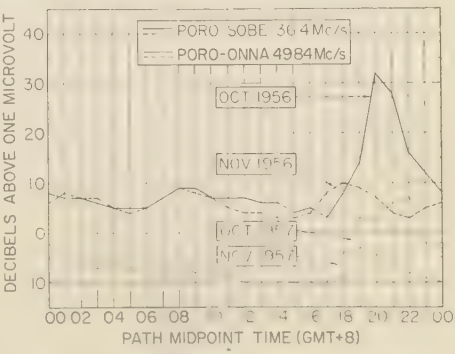

Fig. 1—Diurnal curves of monthly medians of hourly median signal intensities illustrating the effect of the anomaly in the evening hours

TABLE 1

	Path	
	Poro-Sobe	Poro-Onna
Frequency, Mc/s	36.4	49.84
Transmitter power, kw	1	2
Transmitting and receiving antennas	Stacked pair of 5-element Yagis	One 5-element Yagi
Polarization	Horizontal	Horizontal
Surface path length, km	1329	1347

pect to distinguish the anomaly above the level of normal ionospheric scatter up to frequencies of 80 to 90 Mc/s.

Observations of the behavior of the anomaly at 40.2 and 36.4 Mc/s were made for an additional path between Okinawa and the Manila area in the Philippines. For these observations, northbound transmissions were made at 40.2 Mc/s, alternating at half-hour intervals between dipole antennas at each terminal and corner-reflector antennas at each terminal. Southbound transmissions at 36.4 Mc/s were made with the antennas beamed on the great circle path, alternating at half-hour intervals with symmetrical split-beam antennas at each end. The split-beam antennas exhibit a null along the great-circle paths with beam maxima lying about eight degrees on either side of the great-circle path.

The indications are that most of the time during periods of the anomalous propagation the received signals arrive in a range of azimuths predominantly on one side or the other of the great-circle bearing. Occasionally, and usually during the later stages of the anomalous propagation, extremely strong signals were observed with the 'normal' beams aimed on the great-circle path. At such times, the signal intensities observed with the split-beam antennas were characteristically lower than those received with the 'normal' beam.

During September 1958, a series of pulse measurements were conducted over the Poro, Philippine Islands, to Onna, Okinawa, path. The peak-pulse power employed during these special transmissions was slightly less than two kilowatts. For the pulse experiment, independent time standards were used to control the pulse repetition rate at the transmitting terminal and the oscilloscope sweep rate at the receiving terminal. Range-time records were obtained for four nights, two of which (September 22 and 23, 1958) appear in Figure 2. The procedure was to keep the normal E-region echo at the bottom of the record and to display the time delay of the anomalous echo relative to it. Care was taken to make sure that the relative delay times observed were really of the order of one millisecond and not something of the order of 20 milliseconds (an echo of the previous pulse), as might be pertinent to F2-layer-propagated ground backscatter. Occasional readjustments of the receiving synchronization show up as abrupt discontinuities in the films. It is seen that the anomalous signal started abruptly on both nights at a time delay of about 1200 μsec behind the E-region pulse. The commencement time was 1924 on September 22, and 1911 on September 23. The delay time relative to the E-region echo then decreased to 500 μsec at 2300 on September 22 and to about 600 μsec at 2130 (after which the E-region echo drops out) on September 23. From purely geometrical considerations, a delay of 400 μsec relative to the E region corresponds to a signal returned from the midpoint of the great circle path at a height of about 300 km, while 1100 μsec corresponds to a height of about 500 km. A modest lateral deviation would not affect these figures appreciably. The transmitted pulse (50 μsec) when returned by the anomalous propagation mechanism is broadened to about 1500 μsec in the early hours, but this value is seen to have decreased to less than 500 μsec for the later stages of the anomaly.

Recent measurements during this propagation anomaly indicate that at 50 Mc/s the fading rate is of the order of five cycles per second, which is about the same as that of normal scatter fading. The fading rate during periods of sporadic-E transmission is usually much less than this.

The September 1957 periods of anomalous propagation over the Poro-to-Onna path were compared with ionospheric data from the Baguio, Philippine Islands, and Okinawa ionosphere stations. No association between the anomaly and E-region effects could be seen; however, the periods of anomalous propagation did appear to correspond to those of Spread-F

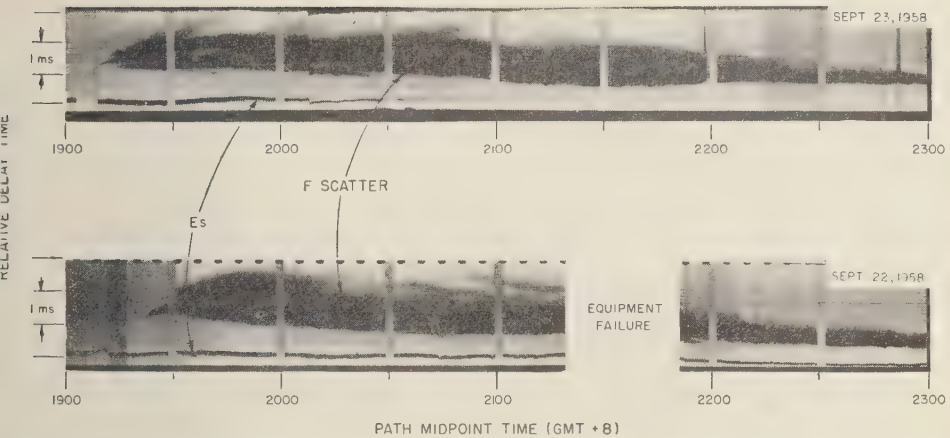

FIG. 2.—Range-time records for the Poro to Onna circuit (1347 km), 49.84 Mc/s illustrating the pulse delay of the evening signal relative to sporadic E; pulse length, 50μsec; prf, 100/sec; receiver bandwidth, 120 kc

at Baguio and high F2 critical frequencies at Okinawa (comparatively little Spread-F is seen at Okinawa). Some of the world's highest values of F2 critical frequencies are observed at the Okinawa ionosphere station during the evening hours. The F2 MUF for the Poro-to-Okinawa path is frequently as high as 35 Mc/s, and on at least one occasion it may have reached 40 Mc/s. It could be argued that the 35 to 40 Mc/s data represent some peculiarity associated with the F2 critical frequency. This hypothesis becomes untenable when the occurrences of the same phenomena at 50 Mc/s are taken into consideration.

There is some evidence of a small negative correlation with magnetic activity. The magnetic dip in the ionosphere at the midpoints of the Philippines-to-Okinawa paths is about 28°. It is interesting that a companion 50 Mc/s circuit from Panama to Guayaquil, Ecuador, operated by National Bureau of Standards during the later part of the IGY has shown few occurrences of the anomaly. This path has roughly the same magnetic configuration as do the Philippines-to-Okinawa paths. A few cases of what appears to be the same anomaly have been observed during winter nights at 50 Mc/s on a path between Panama and the U. S. Naval Base at Guantanamo Bay, Cuba. The magnetic inclination at the midpoint of this last path is about 44°.

The indication, then, is that the anomalous signal is propagated via the F region and is associated with low-latitude Spread-F, as seen on ionosphere sounders. The relatively well-defined lower edge of the anomalous return can either be interpreted as the limiting geometrical distance to the lowest stratum of ionized blobs in the F region or, more probably, as the closest approach of the locus of the 'specular condition' for optimum scattering from field-aligned blobs of ionization in the F region.

Acknowledgments—The authors would like to acknowledge the cooperation and assistance of the Voice of America, the U. S. National Committee of the IGY, and the U. S. Army IGY Support Group, and the U. S. Air Force AACS.

REFERENCES

BAILEY, D. K., R. BATEMAN, L. V. BERKNER, H. G. BOOKER, G. F. MONTGOMERY, E. M. PURCELL, W. W. SALISBURY, AND J. B. WIESNER, A new kind of radio propagation at very high frequencies observable over long distances, *Phys. Rev.*, **86**, 141–145, 1952.

BAILEY, D. K., R. BATEMAN, AND R. C. KIRBY, Radio transmission at VHF by scattering and other processes in the lower ionosphere, *Proc. Inst. Radio Engrs.*, **43**, 1181–1230, 1955.

(Manuscript received January 31, 1959.)

Geotectonics of the Arctic Ocean and the Great Arctic Magnetic Anomaly

E. R. HOPE

Defence Research Board
Ottawa, Canada

Abstract—A tentative description of the structure of the Arctic Ocean floor is presented, in terms of recent data from Soviet sources and of certain representative Soviet theories of Arctic tectonics. Two theories of the Great Arctic Magnetic Anomaly are compared: the anomaly may be related either to an interplatform geosynclinal corridor extending across the Arctic Ocean floor, or to ancient centers of crustal consolidation in the Canadian and Central Siberian Platforms.

Introduction—The Great Arctic Magnetic Anomaly (Fig. 1) has no appearance of being a transient magnetic configuration [*Hope*, 1957]. All the indications are that it is permanent, and therefore presumably has a geological cause; there is no evidence to the contrary. The anomaly cannot be due to a momentary configuration of magnetohydrodynamic disturbances at the surface of the terrestrial core, for these disturbances have lifetimes of the order of a century; the patterns they produce in the geomagnetic field must alter very considerably in a few years' time. Yet the pattern of the anomaly has remained practically unaltered, if allowance is made for a superimposed secular variation, since Fisk's charts of 1925; and the same pattern shows up plainly, in spite of the paucity of data, in Neumayer's magnetic meridians of 1885, three quarters of a century ago. Furthermore the migration of the northern magnetic pole, both within the recorded period and as traced by van Bemmelen back to 1600 A.D., appears to have followed closely the center line of the anomaly; this suggests that the anomaly has existed for three and a half centuries without any great change in position or pattern. The Quaternary pole-positions charted by *Nagata* and others [1957] and by *Roche* [1958], from paleomagnetic studies of lavas in Japan and France, all lie in a band across the Arctic Ocean, a band which coincides remarkably with the disturbed area, Mesozoic plus Hercynian, of Figures 2 and 3. *Brynjólfsson's* [1957] post-glacial pole-positions, found from the paleomagnetism of the Iceland basalts, lie in the same corridor, provided they are corrected for the lateral compressing effect of the 'anomaly trough' [*Hope*, 1957, p. 22].

In a previous paper [*Hope*, 1957] we tentatively associated the magnetic anomaly with the corridor of Mesozoic folding which, according to Soviet authors, crosses the Arctic Ocean from the New Siberian Islands to Ellesmere Island; we suggested that the magnetic effect might be due to some formation underlying this corridor. An alternative theory has been advanced in the USSR: namely, that the magnetic anomaly is due to a concentration of the geomagnetic field in the rocks at two primeval centers of consolidation of the earth's crust, located in the Greenland-Canadian Shield and the Central Siberian Platform. Present data are not sufficient to decide between these points of view. However, a certain elaboration of the first theory is now possible, on the basis of a highly interesting tectonic picture of the Arctic Ocean which is emerging from recent Soviet exploration and theorizing. We are making the present paper the occasion for a fairly extensive summary of this work.

It is understood, of course, that we are merely reporting. The reader must decide for himself what is fact and what is speculation. Those who find the Soviet approach disturbingly unfamiliar should read *Belousov* [1955], whose influential theories provide a good deal of the background for the picture.

Hyperborean Basin and Hyperborean Platform—The schematic chart in Figure 2, recaptioned in English and with certain additions as noted, is reproduced from a paper [1958] by the Soviet oceanographer *Hakkel'* (*Hackel*), in

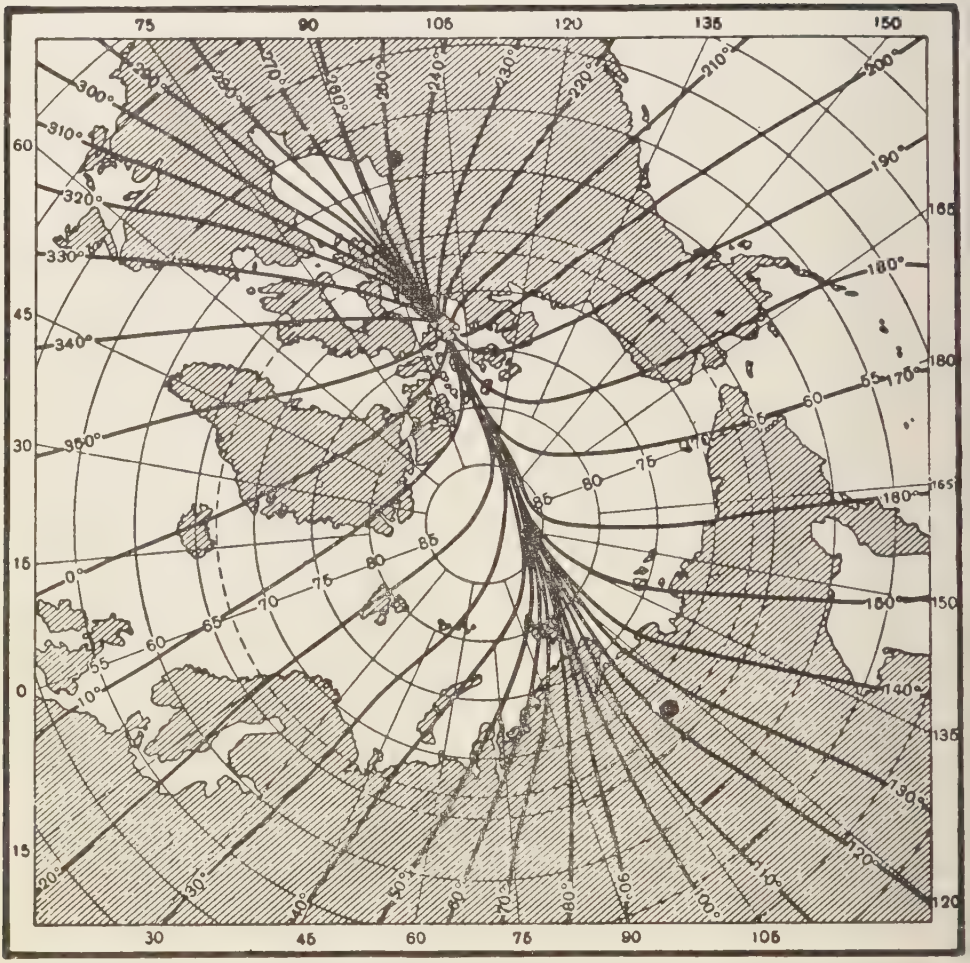

FIG. 1—Magnetic meridians, epoch 1950, after Ostrekin. The two solid circlets mark the poles of maximum intensity of the vertical component of the geomagnetic field, epoch 1945, after Vestine. (Definition: the λth magnetic meridian is a line, continuously following the direction of the magnetic needle, from the point of longitude λ on the equator to the magnetic dip-pole)

which he discusses some recently reported signs of volcanic activity in the Lomonosov Range and in the disturbed corridor. It is, however, the base chart, on which the volcanic data are plotted, that is of principal interest to us. This chart is dated 1955; it is the most recent in a series of diagrams recently published by *Hakkel'* [1957a, pp. 86, 90, 107, 108], showing the progress of Soviet bathymetric work in the Arctic Ocean since the discovery of the Lomonosov Range in 1948. The chart is schematic, and is so described by Hakkel' in his caption. Details in it, for instance the wavy contours in certain areas, must therefore not be considered without due regard to the fact that they may have been intended only as a diagrammatic illustration of some of Hakkel's findings and deductions. But even so they are none the less worthy of attention, since Hakkel' has made a strong case for his deductions, as we shall see.

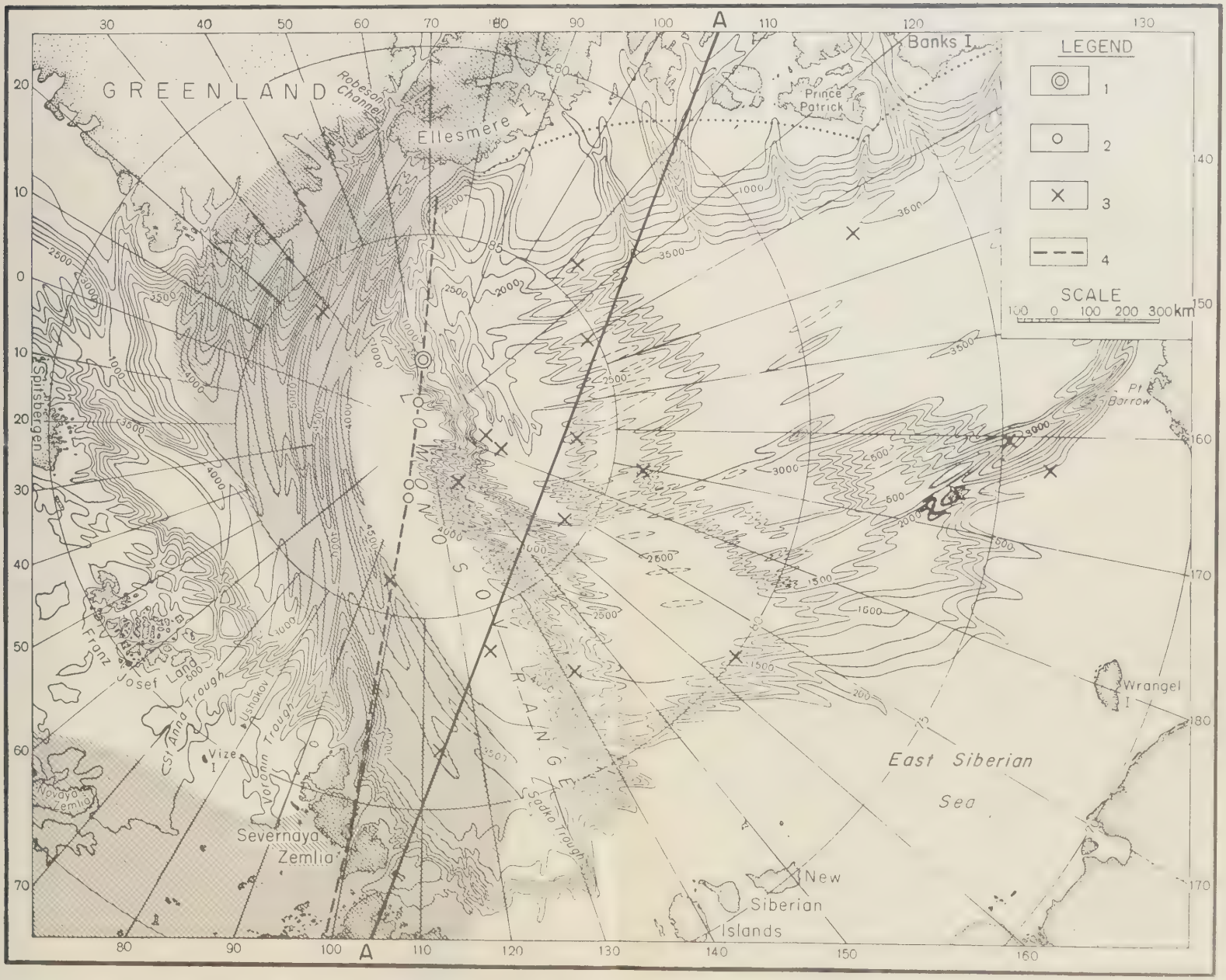

Fig. 2—Chart from *Hakkel'* [1958], with English legend inserted and additions as follows:

—line A-A, marking the axis of the Arctic Magnetic Anomaly (Fig. 1);
—shaded band to mark the corridor of Upper Paleozoic (Hercynian) folding, according to Figure 3;
—dotted line following the edge of the coastal plain. Canadian Arctic Archipelago

Hakkel's original caption read as follows: Schematic chart of volcanism in Arctic Ocean basin. 1. Active submarine volcano in the Lomonosov Range. 2. Points where volcanic glass was found. 3. Points where basaltic hornblende was found. 4. Suggested fracture-line.

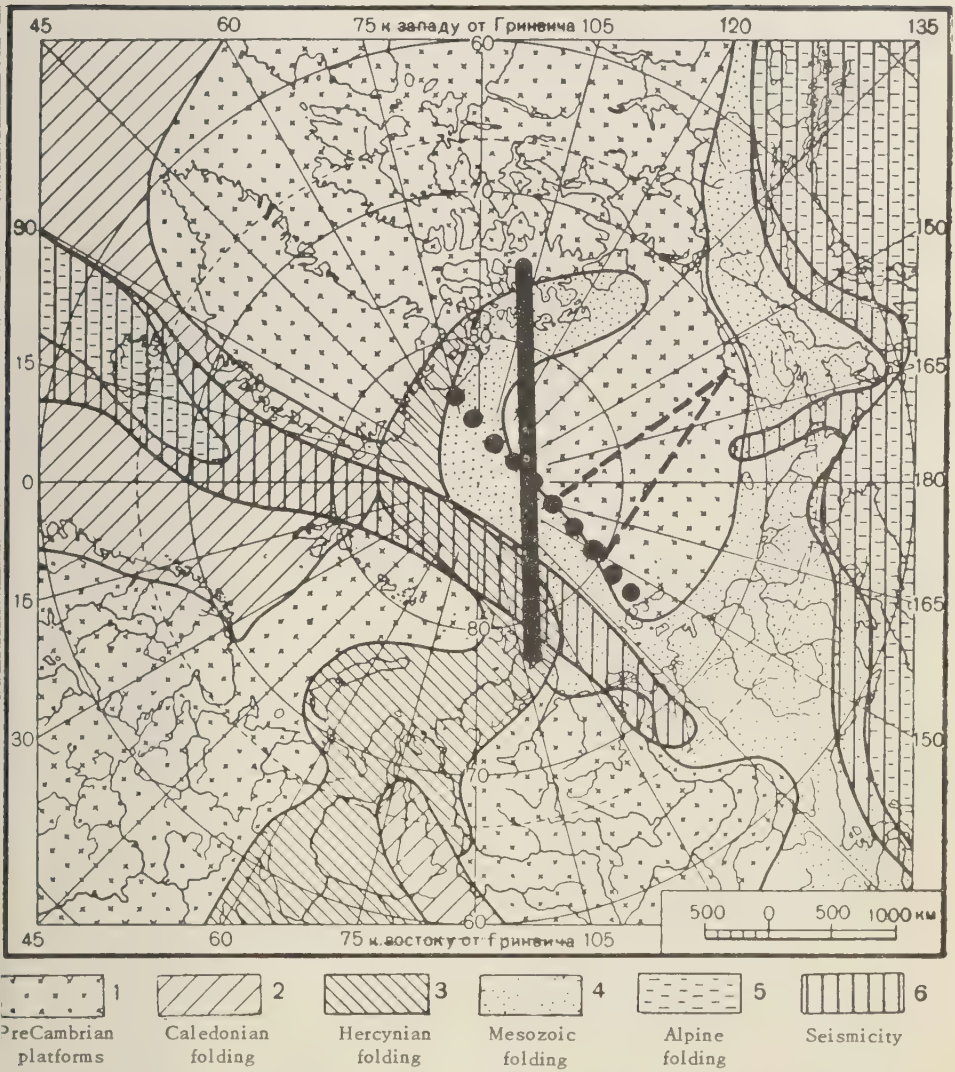

FIG. 3—Diagram of Central Arctic geological structure, showing regions of folding (2,3,4,5) and zone of recent seismic activity. From *Saks, Belov,* and *Lapina* [1955], with additions as follows:

axis of Arctic Magnetic Anomaly

Lomonosov suboceanic mountain range

staircase, from Figure 2

In fact, when this same chart was published in his book of 1957, Hakkel' entitled it simply "Bathymetric Chart of the Arctic Basin, 1955." The 1958 caption, describing it as 'schematic,' is therefore just a cautious afterthought. It appears that in the Lomonosov Range the contours may be taken as basically accurate [*Hakkel'*, 1957a, p. 106]. In other regions this is ob-

viously not so,* and we must always scrutinize the indications in the light of other evidence.

The most prominent feature of the trans-Arctic corridor of Mesozoic folding is the abrupt ridge of the Lomonosov Range, the peaks of which rise to within less than a thousand meters of the surface. The deep part of the Arctic Ocean is thus divided into two basins. That which lies to the left of the Lomonosov Range in Figure 2 may well be called the European Arctic Basin, and we shall refer to the other, which extends toward Alaska, as the Hyperborean Basin (after the Hyperborean Platform which according to Soviet geologists forms its floor).

Now concerning these basins and the Lomonosov Range which divides them, the principal points made by *Hakkel'* [1957a] are the following.

a) The Mesozoic folding of the Lomonosov Range is superimposed, at an angle of about 60°, on an older system of ridges, the strike of which is toward Alaska, parallel to the continental slopes in the Hyperborean Basin. Burkhanov calls them "ancient mountain arcs, which have been traced in an almost north-south direction across the whole of the Pacific part of the Arctic Basin, right into the Beaufort Sea, it would seem, and up to the Alaska continental slope" [*Burkhanov*, 1957a, p. 2 of translation]. The trend of the system is exhibited (Fig. 2) in the elevations and depressions on the floor of the basin, in the wavy contours of the Lomonosov Range and other elevations, and in the indentations of the coastal shelf north of Wrangel Island. We shall refer to it as the *Hyperborean ridge-system.*

b) On the floor of the European Arctic Basin there is a system of ridges and valleys almost at right-angles to the Hyperborean ridges. Just as in the Hyperborean Basin, the structure is roughly parallel to the continental slope (Fig. 2). At the same time it is more or less parallel to the Lomonosov Range. Since it appears to be the suboceanic continuation of the Ural-Tien-shan folding (Fig. 3), which is of Hercynian age, let us call this submarine structure the *Hercynian folding* (Table 1).

TABLE 1

Orogenic Cycles*	Periods or Systems	Eras
Alpine	Quaternary Tertiary	Cenozoic
Mesozoic	Cretaceous Jurassic Triassic	Mesozoic
Hercynian	Permian Carboniferous Devonian	Upper Paleozoic
Caledonian	Silurian Ordovician Cambrian	Lower Paleozoic

**Four* orogenic cycles, named as above, are commonly distinguished by Soviet geologists.

There are, then, three submarine orographic systems distinguished: the Hyperborean ridges, the Hercynian (Upper Paleozoic) folding, and the Mesozoic folding of the Lomonosov Range.

The story behind this is interesting. Hakkel' was one of the airborne exploration group which discovered the Lomonosov Range, on April 27, 1948; on that day a sounding of 1290 m was made at 86°26′N 154°53′E [*Hakkel'* 1957a, p. 84]. By 1954, fairly complete contours of the

* For instance, it is improbable that the Soviet network of soundings was sufficiently close-spaced to justify the detail (Fig. 2) of the gulleys in the Canadian Arctic coastal shelf. *Burkhanov* [1957a] says that the continental slope, along the Canadian Arctic Archipelago and in the Beaufort Sea as far as Alaska, "has been very imperfectly explored. Hence the relief of this part of the Arctic Ocean, particularly the continental slope, is for the time being sketched only in the form of hypothetical isobaths. It is a matter of great scientific interest to check the reliability of this hypothetical picture of the topography in this least studied of all regions."

Hakkel' [1957a, p. 106] gives the total number of depths measured in the Arctic Ocean as over 3000, "distributed, however, far from uniformly." These soundings were made from the Soviet drifting stations and from temporary drifting camps set up by aircraft landing at over 400 points on the ice [*ibid.*, p. 30]; a minor part of the total was contributed by ships and hydroaircraft. A chart of the aircraft landings, up to 1956, is given by *Burkhanov* [1957a]. The temporary drifting camps thus established operated for periods ranging from a few hours to a month [*Hakkel'*, 1957a, p. 85]; a fifteen-day series of hydrographic and oceanographic observations seems to have been regarded as standard.

whole mountain range had been obtained. Hakkel' noticed "the highly important fact that the trend of the Lomonosov Range, or its crest, exhibited certain nodal points, points of inflection, where its direction abruptly altered. From just these points, moreover, there issued some of the spurs of the Lomonosov Range which had by that time been discovered, spurs lying at an angle to the principal mountain chain" [*ibid.*, p. 106]. Hakkel' concluded that the spurs could be predicted from the inflections. On the bathymetric chart of 1954 he tentatively sketched in one of the expected spurs, jutting out at an angle of about 60° (in the direction toward Wrangel Island) from a prominent inflection-point at 86°N 150°E, and extending to 85°N 160°E or beyond [*Hakkel'*, 1957a, chart on p. 107]. This prediction, with several others, was reported by Hakkel' to the Geographic Society of the USSR at its session of February 1955. And indeed in the summer of that year drifting station North Pole 5, during its passage across the Lomonosov Range, discovered the predicted spur. It may be seen in Figure 2.

Several other spurs were found where Hakkel' indicated them to be, all exhibiting the direction of the ancient ridge-system in the Hyperborean Basin.

Moreover, at the nodal points where the Hyperborean ridge-system intersects the Lomonosov folding, the highest mountain elevations are formed. On this basis Hakkel' proceeded to forecast the locations of high points in the Lomonosov Range, and he went looking for them in company with pilots V. V. Mal'kov and A. K. Zhgun. Choosing landing-points on the sea ice in accordance with his predictions, he found a place where the ocean depth was only 965 m; thus 3000 m above the floor level of the adjacent basins. To date, the shallowest recorded depth over the Lomonosov Ridge is 954 m; this was discovered incidentally (that is, without looking for it) by G. V. Sorokin and G. A. Ponomarenko, but it too turned out to agree closely with one of Hakkel's nodal points [*ibid.*, p. 109].

Under these circumstances, it is understandable that Hakkel's structural theory has been one of prestige in the Soviet Union.

It seems that Hakkel' at first described the Hyperborean ridges as folds. Later he concluded that the major ridges were due to a structure of blocks and faults. On the Siberian side of the basin there appears to be a series of fault-terraces or benches, like a staircase with broad steps, by which the floor of the Arctic Ocean, east of the meridian of the New Siberian Islands, descends northward to greater and greater depths [*ibid.*, pp. 108–109]. These terraces can be seen cutting into the continental slope north of the East Siberian Sea (Fig. 2). The picture suggests that the floor of the Hyperborean Basin has been formed by the subsidence of an enormous oblong block, along roughly parallel lines of fracture: the fractures form the continental slope on the North American side and the 'staircase' on the Siberian side.

Of course, the whole of the Hyperborean ridge-system, which creates the inflections and elevated nodes in the Lomonosov Range, is not necessarily due to faulting. Folding on the sunken block, parallel to the continental shelves bordering the oblong, might be due to deformation of the surface layers during subsidence [compare *Belousov*, 1958; *Gzovski*, 1958], or it might be the pattern of the folded basement of the platform, protected from erosion by its submergence and showing through the sedimentary superstructure.

The subsidence theory of the Arctic Ocean floor was considered by Soviet geologists long before the present data had accumulated. [Compare also *Eardley*, 1951, pp. 538–540.] N. S. Shatski had suggested the existence of a great submerged platform, the Hyperborean Shield,* in order to account for the manner in

* Shatski named it the Hyperborean *Shield*, and this name was generally used throughout the 1930's. [See *Arkhangel'ski*, 1941, p. 123, for a historical account.] The term *shield*, however, created some uneasiness, since it implies exposure of the basement rock, and is therefore too explicit. The present tendency seems to be to employ "Hyperborean Massif" or "Hyperborean Platform"; V. A. Tokarev has even suggested "East Siberian Platform" [*Panov*, 1955b; *Saks* and others, 1955]. The term *massif* is intended to imply only a resistant block (though in the Russian literature the word is used in other senses, most of them having in common the idea of an *uplifted* mass). The term *platform* means a two-storied structure, a 'folded basement' of ancient rock which has moved little since its consolidation, plus a superstructure of relatively undislocated strata, generally horizontal. The age of the platform is the age of its consolidation. A *shield* is thus an emergence of the basement of a (Precambrian) platform.

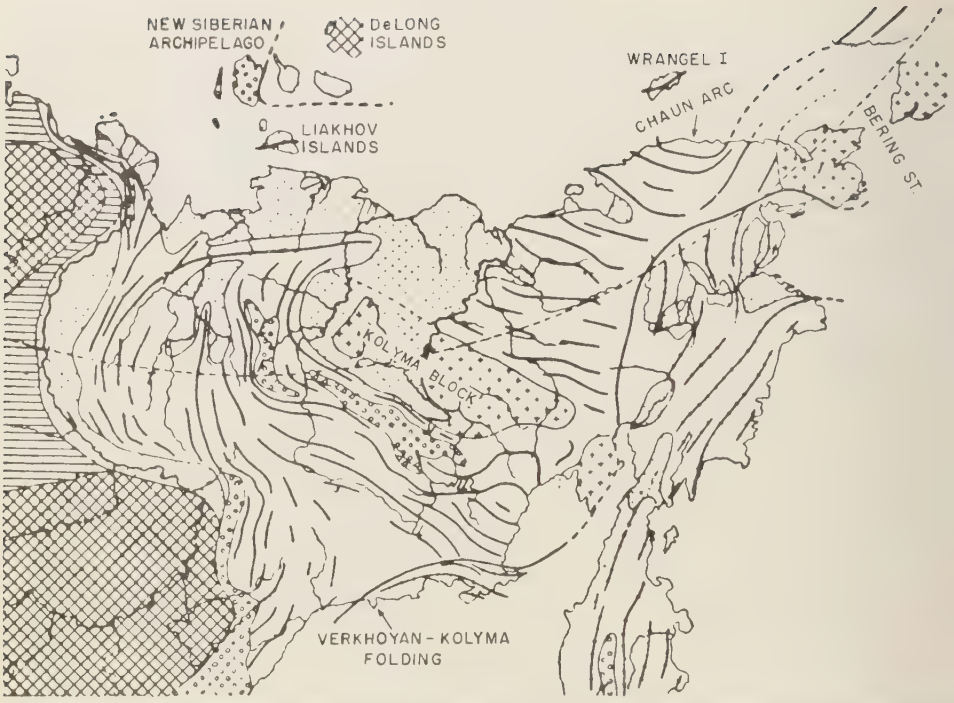

FIG. 4—Folding in Eastern Siberia. Tectonic chart from *Kropotkin* and *Kheraskov* [1939], with added legend. The broken line through the New Siberian Archipeligo represents the corner of the Hyperborean Platform. Compare also *Arkhangel'ski* [1941, Fig 90 (after Obruchev)]

which the Mesozoic folding encircles the entire Hyperborean Basin (Fig. 3, Fig. 4) as though following the rim of a resistant block. Saks (Fig. 3) shows this submarine platform as an extension of the Canadian Precambrian Platform; other Soviet authors show it as an independent structure. Subsidence of the ocean floor is indicated by the escarpments discovered on the continental slopes, escarpments as high as 400 to 600 m [*Panov*, 1955a, §4]. The continental shelf itself, on both sides of the ocean, appears to be a fairly resistant platform-structure, riven by fractures into blocks which are in irregular and independent vertical movement; this is indicated by comparison of strand-line heights on the Arctic islands [*ibid.*, §3].

It will be seen in Figure 3 that Saks' platform extends over the Hyperborean Basin and also over much of the breadth of the Siberian shelf east of the New Siberian Islands. The platform therefore includes the oblong subsided part and a triangular sub-shelf part, separated by the 'staircase' faulting. One corner of the platform boundary intersects the New Siberian Archipelago (compare Fig. 4; also *Eardley* [1951], p. 531 and Fig. 315). The direction of the edge of the platform, in the East Siberian Sea, is given by the strike of the Mesozoic folding on the mainland, and also on Wrangel Island and the Liakhov Islands, as seen in Figure 4. The platform underlies the DeLong Islands (and this part of it has indeed been called the DeLong Islands Platform), as is shown by the horizontal bedding of the Cambrian deposits there, and particularly on Bennett Island [*Kropotkin* and *Kheraskov*, 1939, p. 602 *et seq.*; *Arkhangel'ski*, 1939, p. 303.] At the same time these deposits date the platform as Precambrian.

(It should be noted, however, that *Lobanov* [1957, p. 501] and certain others reject almost every detail in this long-familiar picture, treating the whole archipelago as part of the Verkhoyan folded region and denying that the

eLong Islands, in particular, are included in ıe Hyperborean Platform.)

Between meridians 170° and 175°W, Saks aces the platform boundary across the tip of seismic tongue (Fig. 3) which thrusts northard from Bering Strait; here a "submerged eninsula, dissected by canyons, extends almost 00 km farther north than was previously indiated" [*Burkhanov,* 1957a]. East of this "peninula" is the abrupt descent from the shelf to the ean depression (Fig. 2); that is, from the iangular shelf-portion of the platform to the blong block of the Hyperborean Basin floor. long the north coast of Alaska to the Mackenie River, the platform edge (the end of the epressed oblong block) is shown by Saks as ctually underlying the Alaskan coastal plain, hich is composed of many thousands of feet of early horizontal Triassic, Jurassic, and particlarly Cretaceous sedimentary strata [*Eardley,* 951, pp. 514, 520]. That is, Saks' platform orders the edge of the Central Alaskan geantiline, of Triassic-Jurassic age, shown by Eardley ı his Figure 311. Or, it would be better to say, bordered the antecedent geosyncline of the aleozoic, at which time the platform, or an arly sedimentary superstructure upon it, must ave been high enough to serve as the foreland, he erosion-source for the geosyncline.

East of the Mackenzie, Saks traces the platorm boundary inland, following the edge of the ordilleran geosyncline; it thus forms a neck oining it to the Canadian Shield. Still farther ast, beyond the 'neck,' the platform extends long the continental slope of the Canadian rctic Archipelago, where a belt of folding which we shall call the Franklin folded belt) eparates it from the Canadian Shield [*Dunbar* nd *Greenaway,* 1956, diagram on p. 6]. The ranklin belt may connect with the Cordilleran eosyncline [*Panov,* 1955b]; if so, the neck oining the Hyperborean Platform to the Canaian Shield cannot exist.* *Eardley* [1957, Fig. 7] classes the folding as Palezoic and Mesozoic; Saks shows it as the extension of the trans-Arctic corridor of Mesozoic folding, overlying the earlier corridor of Paleozoic (Hercynian) folding which disappears beneath it on Ellesmere Island. *Panov* [1955b, Fig. 1] shows an even more complicated Franklin belt, with the Paleozoic folding superimposed upon a Caledonian folding, which is an extension of the Caledonian folding of the East Greenland coast. This is, of course, a reflection of earlier concepts, formed before the discovery of the Lomonosov Range [compare *Arkhangel'ski,* 1941, chart VI in pocket at end of book]. Nevertheless it is quite probable that ever since the formation of the Hyperborean Platform, the Franklin belt, separating two great consolidations of the earth's crust, has been repeatedly activated; that Hercynian folding followed Caledonian, and Mesozoic folding remodeled the Hercynian.

On its polar side, Saks' platform is contiguous with the Lomonosov Range; indeed, since the Hyperborean ridge-system and the Lomonosov folding intersect each other, the original platform must have extended through and beyond the present line of the Lomonosov Range. It may be that the very deep ocean depression on the other side of the range is formed by the toe of the original Hyperborean Platform, or more precisely, by the toe of the sunken oblong part of this platform. How far the Hyperborean ridges extend past the Lomonosov Range is of course concealed by the sediments in this catch-basin. The deep depression is bounded by the Hercynian folding, the shaded corridor in Figure 2; the 4000-m isobath, if produced through the Lomonosov Range, coincides with the boundary of the staircase in the Hyperborean Platform. In other words, the Hercynian folding, before there was a Lomonosov Range, followed

* The following facts may have significance: (a) On November 16, 1920, a powerful earthquake occurred, with its epicenter at 72°N 127°W according to closely agreeing determinations at Ottawa and Oxford [*Hodgson,* 1930]. This position is on the continental slope, which may be all the explanation required. But at the same time, it is also at the very tip of the Franklin folded belt as shown by Saks; that is, at the edge of the hypothetical 'neck' joining the platforms. One or two other earthquakes, located not on the continental slope but inland, east of the Mackenzie, have been reported [*Gutenberg,* 1956; *Raiko* and *Lindén,* 1935, Fig. 1]; they lie in the 'neck,' or at the contact of the two platform-blocks. (b) On November 20, 1933, there was a sizeable earthquake, recorded by seismic stations all over the globe, with epicenter at 73°N 69-72°W, in Baffin Bay, an area regarded as seismically inactive (Raiko and Lindén). This too is at a junction or contact of platforms (Canadian and Greenland Shields), north of the deep indentation of Baffin Strait. Gutenberg's chart shows it to be part of a concentrated small cluster of epicenters.

the rim of the platform (as zones of folding are supposed to do). The Lomonosov orogeny later cut across the toe of the platform.

The Alpha Range—In Figure 2, to the right of the Lomonosov Range and roughly parallel to it, there is an elevation extending completely across the deep ocean floor. It now appears that the elevation is the base of another mountain range, of undetermined extent. This new mountain range was reported by the United States drifting station Alpha in August 1957 [*IGY Bulletin No. 6,* Dec. 1957; report in *Science,* 126, p. 499, Sept. 13, 1957]. Let us therefore call it the Alpha Range.* So little is known about it that any discussion is hazardous, but we shall venture one suggestion.

Since the elevation lies entirely within the Hyperborean Platform as outlined by Saks, it may not be a fold-structure, but rather a block-uplift or horst, the result of vertical movements between fractures. There is no evident subaerial continuation of an Alpha folding on either the Canadian or the Siberian sides of the ocean, nor is it to be detected in the contours of the continental slopes. This is in marked contrast with the trans-Arctic corridors of Mesozoic folding (Lomonosov Range) and Paleozoic folding, both of which are continuations of continental structures and have greatly disturbed the continental slope contours (Fig. 2).

It seems possible that the folds of the Chaun Arc (Fig. 4), the Asiatic continuation of the Alaskan Mesozoic folding, may turn north into the Alpha Range, but the indication is feeble and is contradicted by the direction of folding in Wrangel Island. It is more probable that the Chaun folding passes along the rim of the platform to the Liakhov Islands; this is how matters are shown in S. V. Obruchev's diagram reproduced by *Arkhangel'ski* [1941, Fig. 90]. The angles and azimuths involved may be better appreciated in the polar chart of Figure 2, if the data of Figure 4 are transferred to it.

Indeed the theory of the existence of the Hyperborean Platform, which in turn is the very foundation-stone of Soviet tectonic and structural theory for northeastern Siberia, depends upon the thesis that the Mesozoic folding, from the Verkhoyan Arc all the way to Alaska, runs parallel to the edge of the postulated shield. North of the Kolyma block the folding happens to be hidden, but still farther north it reappears in the Liakhov Islands (Fig. 4); its trend in the Chuckchee region is evident; so is the eastward turn of the northeast part of the Verkhoyan folding, to pass around the top of the Kolyma block. [*Arkhangel'ski,* 1941, pp. 232–235; *Kropotkin* and *Kheraskov,* 1939, p. 607.]

The existence of an Alpha folding is therefore doubtful. In contrast, no such doubt exists in connection with the Lomonosov Range, which lies directly in line with the western part of the Verkhoyan folding where it descends into the sea.*

The descent of the Verkhoyan folding into

* The pedestal of the Alpha Range is clearly indicated, not only by Hakkel' in Figure 2, but also in other Soviet bathymetric charts of 1954 and 1955, in Figure 5 of *Saks* and others [1955], and elsewhere. But the mountain ridge itself is not indicated; it seems that in this area the Soviet network of Arctic Ocean depth soundings [see chart in *Burkhanov,* 1957a] was not close-spaced enough to detect the crest. The greatest concentration of soundings was over the Lomonosov Ridge, to the exploration of which a special effort has been devoted since its discovery in 1948. As for the Alpha Range, *Burkhanov* [1957b, translation p. 11] mentions only an "elevation of the sea bottom, of great length." But Hakkel', in his book published in October 1957—that is, after the announcement from Station Alpha—refers to it as "a second, still nameless sub-oceanic mountain range, also extending across the whole Arctic basin, but less high as compared with the Lomonosov Ridge, more deeply submerged below sea level" [p. 87]. Incidentally, Hakkel' informs us [p. 83] that the existence of an elevation, at latitude 81°30'N longitude 180°, and NNW of this point, was predicted in 1946 by I. V. Maksimov, from a study of the ocean-current measurements made by I. I. Cherevichny's N-169 expedition to the Pole of Relative Inaccessibility in 1941. Maksimov concluded that there might be depths of as little as 1000 m in this area.

* As in Figure 4. In Obruchev's diagram of 1938 [*Arkhangel'ski,* 1941, Fig. 90], to which we have already referred, the submerged continuation of the western Verkhoyan folding, plus the westward extension of the Chaun folding past the corner of the Hyperborean Platform, is shown as trending to the northwest along the coast toward the Taimyr Peninsula, not northward into the (then undiscovered) Lomonosov Range. This is evidently incorrect. The Chaun folding presumably does not round the corner of the platform, but turns entirely southward from the Liakhov Islands into the eastern part of the Verkhoyan Arc. [Compare *Lobanov,* 1957, pp. 501, 502.]

the sea was successfully demonstrated by an aerial magnetic survey in 1946–1948. "The actual position of the Lomonosov Range, at that time undiscovered by sounding operations, nevertheless showed up in the trend of anomalies in the vertical component of the magnetic field; these anomalies followed the strike of the Mesozoic folds" [*Saks* and others, 1955]. No mention is made of tracing any continental folding in the direction of the Alpha Range, although Maksimov had already (1946) predicted an elevation in this part of the ocean floor.

The Alpha horst (as we suppose it to be) may have been thrust upward or wedged upward after the general subsidence of the ocean floor. Or again, it may have lagged behind the subsidence, being upheld by some deep formation, by a massive rib in the web of the crust (or even by some rigidity in the Mohorovicic surface, which according to J. Tuzo Wilson is the original "lunar" surface of the planet). The horst may perhaps be taken as extending from the Canadian shelf to a point about halfway across the basin, at which point it has partially shored up and prevented the complete 'staircase' subsidence of the Siberian coastal shelf; at least this is suggested by the sudden and indeed quite remarkable change in the direction of the contours at the 180th meridian.

We have noted that the Hyperborean Platform, in Paleozoic times, must have been sufficiently elevated to serve as foreland for the Alaska geosyncline. The same argument may hold for the entire Mesozoic circuit around the platform. *Panov* [1955b] raises this point in connection with the Lomonosov Range: if of geosynclinal origin it must have had an erosion-source, probably subaerial, on at least one side. Panov therefore supposes that the major subsidence of the floors of the ocean basins began in the Triassic, at the same time as the rise of the Lomonosov Range; there was a second stage in the Tertiary, accompanied by widespread effusions of basalt as seen in the Arctic Islands [*Avsiuk*, 1958; *Dibner*, 1957]. He thus envisages a process similar to the post-Caledonian subsidence of the floor of the Norwegian Sea according to De Geer. The subsidence of the European Arctic Basin, in particular, is seen as a continuation of the process which formed the basins of the Norwegian Sea, and as part of a successive northward extension of the Atlantic Ocean.

How far the reasoning can be extended to the Hyperborean Basin is not clear, since the floor-platforms of the two ocean basins are of very different age and type, as Panov himself emphasizes. But this provisional dating of the subsidences provides at least a point for discussion in dating the Alpha Range.

Hakkel' specifically states that the Alpha Range is intersected by the Hyperborean ridge-system, just as is the Lomonosov Range. He indicates the effects of the intersection by the wavy contours in Figure 2, though this detail is obviously schematic.

The Lomonosov Range—The discovery of the Lomonosov Range was the fulfillment of a long series of prophecies. Early in this century *Harris* [1904, 1911] postulated, from a study of the Arctic Ocean tides, the existence of a central arctic land-mass. One coast of this supposed land, as shown in his 1911 chart, is now seen to be an astonishingly accurate prediction of the position of the Lomonosov Range. [Compare *Nansen*, 1928; *Marmer*, 1928; *Fjeldstad*, 1936.] In 1865 A. Petermann had concluded, from the Arctic Ocean currents, that the east coast of Greenland must extend northward across the pole to Wrangel Island, which was also, at that time, thought to be the tip of a great land-mass; Admiral Sherard Osborn, in a paper read to the Royal Geographic Society in 1873, postulated an archipelago or land extending from near Prince Patrick Island to Wrangel Island [*Harris*, 1911, p. 84; 1904, p. 261]. In the Soviet Union, as *Hakkel'* [1957a, pp. 82, 83, 103] informs us, G. P. Gorbunov examined the collection of Arctic Ocean floor fauna made during the drift of the SS *Sedov*, and showed that the Atlantic species in the Arctic Basin did not extend farther than the New Siberian Islands. The explanation offered, however, was that these islands during the last glaciation were practically united with the mainland, thus dividing the continental shelf and isolating the shallow-water fauna. (The deep Arctic waters were long believed to be sterile [*Nansen*, 1928].) In 1947, Ye. F. Gur'yanova ascribed the faunal separation to a *suboceanic ridge* extending north of the islands. Other long-known facts, for instance, the existence of two separate Arctic walrus packs, could be explained if a recent emergence of the ridge were assumed (and indeed, glacial deposits dredged from the Lomonosov Range

do indicate that the crest was lately above water [*Hakkel'*, 1957a, p. 87; *Burkhanov*, 1957a, p. 3 of translation]). V. A. Tokarev, who participated in the aerial magnetic survey of 1946–1948, concluded from the magnetic data that there must be shallow ocean depths north of the New Siberian Islands [*Hakkel'*, 1957a, p. 83].

The most interesting prediction is that of *Süss* [1909, ch. 16, pp. 283, 284; ch. 26, p. 730], who suggested, in view of geological similarities, that the New Siberian Islands and Ellesmere Island were connected across the Arctic by a suboceanic structure, a prolongation of the Mesozoic folding of the Verkhoyan Range. He thus set the age of the Lomonosov folding as Mesozoic, a dating which all the recent Soviet exploratory work appears to confirm. The principal Verkhoyan folding is indeed clearly Mesozoic [*Atlasov*, 1957, pp. 457, 458]. Traces of a Caledonian folding do appear, but there are only infrequent and obscure signs of Hercynian folding [*Arkhangel'ski*, 1941, p. 235], aside from some local manifestations confined to the edge of the Kolyma block [*ibid.*, Fig. 90; *Kropotkin* and *Kheraskov*, 1939, p. 606]. The Upper Carboniferous and Permian rocks are dislocated conformably with the Mesozoic; they constitute, with the Triassic, "a single formation difficult to resolve" [*Arkhangel'ski*, 1939, p. 305; see also p. 309; *Kropotkin* and *Kheraskov*, 1939, pp. 602, 604]. The most energetic folding seems to have taken place at the end of the Jurassic and again in the second half of the Cretaceous [*Suslov*, 1947, p. 218]. Since then the area has been generally quiet; the Mesozoic deposits are thin and little dislocated [*Arkhangel'ski*, 1939, p. 305]. Tectonic movements were already feeble in the Tertiary, if one may judge from the history of terraces in the adjacent Lena River valley [*Chebotareva* and *Kuprina*, 1958; *Atlasov*, 1957, p. 458; *Lazurkin*, 1957, p. 480]; throughout the Quaternary there has been little movement other than a general uplift.

This picture is in fortunate contrast to the obscure situation in Ellesmere, though Süss based his prediction on his ability to identify the corresponding Mesozoic formations there.

The Verkhoyan region is seismic; through it passes the belt of seismic activity shown in Figure 5. The Lomonosov and Alpha Ranges, on the other hand, are not seismic; they have long since been deserted by such activity. They do, according to Hakkel', give evidence of recent volcanic activity, in the form of volcanic glass and basaltic hornblende in the bottom sediments (see Figure 2 and caption). This volcanism, having no seismic background, is not of a tectonic character; it is probably no more than a reactivation of old foci by glacial and postglacial isostatic adjustments. It will be seen that the volcanic evidence (the crosses and circlets in Figure 2) was mostly found in the area of the Lomonosov and Alpha Ranges, aside from some points on the continental slopes. Only a few traces of the recent volcanic activity were found in the ocean depressions, where they may represent material carried down from the slopes by turbidity currents and slumps.

Hakkel's Fracture and the Sadko Trough—Quite aside from the Hyperborean structure that crosses it, the Lomonosov Range, which has disrupted the edge of a platform, is itself likely to have been formed by a combination of folding and large-scale faulting. This, according to *Panov* [1955b], is indicated by fault-troughs, filled with Mesozoic sediments, in the New Siberian Islands and in Ellesmere.

In Figure 2 the double circlet represents the location of a supposed submarine volcanic eruption [*Hakkel'*, 1958] recorded by the Soviet drifting station North Pole 3 on November 21–24, 1954. The single circlets mark places where volcanic glass, recent (< 5000 years B.P.) and uncrystallized, was found in ocean floor sediments. All four points, together with one of the crosses marking slightly older evidences of volcanism (> 5000 years B.P.), lie on a single straight line or great circle arc. Accordingly, Hakkel' believes that the recent volcanic activity here exhibited must mark a deep fault or crustal dislocation extending from within Eurasia across the entire Arctic Ocean (broken line of the chart). The line passes through the straight cleft of Shokal'ski Strait (in Severnaya Zemlia), then to the lower Taimyr River, and, "as Soviet geologists now believe, these latter features, together with Lake Taimyr, lie on a deep fracture of the earth's crust, with the River Kotui, it would seem, as its southward extension" [*ibid.*].

The Shokal'ski Strait is said to be a quite recent formation. "*At the end of the glacial epoch*, the earth's crust in Severnaya Zemlia and the Taimyr Peninsula was broken up by a series of

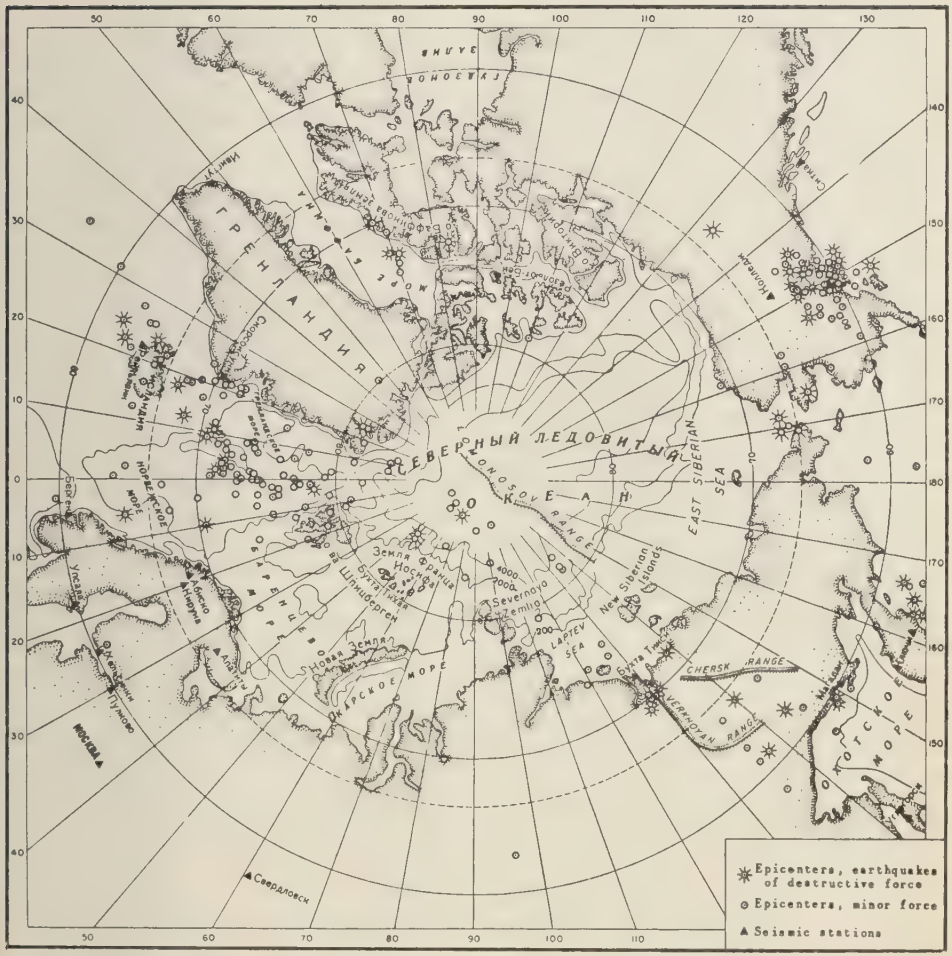

FIG. 5—Arctic seismic zone, according to N. A. Lindén. From *Savarenski* [1956]. For antecedent information, see *Hodgson* [1930], *Raiko* and *Lindén* [1935], *Mushketov* [1935]; cf. also *Gutenberg* [1956].

tectonic faults, whereby the archipelago was severed from the continent, and various parts displaced in relation to each other; some parts, sinking below sea level, were flooded and, for instance, the Vil'kiçki and Shokal'ski Straits were formed" [*Suslov*, 1947, p. 182; see also *Mushketov*, 1935, p. 10]. This, however, does not necessarily mean that the Shokal'ski-Taimyr fracture is recent, though the Shokal'ski graben may be; in fact, the absence of seismicity suggests that the fracture is an ancient, long-quiet feature.

North of the Shokal'ski Strait, along the meridian of 100°E, the course of the fracture is marked by the abrupt rectilinear eastern wall of the submarine promontory extending from Severnaya Zemlia.

If Hakkel' is right and the fracture does extend across the ocean, then we see that the circlets and crosses in Figure 2 (with the exception of one cross on the Greenland continental slope) all lie on or to the right of the fracture. That is, the fault-line appears to be a boundary for the volcanism, the reactivated foci in the disturbed

area of the Lomonosov and Alpha Ranges. One might suspect that this is due to lack of data from the oceanic depressions, but Hakkel' seems to have no doubt that the absence of volcanic indications in the deeper ocean is real.

Toward Ellesmere the great fracture, as Hakkel' shows it, crosses over the Lomonosov Range, "forming a fault in the shape of the western slope of the Lomonosov Range in this sector" [*Hakkel'*, 1958]. Or in other words, the Lomonosov folding overleaps the fracture and utilizes it, for a distance of 300 miles, as its western boundary. This does not suggest that the fracture is recent; rather it suggests a pre-existing feature which guided the formation of this part of the Lomonosov Range.

"The western slope of the Lomonosov Range in this sector" is at the same time the eastern wall of a large kite-shaped cirque in the continental shelf (and, of course, in the basement formation underlying the shelf). The southern end of the cirque closely approaches the shores of Ellesmere Island. Its western side, on the meridian of 90°W, is also rectilinear; if this detail is accurate, it likewise represents a structural line of some kind. The southern end of the kite-shaped cirque, along the Ellesmere coast, coincides with the extension of the 4000 m isobath, the apparent boundary of the Hercynian corridor in the European Arctic Basin.

On the Greenland side of the Lomonosov Range there is a series of enormous gulleys and ridges which extend toward Ellesmere and interrupt the Lomonosov folding. The largest of the gulleys continues into the straight cleft of the Robeson Channel. Nansen's sill might also be related to the system. As Figure 2 shows plainly, these gulleys and ridges are the extension of the Hercynian folding on the floor of the European Arctic Basin.

At the other end of the Lomonosov Range there is the Sadko Trough, which, if Hakkel's detail can be trusted, is bordered on the east by a wall 150 miles long and of maximum height two miles. In the neighboring gulleys we see a change of direction from that of the Hyperborean ridge-system to that of the Sadko Trough. The gulley immediately to the east of the Sadko Trough runs precisely toward the corner of the Hyperborean Platform in the New Siberian Islands; it might be taken as outlining the tip of the triangular sub-shelf part of the said platform. It is directly in line with the 3500 m isobath of the European Arctic Basin, just as the 4000 m isobath is in line with the 'staircase.' It is as though these isobaths were diverging in order to accommodate the point of the triangle.

The Sadko Trough, from the steepness of its initial descent, appears to be a structural rather than an erosional (Lena River) feature. It may originally have belonged to the Hercynian system. Only on one side has it a high wall, which thus marks the edge of a straight bite out of the continental shelf—a subsidence, it would seem. The subsidence may have been part of the presumed general sinking of the floor of the European Arctic Basin. In the Permian and Triassic there was an uplift in the area of the present Laptev Sea, high enough to serve as an erosion-source for terrigenous drift deposited on the Taimyr Peninsula, which was then in a synclinal stage [*Kalinko*, 1956]. The said land probably extended well to the north beyond the present shelf limit, very likely to the rim of the Hyperborean Platform. At this time, of course, the Lomonosov Range did not yet exist. By the beginning of the Triassic period the northern Taimyr had become a mountainous country. Drift still continued to come from Kalinko's land-mass in the northeast. This land may have subsided only with the elevation of the Lomonosov Range. The Sadko Trough, close to the original edge of the Hyperborean Platform, was one boundary for the subsidence, and the other boundary may have been Hakkel's fracture (or rather, the Shokal'ski-Taimyr fracture, concerning the existence of which there is less doubt). If the subsidence was in the Mesozoic, this would account for the crosses in this area of Figure 2 and permit a generalization: the recent volcanic activity everywhere retraces the Mesozoic tectonic activity.

It will be noticed in Figure 2 that the prominent ridges and gulleys in the edge of the European shelf between 80° and 100°E, which belong to the Hercynian fold-system, are abruptly wiped out to the east of Hakkel's fracture, although the deep-sea Hercynian contours do seem to continue across it. This change in the character of the continental slope is confined to the sector between the straight wall of the Sadko Trough and the above-mentioned straight wall on the 100th meridian, which follows Hak-

kel's fracture north of the Shokal'ski Strait. The suggestion is very strong that the Hercynian features of the continental slope were wiped out by a (Mesozoic?) subsidence between these limits, accompanied by slumping of the sedimentary shelf.

All the above discussion depends on the accuracy of Hakkel's chart in this region. Since Hakkel' himself describes it as a schematic chart, it is natural to ask how far one may rely on it. The only answer that can be given is that the Soviet exploratory effort has been concentrated on the Lomonosov Range and its vicinity; that Hakkel' himself was a participant; that one of Hakkel's special interests is the continental shelf and slope, to which he devotes a chapter of his book [1957a] and at least one paper [1957b].

The Ewing-Heezen Rift—F. *Nansen* [1928] suspected that there might be a ridge or sill across the Arctic Ocean, dividing it into two basins and thus continuing the series of transverse sills and basins of the Norwegian Sea. To others, the concept of the Arctic Ocean as a continuation of the Atlantic suggested that the Mid-Atlantic Ridge should extend, as a longitudinal rather than a transverse feature, through the Arctic Ocean. The discovery of the Lomonosov Range has revived this latter idea. The Mid-Atlantic Ridge is now known to be a double mountain-chain with a deep median rift [*Heezen* and *Tharp,* 1957]. According to *Ewing* and *Heezen* [1956; see also *Science News Letter,* Feb. 16, 1957, p. 90; *Scientific American,* March 1957, p. 66] it is a segment of a great fracture-system encircling the entire globe. Might not the Ewing-Heezen rift, after bisecting Iceland, pass across Greenland (or if the icecap were removed, through the middle of a Greenland Archipelago) and continue across the Arctic Ocean in association with the Lomonosov Range?

Unfortunately for such an idea, it is now proven that the Lomonosov Range does not proceed into the Atlantic nor toward the Greenland coast; on the contrary, it proceeds to Ellesmere Island, and there is a deep depression, the continuation of the Robeson Channel, separating it from Greenland. These facts are very positively stated by the Soviet writers [for example, *Saks* and others, 1955]. It transpires, indeed, that I. I. Cherevichny led an airborne reconnaissance group into the Lincoln Sea area in April-May of 1954 for the express purpose of deciding the matter. His findings, reported in *Pravda* in July [*Burkhanov,* 1954] were confirmed by more extensive work in the spring of the next year. From U. S. reports it appears that Ice Island T-3, in 1952 to 1954, crossed some spurs of the Lomonosov Range north of Ellesmere.

For still another reason it is improbable that the Lomonosov Range has anything to do with the Mid-Atlantic Ridge. *Ewing* and *Heezen* [1956, p. 80] establish a sharp distinction between oceanic ridges of fold type and of rift type, and they state criteria for the distinction. The Lomonosov Range belongs to the folded category of ridges; that is, it is not of the same type as the Mid-Atlantic Ridge.

One criterion for the rift-and-ridge system is seismicity. Ewing and Heezen therefore unhesitatingly orient their rift-zone, not toward the Lomonosov Range, but along the Arctic seismic belt of Figure 5, to join the Verkhoyan Arc in Siberia.

The Verkhoyan Arc, as we have noted, has been tectonically inactive since the Tertiary, but it is now seismic, especially just at its seaward end. Does this mean a new phase of activity, connected with a quite recent thrust of the Ewing-Heezen rift across the Norwegian Sea and the European Arctic Basin? If these seas are Mesozoic extensions of the Atlantic, as is widely believed, then the extension of the Mid-Atlantic rift-and-ridge system across them would seem to be the logical next step in a global process. Unfortunately the character and causation of this process are still an enigma.

On the other hand, Saks and his associates see, in the European Arctic Basin with its accumulation of sediments, an incipient geosyncline, a geosyncline which may in due course produce a new Arctic orogeny. What relation geosynclinal orogenies may have to rift-and-ridge systems of the Mid-Atlantic type is, of course, part of the enigma.

It is reported [*Frolov* and *Paseçki,* 1958] that the Soviet vessels Lena and Ob' have during the last year discovered a deep-water trough completely piercing Nansen's sill [compare Fig. 2, at latitude 80°N longitude 0°; compare also *Nansen,* 1928, p. 12]. On the 80th parallel the trough is 3000 m deep, and 50 km wide between the 1000-m isobaths (T. A. Harwood, from con-

versation with the Soviet oceanographers P. A. Gordienko and A. F. Laktionov). Its orientation is roughly northward. This trough, then, lies in the seismic belt, and it could mark the continuation of the Ewing-Heezen rift north of Iceland and Jan Mayen.

At the other side of the Arctic Ocean, the seismic belt follows close to the Sadko Trough, possibly tracing an ancient break.

The Arctic Ocean Floor-Platforms—The notion of a platform, common to Soviet geologists, is a useful one, but there are intricacies in the understanding of the term. In particular, the floor of the European Arctic Basin is frequently described as a platform, thus suggesting an exact parallel with the Hyperborean Platform. The two oceanic basins are, however, very different entities, historically and physically. There is a snare in the matter-of-fact statement that the Lomonosov Range divides the Arctic Ocean depression into two basins.

Platforms are consolidated areas of the earth's crust. To the irresistible epeirogenic movements of the restless earth, platforms respond by fracturing, vertical block-movements, and perhaps overthrusting, but not generally by folding except at the very edges. This characterization implies that platforms will be bordered by areas which *are* subject to folding, and for which we might adopt Arkhangel'ski's term "geosynclinal regions." [*Arkhangel'ski,* 1941, p. 44: "My own researches have compelled me to broaden the concept of the geosyncline to that of the *geosynclinal regions,* within which geosynclinal, subsiding sectors alternate with geanticlinal sectors of uplift."] A geosynclinal region is the antithesis of a platform [compare *Krishtovich,* 1955, vol. 1, p. 160]. In an area of platforms and geosynclinal regions, any epeirogenic movement will expend most of its power in reworking the geosynclinals [*Arkhangel'ski, loc. cit.*].

According to some authors, the formation of platforms is a one-way process. "Whereas the conversion of geosynclinal areas of the terrestrial crust into [resistant] blocks is a fact known to all, in the opinion of the majority of geologists the reverse transition of blocks, once consolidated, in geosynclines is not observed, particularly when they are ancient blocks" [*Arkhangel'ski,* 1941, p. 45]. But other authors speak of "reactivation" of platforms. In part, the disagreement would seem to be a matter of platform age. Since 'Precambrian' refers to a period many times longer than the whole 'historical' period of geology, the average Precambrian platform will be very old; it will have survived aeons of epeirogenic stresses. Younger platforms may not be so resistant, and are very likely subject to reactivation. The strength of platforms is not a function of thickness, but is no doubt geochemical (in the broadest sense), and the geochemical conditions of platform formation may have changed radically since Precambrian days—for instance, with the decay of crustal radioactivity.

Now the Hyperborean Platform, as we have noted, must be of Precambrian age. The floor of the European Arctic Basin, however, is nearly all occupied by Hercynian folding, a submarine extension of the Ural-Tienshan folding of the Eurasian continent. Here the consolidation was completed, more or less, only in Upper Paleozoic times.* Therefore, if the floor of the European Arctic Basin is called a platform, it is only an Upper Paleozoic platform, just as the Ural-Tienshan folded region is sometimes called "the Ural-Siberian *Paleozoic* Platform" [*Arkhangel'ski,* 1939, p. 303]. On this basis we can understand the seismicity and signs of restlessness in the European Arctic Basin, in contrast to the Hyperborean Platform which is quite aseismic, in conformity with its age.

The only truly archaic consolidation in the European Arctic Basin is the small Barents Sea Platform (Fig. 3), a submerged extension of the East European Platform. Its presence is demonstrated by the sweeping curve of the western part of the Ural-Tienshan folding through Novaya Zemlia [*Arkhangel'ski,* 1941, Fig. 80]. Running lengthwise of Novaya Zemlia, this folding turns directly east towards Severnaya Zemlia; then, of course, it must again veer sharply to the northwest in order to parallel the

* The Ural-Tienshan geosynclinal region was strongly active in the Caledonian cycle, and the Caledonian folding was reelaborated by the Hercynian [*Krishtovich,* 1955, vol. 1, p. 287; *Suslov,* 1947, p. 198]. Some Mesozoic folding was superimposed on the Hercynian [*Arkhangel'ski,* 1939, p. 304], indicating a not quite complete consolidation.

folding which is seen in Severnaya Zemlia [*Yegiazarov*, 1957, pp. 419–420]. This unmistakably indicates a resistant block in the Barents Sea.

On the other hand, it is the Barents Sea Platform and the Greenland-Canadian Platform on one side, and the Hyperborean Platform on the other side, that determine the course of the Hercynian folding across the ocean depression and through the Franklin corridor. The folding both fits and fills the space between these platforms, only jumping across the gap between Spitsbergen and Northeast Greenland (Fig. 3).

Now the Lomonosov orogeny appears to have chewed up the edge of the Hyperborean Platform (just as the Verkhoyan folding swallowed the edges of the Anabar and Aldan Shields, as explained by *Kropotkin* and *Kheraskov* [1939, p. 602]). But with this exception, the directions of all the Arctic foldings can be explained quite simply in terms of corridors between platforms, without any special hypotheses. No doubt this is due to the particular character of the Arctic region, enclosed on every side by ancient platforms.

The suggested historical picture is as follows. Archaic consolidations (Greenland-Canadian, East European and Central Siberian Platforms) were separated by geosynclinal corridors thinly crusted over (oceanic crust), so that these corridors were subject to folding. (Perhaps in earlier times, when the radioactive heat flux was greater, an oceanic crust was less effective than at present in impeding the movements of platform blocks; some of the corridors may be channels opened by continental drift.) The geosynclinal regions successively consolidated, after many foldings which thickened the crust. The most recent consolidations were probably in the areas of weakest oceanic crust. In some cases (Ural-Tienshan and Verkhoyan arcs) the crust was built up to continental thickness by folding and magmatic activity, and the geosynclinal regions then became incorporated into the continents. Elsewhere they subsided and reverted to oceanic status [*Arkhangel'ski*, 1941, p. 48].

Parallel Structures—The apparent subsidences of the Arctic Ocean floor are associated with large-scale fracturing, the pattern of which has no visible connection with platform boundaries; for instance, the 'staircase' faulting has broken the Hyperborean Platform into two parts. Hakkel' is impressed by the parallel orientations of such features. The 'staircase' is parallel to the Canadian Arctic continental slope, and the Hyperborean ridges are part of this system. Another system is formed by the Lomonosov Range, which is roughly parallel to the European Arctic continental slope and to the Hercynian folding on the floor of the European Arctic Basin.

In particular, Hakkel' repeatedly emphasizes that the *continental slopes* belong to these parallelisms.

The cause of the fracturing may have been changes in the shape of the terrestrial globe, due to polar wandering or variation of the earth's rotation. Under the assumption that the axis of the geomagnetic field, if averaged over several thousands of years, will coincide with the earth's rotational axis, paleomagnetic data suggest that the position of the rotational pole, relative to the earth's crust, has not been constant. These data show good agreement with the present geographic pole as far back as the middle of the Tertiary Period [compare, however, *Roche*, 1958], but before that, with few exceptions, they generally fail to agree, while for the Triassic and earlier there is never such agreement [*Irving*, 1958, p. 224]. But if the position of the pole has shifted, so has the geospheroid shifted with respect to the crust. If the pole moved into what is now the Arctic region in early Mesozoic times, then crustal compression and flattening of the crustal curvature have occurred here.

Even if no migration of the pole has taken place, change of the earth's rotation rate, whether a steady variation or irregular fluctuation, would have similar effects. This is the theory preferred by *Hakkel'*, who points out [1957a, p. 119] that the increase in the length of the day since Archean times, as calculated by certain astronomers [*Stovas*, 1957], would imply a 44-km increase in the length of the earth's axis. When this figure (or one half of it) is compared with the 5-km maximum depth of the Arctic Ocean, we are able to visualize the possible scale of hypsometric adjustments.

Fluctuations in the earth's rotation would maintain a continual working of every type of fault or dislocation (such as Ewing's world-wide rift system).

To account for the parallel features, Hakkel' accepts a theory which was put forward by *Rikhter* [1955], at the 1955 Session of the Geographic Society of the USSR (the same session at which Hakkel' predicted the spurs of the Lomonosov Range). According to this theory, the parallel features are actually segments of concentric arcs, belonging to two great systems of concentric and radial faulting centered at 68°N 77°W in the Foxe Basin, and at 71°N on the meridian of Greenwich in the Norwegian Sea. It is supposed that change in the crustal radius of curvature has produced these fracture-systems, which resemble the cracks in an egg-shell crushed in with a spoon. In terms of circles and radii extending outward from the two centers, Rikhter explains the directions of tectonic faults, rivers, coastlines, coastal indentations, and a great number of natural features in North America, Greenland, Europe, and Siberia. Moreover [*ibid.*, p. 33]: "In the relief of the ocean depression adjacent to the Canadian Archipelago, the arcuate lines of elevation and depression of the ocean floor take a direction corresponding to concentric fractures in the Canadian Shield, while in the ocean depression adjacent to Greenland, Spitsbergen and Franz Josef Land the direction of the long narrow arcs is extremely close to that of the concentric arcs around the center in the Scandic Deep." All this is set forth in two charts published by Rikhter in the above-cited paper. Since they are self-explanatory and readily available, we shall not reproduce them here.

Rikhter is strongly criticized by *Aprodov* [1956] for pushing the schematization too far. With this criticism one must agree, for Rikhter's structural lines are in wild contradiction with the known geomorphology of (at least) the Canadian Arctic. As regards Eurasian geographical features he may have a better basis, since a good deal of prior work is consulted. But the scheme is patently inapplicable to the Hercynian ridges in the European Arctic Basin, for they do not form arcs centered in the Norwegian Sea; they have neither the right direction nor the right curvature (Fig. 2).

As a matter of fact, the parallelisms noted by Hakkel' are found, upon examination, to be not very significant. The Lomonosov Range is actually at a considerable angle to the European Arctic continental slope. Neither of these formations has anything directly to do with the Hercynian folding which fills the space between them, since the direction of this folding is determined by the edges of the Hyperborean and Barents Sea Platforms. The continental slope happens to have the same trend because, in this region, it closely follows the edge of the Barents Sea Platform. As for the Hyperborean Basin, the lowest isobaths of the 'staircase' and the Canadian Arctic continental slope are certainly parallel to each other and to the Hyperborean ridges. The most probable explanation for this is that the oblong floor of the basin subsided along fractures which followed the Hyperborean folding; the staircase and the opposite continental slope were formed by the subsidence.

The Trans-Arctic Hercynian Corridor of Folding—From Saks' diagram, Figure 3, we have lifted the corridor of Hercynian folding as there shown and superimposed it on Figure 2 (shaded band). The result is most revealing. Saks' corridor precisely encloses the ocean-floor folding shown by Hakkel', thus indicating that Saks and Hakkel' have employed the same bathymetric data (of 1955). The boundary isobaths and the ocean-floor ridges trend with the corridor; so do the great indentations in the shelf north of Greenland. On the European side, it appears that Saks' corridor should be widened to include the shelf features west of Severnaya Zemlia, which have precisely the right trend; so too it should perhaps be widened eastward to the Sadko Trough. In Northeast Greenland we see that Independence Fjord, Frederick E. Hyde Fjord, and other indentations are concordant with the Hercynian folding; so too, on Ellesmere Island, are Archer Fjord and Lake Hazen; on the west coast, Greely Fjord. The right-hand boundary of the shaded corridor in Figure 2, once it is past the violent irruption of the Lomonosov folding, follows the isobaths of the kite-shaped cirque, then the northern coast of Ellesmere, and from there its smooth extension (dotted line in Figure 2) precisely follows the edge of the sedimentary coastal plain of the Canadian Arctic Archipelago as far as the very western tip of Prince Patrick Island. It is strange that the ephemeral shoreline should so closely follow the Hercynian trend. Nevertheless the arc of the coastline is obvious, and so is its continuity with the isobaths north of Ellesmere and in the European Arctic Basin.

At the western end of Prince Patrick Island another great arc seems to begin, extending to Point Barrow in Alaska. It is more obscured by casual indentations such as Mackenzie Bay, but its existence seems unmistakable. One would say, then, that the Hercynian folding must have ended at Prince Patrick Island, where it is intercepted, at an angle, by another (Cordilleran?) system.

Now all this picture is strongly dependent on Hakkel's isobaths and ridge-system in the European Arctic Basin. How reliable these are the future will certainly show, but for purposes of present assessment the following considerations are suggested.

a) The existence of the mountain ridges on the floor of the European Arctic Basin is independently attested. Thus Burkhanov (at the time, Director of the Northern Sea Route Authority), in May 1957: "In the best-explored Atlantic part of the Polar Basin, bounded on the east by the Lomonosov Range, several mountain ranges have been traced over almost the full distance from Greenland and Ellesmere Land to the Kara Sea and Severnaya Zemlia. In the opinion of Arctic Institute scientists, these mountain systems were developed in the Caledonian and Hercynian epochs of folding." [*Burkhanov*, 1957a.] This statement carries weight. The ridges exist.

b) We have noted that Hakkel' favors Rikhter's theory, according to which the mountain ridges should form arcs centered on a point in the Norwegian Sea. But in Figure 2 they do nothing of the kind. If these contours were mere diagrammatic detail, intended only to illustrate Hakkel's ideas, then he would certainly not have drawn them as in Figure 2.

c) Hakkel's contours fit Saks' corridor; Saks and Hakkel' have used the same data. Therefore if we suppose anything tentative, not to say imaginary, about these contours, then we are obliged to assume that more than one highly regarded Soviet scientist has been deceived.

10) *The Great Arctic Magnetic Anomaly*—The Great Magnetic Anomaly is quite as real an Arctic feature as the Lomonosov Range, or the Arctic seismicity and volcanism. It is indeed more notable than these, because it is unique on the face of the earth. Therefore it is reasonable to say that no account of Arctic geotectonics will be complete without reference to the Great Arctic Magnetic Anomaly.

As the Soviet authors inform us, the descent of the Verkhoyan folding into the sea was successfully traced by the behavior of the geomagnetic field, which exhibits anomalies following the strike of the Mesozoic folds. The rock, above the Curie point level, is of such nature that a local fold will produce a local magnetic anomaly. A major formation might therefore produce a major anomaly. On this basis Tokarev, before the discovery of the Lomonosov Range, predicted an elevation of the ocean floor to account for the Great Arctic Anomaly.

The outstanding puzzle was the direction of the Lomonosov Range, which does not follow the axis of the anomaly (Fig. 2, Fig. 3).

In a previous paper [*Hope*, 1957] we have suggested that if the Franklin belt of folding, along the edge of the Canadian Arctic Archipelago, is included with the Lomonosov folding, then the axis of the anomaly does pass through the centroid of the Mesozoic corridor as a whole. This is clearly seen in Figure 3. We had to suppose that the corridor was no more than the erratic surface trace of a deep-lying and magnetically active formation (deep, but above the Curie point level); the surface trace might be deflected by the edge of the Canadian Precambrian Platform, just as a fissure in sea ice is deflected along the edge of a frozen-in iceberg.

The picture is now modified and improved by the discovery of the Alpha Range, which fills in the corner between the Lomonosov and Franklin foldings. Moreover, it will be seen that six of the crosses in Figure 2 lie almost on the anomaly axis, while six more are equally distributed on the two sides of the axis. If the recent volcanism marked by these crosses is associated with the area of Mesozoic movements (see above), then the anomaly axis too is associated with the area of Mesozoic disturbance.

The magnetic pole tends to be confied to the anomaly 'trough' [*Hope*, 1957]. Now we find that the average Quaternary poles, as derived by *Nagata* and others [1957, Fig. 5] from paleomagnetic evidence in Japan, all lie in a band across the Arctic, parallel to the anomaly axis. True, the band is displaced somewhat, passing across North Greenland to the Kara and Barents Seas; that is, it follows the Hercynian corridor

very closely, rather than the Mesozoic corridor. Possibly this indicates that the Hercynian corridor in the past had a greater geomagnetic importance. On the other hand, the displacement may not be too significant. Observations of the magnetic vector in any one region of the globe do not yield a magnetic pole position without a considerable systematic error (note the direction of curvature of the magnetic meridians through Japan, in Figure 1), and this would be as true of paleomagnetic as of modern determinations.

Roche [1958], from well-dated volcanic formations in France, likewise places a Quaternary (Pleistocene) magnetic pole near the north coast of Greenland, at 84°N 50°W. But obviously this position also requires a correction, since it is found from a paleomagnetic declination and dip (7°W and +62°), which are nearly the same as the present values (6°W and +62°), and of course the present declination and dip do not mean a magnetic pole north of Greenland. The indicated correction would put Roche's Pleistocene magnetic pole only 40-odd miles from the present magnetic dip-pole.

The recent (< 5000 B.P.) magnetic poles, as charted by *Brynjólfsson* [1957, Fig. 3] from the vantage point of Iceland, are scattered over the Mesozoic corridor, including the Franklin belt, and the European end of the Hercynian corridor. For the period since 900 A.D. they lie generally in a band extending from the Boothia Peninsula to Severnaya Zemlia; that is, symmetrically with the present anomaly axis. The lateral scatter of Brynjólfsson's points is greatly reduced if we correct for the influence of the anomaly itself. The magnetic pattern on the earth's surface is compressed toward the anomaly axis [*Hope*, 1957, Fig. 1], so that a circling or oval motion of the magnetic vector in lower latitudes will correspond to a linear or narrowly oval motion of the magnetic pole. For instance, with the indicated correction, Brynjólfsson's broad looping pole-path for 1554–1950 A.D. will be very similar to the narrow oval path reconstructed by van Bemmelen [*Hope*, 1957, Fig. 4].

Hakkel' [1957a] presents an entirely different theory of the Great Arctic Anomaly. On page 115, he shows an isoline chart of the vertical component of the geomagnetic field, which, as is well known, has not one but two points of maximum intensity (Fig. 1). One of them is in Canada (about 58°N 97°W, just west of Hudson Bay) and the other in Siberia (about 67°N 105–115°E). These maxima, which are of equal intensity, lie practically dead-center in the Canadian and the Anabar crystalline shields, two of the most ancient centers of consolidation of the earth's crust. [See, in particular, *Arkhangel'ski*, 1941, chart I in pocket at end of book.]

Hakkel's interpretation seems to be as follows. The earth's magnetic field is preferentially channeled through the great crustal shields, so that instead of a single maximum concentration of geomagnetic lines of force in the Arctic, there are two such maxima. However, this interpretation is based on the vertical component alone. If matters were so simple, then, since the two vertical maxima have practically equal intensities, the pattern of the horizontal component, around each vertical maximum, would be symmetrical, and the dip-pole would lie about halfway between them. But as may be seen in Figure 1, this is not the case. It appears that there must be modifying features distributed corridor-wise along the axis of the anomaly. Indeed no one can examine the extraordinary compressed sheaf of the magnetic meridians in Figure 1 without coming to this conclusion. The picture is equally impressive in the isolines of the horizontal field-component, which form a straight-sided trough* [*Hope*, 1957, Fig. 1]. This configuration could scarcely be reproduced by two dipoles separated by about 75° of the earth's circumference, but rather would call for a row of dipoles.

The Anabar Shield is quite small, smaller than the Fenno-Scandian Shield. Why should the former have a great influence on the geomagnetic field, and the latter none? The same size-relationship holds for the two respective platforms, the East European and the Central Siberian, as shown in Figure 3. The East European crystalline rock extends far north under

* The two maxima of the vertical component are thus simply associated with the maximum curvature of the isolines of the horizontal component, where they round the ends of the 'trough.' Incidentally, the said maxima are not fixed but in motion, though this of course does not disprove a crustal theory of their origin. As in the case of the dip-pole, the motion is the effect of a superimposed cyclic variation originating in the earth's core [*Hope*, 1957].

ne Arctic Ocean in the form of the Barents Sea latform. Why has it no influence?

Similarly there is the Greenland Shield, within hich the Gaussian axis-pole is located; it is ertainly connected with the Canadian Shield, nd it extends much farther north. Why is its nfluence not felt? Is it counteracted by the pposing mass of the Hyperborean Platform? hen the whole Arctic region has the appearance f a cap of magnetically active rock, broken by disturbed corridors of comparatively small area. f one postulates that the shield rocks attract he magnetic field, there seems to be no reason hy the magnetic meridians should be concen-rated in one direction rather than another.

Figure 3, in fact, gives one the impression that the shields or platforms are repelling rather than attracting the magnetic field; that they are packing the magnetic meridians into the Central Arctic corridor-region which they enclose.

This gives us a possible clue. The earth's crust is thickest, not in platforms, but in folded regions. (The strength of a platform is in its composition and cohesion, not in its thickness.) Now in the Soviet Arctic coastal region the thickest crust (43 km) is said to be in the strip containing Novaya Zemlia and the Taimyr Peninsula, and extending eastward through the Laptev Sea [*Leonov,* 1956, Fig. 65, after V. F. Bonchkovski]; that is, just where the trans-Arctic corridors of Hercynian and Mesozoic folding descend into the sea. The anomaly axis crosses the very center of this strip, in the Taimyr-Severnaya Zemlia sector of the coast. Here, in Severnaya Zemlia, the land extends farthest north, and also, no doubt, the thickest continental rock. Severnaya Zemlia and the northern Taimyr are part of a land-mass which in the Paleozoic extended much farther north (see isobaths of Figure 2) and was already a mountainous country with a spine of Precambrian rock [*Suslov,* 1947, p. 182]. Severnaya Zemlia was most intensively folded in the Caledonian cycle, but by Hercynian times reacted almost as a platform [*Yegiazarov,* 1957, pp. 419–422], a resistant block within the Hercynian corridor of disturbance.

We note particularly, in Figure 1, that the convergence of the meridians is toward Severnaya Zemlia rather than toward the Anabar Shield (70°N 110°E). It was in the northward-thrusting finger of Severnaya Zemlia that a second magnetic dipole was believed (until 1948) to exist.*

As to why the thicker crustal rock should influence the geomagnetic field, speculative hypotheses are easy to construct. For instance, differences in thermal conductivity of the rocks may produce considerable differences of temperature-distribution in depth, and consequently different depths of the Curie point level as between geosynclinal and platform regions. However, in the absence of definite information, we should be satisfied for the present to point out the apparent relationships, without forcing an explanation.

Under the Arctic Ocean the crust thins out as compared with the continent, but it is possible that the same *relative* difference of thickness is maintained between platform areas and folded areas. In Figure 6 we reproduce a diagram of the terrestrial crust under the European Arctic Basin according to R. M. Demeniçkaya (though the status of the information in this diagram is unknown). In the ocean depression Demeniçkaya shows only an oceanic thickness of crust (5 to 8 km), but under the Lomonosov Range it increases to 15 km. Both granite and basalt are thickened. The path of the magnetic anomaly across the Arctic may be determined by this configuration.

In the trans-Arctic Hercynian corridor, Figure 6 shows smaller thickenings of the granite and basalt. It is possible that the roots of this ancient Hercynian mountain system have been resorbed and degranitized [*Belousov,* 1955], a process of which there are indications elsewhere on the globe. (If so, it is an interesting possibility that the thermal conductivity and other characteristics of the Hercynian formations may have been gradually changing, and simultaneously their geomagnetic influence.)

* The idea is an old one; it was advanced by Christopher Hansteen a century ago, on the basis of observations which he had conducted in Norway, Finland, and, with G. A. Erman, in Western Siberia (1828–1830). In the 1930's the Soviet magnetologist, B. P. Vainberg (Weinberg), studying the magnetic data obtained during the drift of the SS *Sedov,* revived the hypothesis of a second dipole, but its existence was finally disproved by Soviet exploration in 1948 [*Hakkel'* 1957a, p. 114]. However, as Hakkel' remarks, there is no cloud without a silver lining, and the loss of the second magnetic pole was at the same time the discovery of the Great Arctic Anomaly.

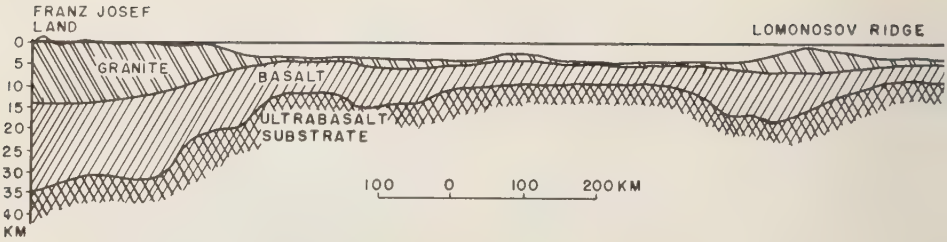

FIG. 6—Section of the terrestrial crust across the Atlantic Arctic Basin from Franz Josef Land to the Lomonosov Ridge, in the direction toward Alaska, according to R. M. Demeniçkaya. From *Hakkel* [1957a, p. 95]. The crust under the archipelago is shown as of continental thickness, 35 km; in the depression it is of oceanic thickness, 5-8 km; under the Lomonsov Range it thickens to 15 km.

Now returning to the theory which relates the Great Arctic Magnetic Anomaly to the Canadian and Anabar Shields, let us say in conclusion that we cannot afford to ignore this theory. But if it is to be maintained, then the Canadian and Anabar Shields must be shown to differ essentially in constitution from other ancient centers of crustal consolidation. *Hakkel'* [1957a, pp. 115, 116] attempts to do so by an argument which invokes, among other things, the Siberian diamonds, volcanic pipes, and kimberlites. To him they are evidence that the Anabar rocks or geological formations are of a very special character. It is curious to recall that the Chubb meteor crater of Ungava, in the Canadian Shield, is named after a prospector who thought it might be a volcanic formation and a good place to look for diamonds.

Acknowledgments—The author is grateful to the Defense Research Board of Canada for permission to publish this communication, and to Brigadier E. D. Baldock, Chief Cartographer of the Department of Mines and Resources, Ottawa, for facilities extended. Cordial thanks are due to W. W. MacLarty and J. B. Roberts for preparation of the charts.

REFERENCES

APRODOV, V. A., Morphotectonics of the Arctic regions, *Izvest. Akad. Nauk SSSR., Ser. Geog.*, no. 1, 144–146, 1956.

ARKHANGEL'SKI, A. D., The geological structure and geological history of the USSR, *Mezhdunarod. Geol. Kong., Trudy XVII Sess. 1937* [*Trans. 17th Sess. (1937)*, *Intern. Geol. Congr.*], vol. 2, 301–321, GONTI, Moscow, 1939.

ARKHANGEL'SKI, A. D., *Geologicheskoye Stroyeniye i Geologicheskaya Istoriya SSSR* [*Geol. Structure and Geol. History of the USSR*], ONTI, Moscow, 1941.

ATLASOV, I. P., Geological structure of the northern part of the Verkhoyan Range, In *Geol. Sovet. Arktiki*, vol. 81 of *Trudy NIIGA* [*Trans. Research Inst. Arctic Geol.*], pp. 424–460, Gosgeoltekhizdat, Moscow, 1957.

AVSIUK, G. A., *Modern glaciation of the Soviet Arctic*, presented at International Conference on Sea Ice, Washington, 1958.

BELOUSOV, V. V., The geological structure and evolution of the oceanic depressions, *Izvest. Akad. Nauk SSSR, Ser. Geol.*, no. 3, 3–18, T 284 R,* 1955.

BELOUSOV, V. V., A promising new orientation in geology, *Vestnik Akad. Nauk SSSR*, 28, 9, 3–10, T 310 R,* 1958.

BRYNJÓLFSSON, *A.*, Studies of remanent magnetism and viscous magnetism in the basalts of Iceland, *Advances in physics* (*Quart. Suppl. Phil. Mag.*), 6, 247–254, 1957.

BURKHANOV, V. F., *Pravda*, no. 199, July 18, 1954.

BURKHANOV, V. F., Soviet Arctic research, *Priroda*, no. 5, 21–30, T 265 R,* 1957a.

BURKHANOV, V. F., Achievements of Soviet geographic exploration and research in the Arctic, *Cherez Okean na Dreifuyushchikh L'dakh* [*Across the ocean on drifting ice*], Geografgiz, Moscow, T 253 R,* 1957b.

CHEBOTAREVA, N. S., AND N. P. KUPRINA, History of the Valley of the Lena, *Izvest. Akad. Nauk SSSR, Ser. Geog.*, no. 5, 42–46, 1958.

DIBNER, V. D., Geological structure of Franz Josef Land, In *Geol. Sovet. Arktiki*, vol. 81 of *Trudy NIIGA* [*Trans. Research Inst. Arctic Geol.*], pp. 11–20, Gosgeoltekhizdat, Moscow, 1957.

DUNBAR, M., AND K. GREENAWAY, *Arctic Canada from the air*, Defence Research Bd. Can., Ottawa, 1956.

EARDLEY, A. J., *Structural geology of North America*, Harper and Bros., New York, 1951.

EARDLEY, A. J., The cause of mountain building—

* The starred numbers are the serial numbers of Defence Research Board (Canada) translations. These translations are deposited in the Library of the National Research Council, Sussex Street, Ottawa, Canada, and in many other libraries, from where photocopies may be obtained.

an enigma, *Am. Scientist,* 45, 189-217, 1957.

Ewing, M., and B. C. Heezen, Some problems of Antarctic submarine geology, *Geophys. Monograph No. 1: Antarctica in the IGY,* Am. Geophys. Union Publ., 75–81, 1956.

Fjeldstad, J. A., *Results of tidal observations (Maud Expedition),* John Greig, Bergen, 1936.

Frolov, V. V., and V. M. Paseçki, Arctic Ocean research center, *Priroda,* no. 8, 56–62, 1958.

Gutenberg, B., Earthquakes in the Arctic area, *The dynamic north,* book 1. Bur. Naval Operations, Washington, 1956.

Gzovski, M. V., The modeling method in tectonophysics, *Sovet. Geol.,* no. 4, 53–72, T 311 R *, 1958.

Hakkel' (Hackel), Ya. Ya., *Nauka i Osvoyeniye Arktiki [Science and the conquest of the Arctic],* Morskoi Transport Press, Leningrad, 1957a.

Hakkel', Ya. Ya., The continental slope as a geographic zone of the Arctic Ocean, *Izvest. Vses. Geog. Obshch. [Izvestiya of the All-Union Geog. Soc.],* 89, 493–507, 1957b.

Hakkel', Ya. Ya., Signs of recent submarine volcanic activity in the Lomonosov Range, *Priroda,* no. 4, 87–90, T 296 R *, 1958.

Harris, R. A., Some indications of land in the vicinity of the north pole, *Natl. Geog. Mag.,* 15, 255–261, 1904.

Harris, R. A., *Arctic tides,* Govt. Printing Office, Washington, 1911.

Heezen, B. C., and M. Tharp, *Physiographic diagram, Atlantic Ocean,* Lamont Geol. Observatory, Columbia Univ., New York, 1957.

Hodgson, E. A., The seismicity of the Arctic, *J. Roy. Astron. Soc. Can.,* 24, 201–210, 1930.

Hope, E. R., Linear secular oscillation of the northern magnetic pole, *J. Geophys. Research,* 62, 19–27, 1957.

Irving, E., Palaeogeographic reconstruction from palaeomagnetism, *Geophys. J. Roy. Astrom. Soc.,* 1, 224–237, 1958.

Kalinko, M. K., Sources of terrigenous material in the Permian and Triassic periods in the north of Central Siberia, *Doklady Akad. Nauk SSSR,* 108, 131–134, T 225 R,* 1956.

Krishtovich, A. N., (ed.) *Geologicheskii Slovar' [Geol. Dictionary],* Gosgeoltekhizdat, Moscow, 1955.

Kropotkin, P. N., and N. P. Kheraskov, Tectonics of northeastern Asia, In *Mezhdunarod. Geol. Kong., Trudy XVII Sess. 1937,* vol. 2, 601–611. GONTI, Moscow, 1939.

Lazurkin, V. M., Geological structure in the region of the lower reaches of the Lena River (Lena Depression), *Geol. Sovet. Arktiki,* vol. 81 of *Trudy NIIGA [Trans. Research Inst. Arctic Geol.],* pp. 461–483. Gosgeoltekhizdat, Moscow, 1957.

Leonov, G. P., *Istoricheskaya Geologiya,* Moscow Natl. Univ. Press, Moscow, 1956.

Lobanov, M. F., Geological structure of the New Siberian Islands, In *Geol. Sovet. Arktiki,* vol. 81 of *Trudy NIIGA [Trans. Research Inst. Arctic Geol.],* pp. 484–503, Gosgeoltekhizdat, Moscow, 1957.

Marmer, H. A., Arctic tides, *Problems of polar research,* Spec. Publ. no. 7, Am. Geog. Soc., New York, pp. 17–24, 1928.

Mushketov, D., Seismicity of the Arctic, *Trans. Seis. Inst., Acad. Sci. USSR,* no. 61, 9–15, 1935.

Nagata, T., S. Akaimoto, S. Uyeda, Y. Shimizu, M. Ozima, and K. Kobayashi, Paleomagnetic study on a Quaternary volcanic region in Japan, *Advances in physics (Suppl., Phil. Mag.),* 6, 255–263, 1957.

Nansen, F., The oceanographic problems of the still unknown Arctic regions, *Problems of polar research,* Spec. Publ. no. 7, Am. Geog. Soc., New York, pp. 3–14, 1928.

Panov, D. G., Neotectonic movements in the Arctic region, *Doklady Akad. Nauk SSSR,* 104, 462–465, T 204 R,* 1955a.

Panov, D. G., Tectonics of the central Arctic, *Doklady Akad. Nauk SSSR,* 105, 339–342, T 207 R,* 1955b.

Raiko, N. V., and N. A. Lindén, The earthquake of Nov. 20, 1933, in Baffin Bay and the distribution of seismic foci in the Arctic, *Trans. Seis. Inst., Acad. Sci. USSR,* no. 61, 1–8, 1935.

Rikhter, G. D., Basic features of the orography of the Arctic regions, *Izvest. Akad. Nauk SSSR, Ser. Geog.,* no. 4, 29–34, 1955.

Roche, A., Sur les variations de direction du champ magnétique terrestre au cours du Quaternaire, *Compt. rend.,* 246, 3364–3366, 1958.

Saks, V. N., N. A. Belov, and N. N. Lapina, Present concepts of the geology of the Central Arctic, *Priroda,* no. 7, 13–22, T 196 R,* 1955.

Savarenski, Ye. F., Research on seismicity of inaccessible regions, *Vestnik Akad. Nauk SSSR,* no. 6, 78–81, T 226 R,* 1956.

Stovas, M. V., Irregularity of the earth's rotation as a planetary-geomorphological and geotectonic factor, *Geol. Zhur. Akad. Nauk Ukrayin. RSR,* 17, 58–69, 1957. [See *Geophys. Abstr.,* no. 172–92, 1958.]

Suslov, S. P., *Fizicheskaya Geografiya* SSSR, Uchpedgiz, Moscow-Leningrad, 1947.

Süss, E., *Das Antlitz der Erde,* vol. 3, part 2, F. Tempski, Vienna, 1909.

Yegiazarov, B. Kh., Geological description of the Severnaya Zemlia archipelago, In *Geol. Sovet. Arktiki,* vol. 81 of *Trudy NIIGA [Trans. Research Inst. Arctic Geol.],* pp. 388–423, Gosgeoltekhizdat, Moscow, 1957.

(Manuscript received December 22, 1958.)

Observations of the Development of Rayleigh-Type Waves in the Vicinity of Small Explosions

Carl Kisslinger

St. Louis University
St. Louis, Missouri

Abstract—Study of the particle motion and dispersive properties of waves generated by small explosions has led to the identification of the fundamental M_2 mode and possibly a higher mode of this branch of the solution of the Rayleigh wave equation. In the particular field models, consisting of loess and clay over limestone, variations in near-surface conditions at the source have a greater effect on the recorded motion than do similar variations at the recording sites.

The features within the complex motion close to the source can be identified with specific wave types, which are well-separated at the larger distances.

Introduction—Steady progress has been made in explaining observed surface waves in terms of the normal modes of propagation in the layered system transmitting them. The number of unexplained events in the surface wave portion of seismograms from both natural and artificial sources has been greatly reduced, and this increased understanding has enhanced the usefulness of ground motion records for the determination of the physical characteristics of the medium through which the waves have been propagated.

The approaches to this problem have been: (1) theoretical, with theory now developed to account for almost all observations in sufficiently simple elastic systems; (2) observational, using model studies to gain solutions for systems complex enough to approach real geological situations; and (3) observational, using data from small explosions in field models of known characteristics. The third approach gives confirmation of theoretical and laboratory results in a real situation and, as an inevitable by-product, brings out new features to be explained.

The present study is of this last kind. Displacements of the ground surface at known distances from a number of small explosions have been recorded, and the results examined in the light of established theory and earlier experimental investigation. The purpose was to determine what is produced in the particular field model by a simple source, as a preliminary to understanding the results of more complicated experiments.

The site—The first decision in a study of this type is the selection of a suitable site. It is obviously desirable that the formations making up the earth model be approximately homogeneous within the areal limits of the observations and that the geological sequence be well known. The results in any case will be the solution only for the particular model, and they must be compared with other observations on that basis.

An open field on the grounds of St. Stanislaus Seminary, Florissant, Missouri, was selected as the test site. The physical properties of the field model are known from refraction seismic data, electrical resistivity results, and a limited amount of coring. Knowledge of the pertinent parameters is not as complete as would be desirable for a detailed analysis of wave propagation, but enough is known to explain the important characteristics of the observed ground motion.

The surface material is loess, underlain by Pleistocene silt and clay. Mississippian limestone of unknown, but probably great, thickness forms the bottom of the model. The densities in the sequence are: 1.2 to 2.0 g/cm^3 above the water table; 2.1 to 2.3 g/cm^3, with an average of 2.25 g/cm^3, from the water table to the limestone; and 2.67 g/cm^3 for one sample of the compact, crystalline limestone.

The only discontinuity in compressional wave velocity above the limestone detected by refraction shooting was at the water table. These velocities are indicated in Figure 1. The materials above the limestone are very uniform in

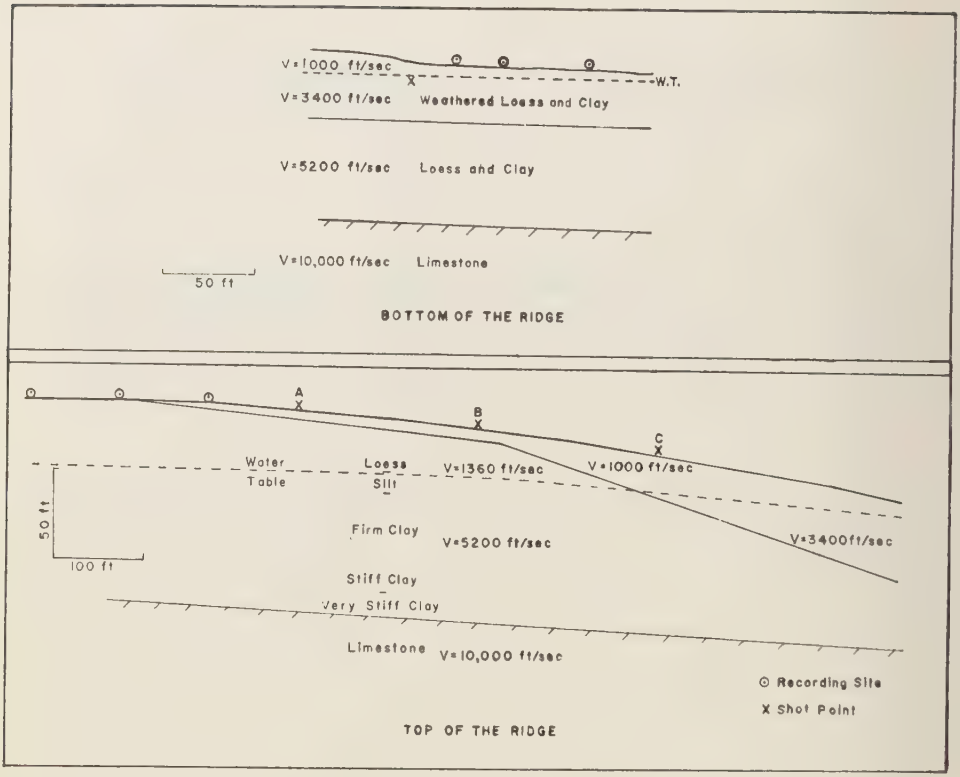

FIG. 1—The two models studied

texture. A silt layer with a maximum thickness of 15 ft at a depth of 30 ft may represent a velocity inversion. While no measurements of the rigidity modulus were carried out on the materials, standard penetration tests made at the time of coring indicate a definite increase in the rigidity of the clay at a depth of about 85 ft. The number of hammer blows per foot of penetration increased from 11 to 16, corresponding to a change from a stiff to a very stiff clay [*Terzaghi* and *Peck*, 1948, p. 300]. The depth to limestone is about 110 ft.

Observations were obtained in two distinct models in the selected area (Fig. 1). In one, records were made along a line at the bottom of a broad ridge. The depth to water was only 9 ft. In the second case, measurements were made along the top of this feature. The depths referred to in the preceding paragraph are below the top of the ridge.

Instrumentation—The ground displacements were determined by the use of Sprengnether three-component portable seismographs. These are mechanical-optical instruments, using inverted pendulums for the horizontal components and a spring-supported hinged lever for the vertical. The undamped periods are 0.75 sec, and the systems are damped to 0.55 critical. For the periods involved in this study, the instruments are essentially displacement measuring devices, and the traces were reduced on this assumption.

A choice of two magnifications is available in each instrument, one being exactly double the other. The static magnification was determined by tilt table measurements and by direct displacement of the center of oscillation of each pendulum. The value of magnification for each trace is denoted by V_0 in Figures 2, 3, and 5.

Although the instruments give a reliable record of ground displacements (the function for which they were intended), they contain no

method for putting the firing time on the record. This lack of a time tie between the records is a handicap in studying dispersion. The problem was at least partly solved by setting up a standard refraction profile at the same sites and recording on both types of equipment simultaneously. The particle motion diagrams presented here are of a higher order of reliability than the travel-time information and the dispersion data computed from it.

Experimental procedure—The records which form the basis of the principal part of this report were made at three sites, 100 ft apart, on a line along the top of the ridge. Small charges were fired in shallow holes at distances of 100, 300, and 500 ft from one end of this array. The overlap between shots made it possible to distinguish between effects due to changing distance and those due to changing conditions at the shot point. The instruments were carefully aligned so as to separate the radial and tangential components of ground motion. Shots were recorded at various other points along the ridge to fill out the picture.

A second series of shots was fired in a bore hole at the bottom of the ridge. These were recorded at 25, 50, and 100 ft.

All records were scanned with a micrometer microscope. Only the vertical and radial components are considered here. In all cases the tangential component was small compared with the other two. Particle motion diagrams in the vertical-radial plane were constructed for each record, and the most significant of these are presented in the accompanying figures.

Description of the recorded motion—Samples of the wave forms recorded in the two models are shown in Figure 2, for the top of the ridge, and Figure 5, for the bottom. Clearly defined body waves are not found here beyond 300 ft. The most striking difference in the two sets of records is the greater spread between the first arrivals and the surface waves at the bottom of the ridge. This is readily explained by the shallow water table, which is the refracting horizon producing the first arrivals. Thus, the body waves arrive at the stations on top of the ridge only slightly before the surface wave arrivals because of the much greater depth of the refracting boundary. The water table does not, of course, act as a velocity discontinuity for shear waves [*Dobrin* and others, 1954; *Ewing* and others, 1957].

The features characteristic of the waves which developed on top of the ridge are clearly seen at 700 ft (Fig. 3). The motion has separated into distinct events, which can be followed back to the smaller distances where they combine to form complex particle orbits. The dominant surface wave motion, as seen on the record and particle motion diagram, Figure 3, consists of three events. There first develops a prograde elliptical motion, designated E_1, with the major axis tilted forward at about 65° from the vertical. The periods decrease from 0.17 to 0.09 sec in three cycles, while the amplitude gradually increases until the motion changes, abruptly on the vertical, to a second prograde event.

This second event, called E_2, is more nearly circular. It starts with a period of 0.09 sec, which increases to 0.11 sec, and then decreases to 0.06 sec in about 2½ cycles. The last part of this orbit is tilted back, almost at right angles to the first prograde event. The E_2 motion stops abruptly, and the retrograde motion of the familar Rayleigh wave begins. The Rayleigh orbit is somewhat elongated horizontally, and the one large ellipse has a period of 0.15 sec. The large Rayleigh motion diminishes quickly into a short train of small amplitude, higher frequency retrograde waves.

The most significant fact established by these observations is the succession of two prograde events, of quite different orbital shape, appearing as two separate phases on the vertical, but as a continuous motion of first decreasing, then increasing, and finally decreasing period on the longitudinal. Also, the pulse-like nature of the large Rayleigh motion is to be noted.

The development of these features from the motion at the smaller distances can be readily traced. At the smaller distances, each event is cut off at an earlier part of its motion, so that at the closest stations the distinct nature of the wave types is no longer apparent. The general shape of each orbit and the orientation of the axes are maintained all the way through.

Figure 4 is included to illustrate the extent to which the results are reproducible when the shot point and recording locations are changed, but the distance kept constant. The records at 300 ft are strikingly similar because conditions

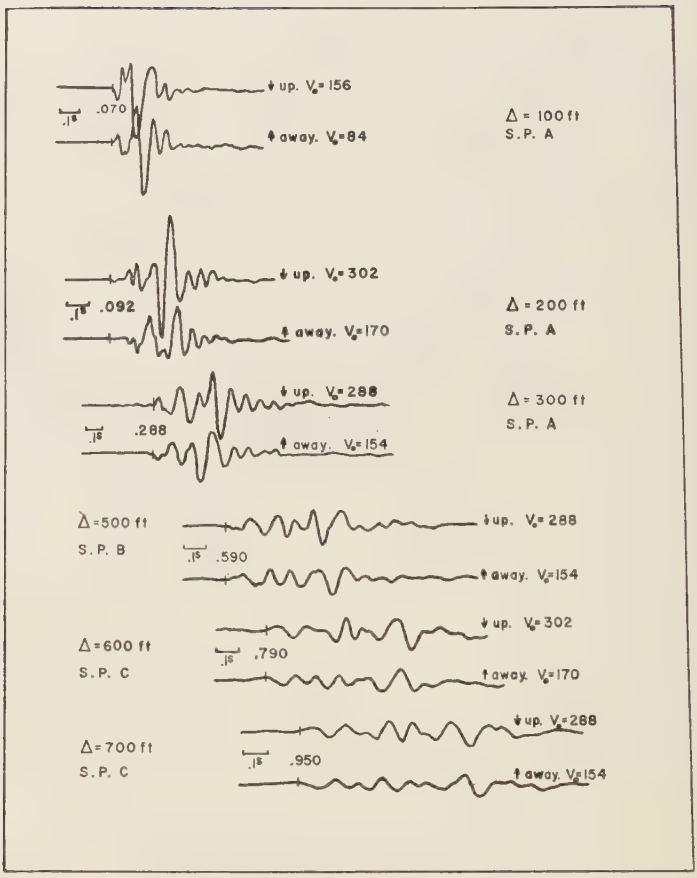

FIG. 2—Records of the longitudinal and vertical components, top of ridge

at shot points *A* and *B*, Figure 1, are much the same.

The two particle-motion diagrams at 500 ft are obviously not identical, but their principal features are certainly similar. The differences, which are chiefly in the shape of the retrograde orbit, must be ascribed to the difference in conditions at the two shot points. Shot point *C* is low on the ridge, in the layer of very low velocity material that blankets the area and wedges out toward the top. Shot point *B* is located near the top, where this layer has become very thin. In general, it has been found that the radial component is excited more strongly relative to the vertical for shots high on the ridge, while the motion is more regular, with smoother orbits, for shots low on the hill.

Evidence from other records, not shown here, supports the conclusion that the basic wave types are not altered by even rather extreme differences in near surface conditions at the recording sites when conditions at the shot points are not greatly different. The shallow conditions affect only the excitation of the events, while the overburden-limestone system controls the propagation.

The records at the bottom of the ridge were made at distances of 25, 50, and 100 ft from a series of charges fired in a bore hole. Depths of the charge ranged from 5 to 15 ft. The records were all similar, and those for the 11 ft depth are shown in Figure 5.

The motion recorded is relatively more simple than that found at the top of the ridge,

pecially on the vertical component. In addi-
n, the longitudinal amplitudes are smaller
ative to the vertical than in the previous
se. The Rayleigh ellipse is well developed,
en at 50 ft, in striking contrast to the close
ations in the other model. No definite evidence
the presence of the prograde events appears,
t the simplicity of the diagrams suggests that
ese waves have not been strongly excited.

The Rayleigh ellipse at 50 ft has a period of
06 sec and an axis ratio of 2.1:1, with the
ajor axis inclined forward at 25°. At 100 ft,
e period is 0.09 sec, axis ratio 1.7:1, with the
ajor axis inclined back at 40°.

Observed dispersion and the identification of e prograde motion—The dispersive character-
ics of the various waves can only be examined
the larger distances where the events are
ell-separated.

The dispersion data taken from the records
om the top of the ridge are presented in
gure 6. E_1 data are shown by an X, E_2 by a
iangle, and Rayleigh wave data by a dot.
ost of the data were taken from the records
600 and 700 ft, though values for the small
nplitude trains following the large Rayleigh
ave at 300 and 500 ft are included. The
nited time resolution of the equipment made
termination of wave periods to closer than
01 sec insignificant. The point corresponding
the maximum amplitude within each phase
marked with an m.

The observed dispersion data were compared
ith a variety of theoretical curves in an at-
mpt to discover the identity of the prograde
vents. The curve which fitted best, shown in
igure 6, is taken from *Tolstoy* and *Usdin* 1953]. It represents the dispersion of the first
odes of the M_1 and M_2 branches in a system
onsisting of a layer 110 ft thick, with a shear
elocity of 540 ft/sec, overlying an infinitely
gid half space. Poisson's ratio is taken to be
.25, although it obviously is not the correct
alue for the materials in the field model.

The assumption of an infinite rigidity for the
mestone relative to the overburden does not
em unreasonable. With regard to Poisson's
atio, *Giese* [1957] has demonstrated that
ariation in this number from 0.25 to 0.45 has
nly slight effect on the shape of the dispersion
urves for the fundamental Rayleigh modes for
his case.

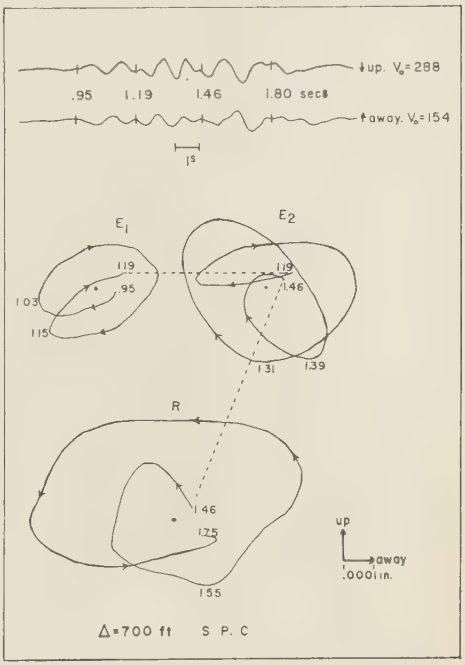

FIG. 3—Particle motion at 700 ft, top of ridge

No agreement at all was found with *Nagamune's* [1956] Case I for two surficial layers. However, this may still be a three-layer problem, as the constants for this theoretical curve are far from those that describe the model under consideration.

The points representing the large retrograde motion fit the Rayleigh wave (M_{II}) curve quite well from 5 to 10 cps. These include all of the large amplitude Rayleigh motion. The high frequency waves fall below the curve, an effect which may be explained as due to the presence of the thin layer of very low velocity material at the surface. Thus, we observe on the micro-scale an effect similar to that observed by *Oliver* and *Ewing* [1958] for continental surface waves from earthquakes. The few points at frequencies below five cycles per second are of doubtful significance, as they are taken from very small amplitudes late in the records.

The motion previously called E_2 fits the M_{II} curve well from 9 to 14 cps. Again the high frequencies drop below the predicted curve, indicating the effect of the thin surface layer. The identification of this event as the fundamental

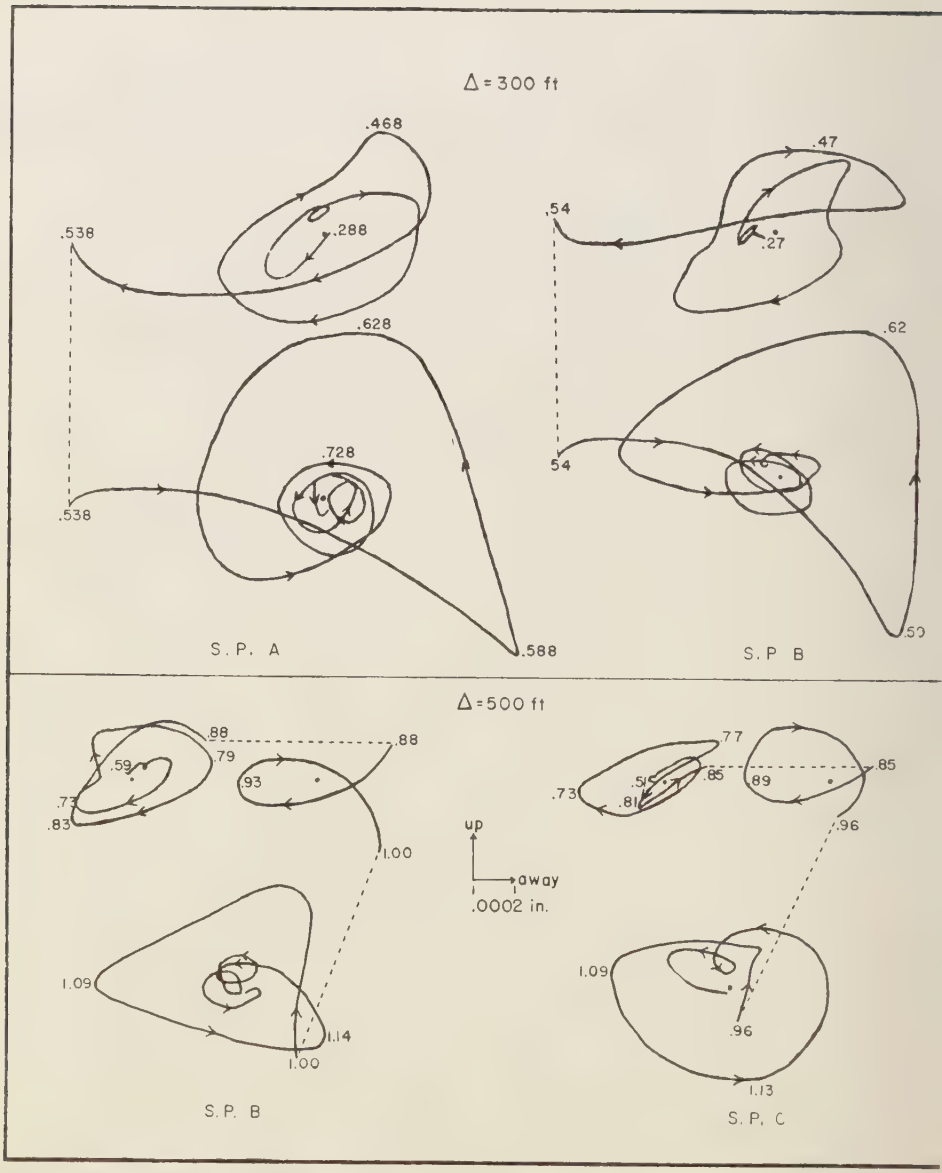

FIG. 4—Comparison of motion obtained at a given distance when source and seismometer location are changed

mode of the M_2 branch seems to be well-supported by both the dispersive properties and the nature of the particle motion.

The E_1 data do not fall on the theoretical curves, though they seem to approach the M_{21} curve at the lower frequencies. The fact that th largest amplitudes occur at the end of the trai would indicate arrivals at a minimum of grou velocity. The actual velocity values are too hig to correspond to the pronounced minimum i

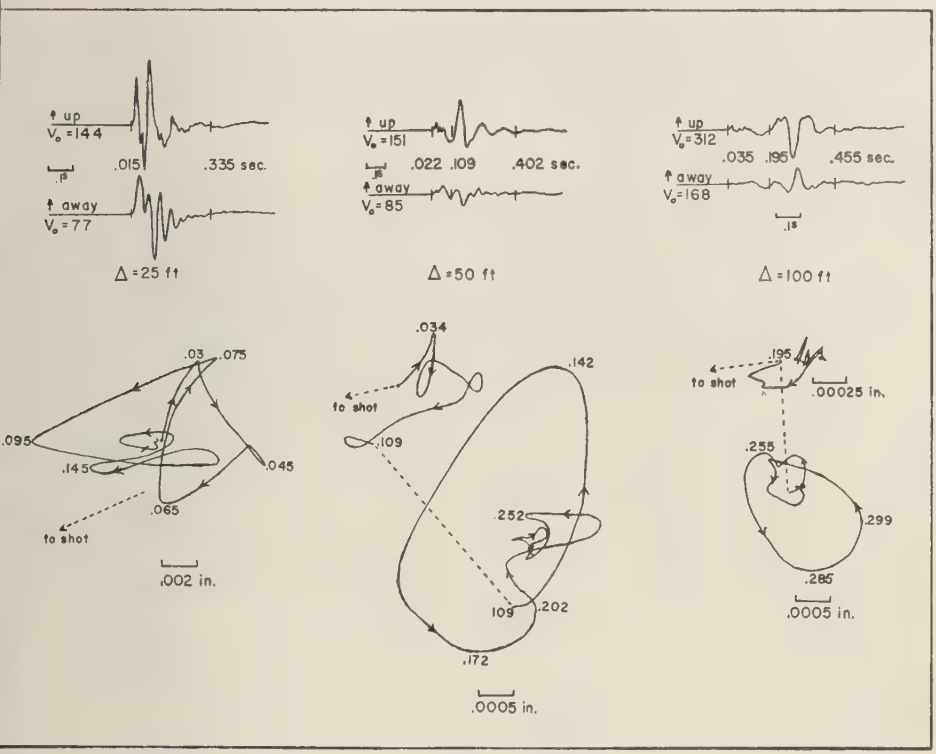

FIG. 5—Records and particle motion diagrams, bottom of ridge

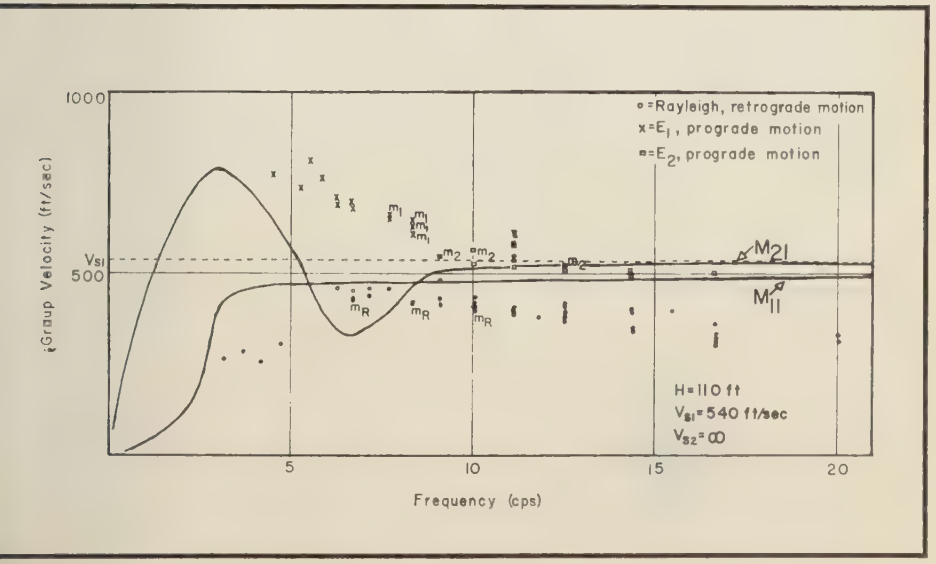

FIG. 6—Dispersion curves, top of ridge

the M_{21} curve; therefore this event must be tentatively identified as a higher mode of one of the branches, perhaps M_{22}.

Summary—The surface wave motion in the longitudinal-vertical plane at the top of the ridge, from a point source at shallow depth, is made up of three distinct events. First, a normally dispersed train with prograde motion and increasing amplitude appears. This is followed by a second prograde event, showing less dispersion in the distance range covered by the observations. The Rayleigh motion is the largest phase at all distances. It consists of a single large retrograde ellipse, followed by a train of much smaller, higher frequency waves.

The dispersion of the Rayleigh wave fits the curve for a layer of thickness equal to the known overburden, overlying a rigid half-space. The second prograde event is identified as the fundamental mode of the M_2 branch of the Rayleigh wave equation, while the first is tentatively identified as a higher mode.

The motion at small distances is a complex combination of these normal modes.

The motion at the bottom of the ridge is much more simple. Well-developed Rayleigh motion is observed at only 50 ft. The higher modes do not seem to be strongly excited.

Acknowledgment—The research upon whic this report is based is part of a program being sup ported by an unrestricted grant to the Departmen of Geophysics and Geophysical Engineering of S Louis University from the Shell Companies Foun dation. The author wishes to express his gratitud for this generous assistance.

References

Dobrin, M. B., P. L. Lawrence, and R. Sengbush Surface and near-surface waves in the Delawar Basin, *Geophysics,* 19, 695–715, 1954.

Ewing, M., W. S. Jardetzky, and F. Press, *Elasti waves in layered media,* McGraw-Hill, Ne York, p. 200, 1957.

Giese, P., Die Bestimmung der elastischen Eigen schaften und der Machtigkeit von Lockerböde mit Hilfe von speziellen Rayleigh-Wellen, *Beit Geophys.,* 66, 274–312, 1957.

Nagamune, T., M_2 waves in a medium with doubl surface layers, *Geophys. Mag. Tokyo,* 27, 345 352, 1956.

Oliver, J., and M. Ewing, The effect of surficia sedimentary layers on continental surface wave *Bull. Seis. Soc. Am.,* 48, 339–354, 1958.

Terzaghi, K., and R. B. Peck, *Soil mechanics i engineering practice,* John Wiley and Sons, Ne York, p. 300, 1948.

Tolstoy, I., and E. Usdin, Dispersive propertie of stratified elastic and liquid media: a ra theory, *Geophysics,* 18, 844–870, 1953.

(Manuscript received May 5, 1958; revised De cember 24, 1958.)

On the Damping of Gravity Waves Propagated over a Permeable Surface

J. N. HUNT

School of Mathematics
Georgia Institute of Technology
Atlanta, Georgia

Abstract—The problem of the damping of small amplitude gravity waves propagated over a permeable sea bed is examined in terms of viscous-flow theory. Previous solutions for the exponential loss of wave height with distance consider either viscous damping over an impermeable bed, for example, *Biesel* [1949], or inviscid potential flow over a permeable bed, *Reid* and *Kajiura* [1957]. A solution is obtained which satisfies the full viscous boundary conditions, and for small values of the viscosity and permeability the damping is found to be the sum of these two solutions. This result agrees reasonably well with measurements by *Savage* [1953] on waves over a smooth sand bed.

It is also found that to a first approximation viscosity slightly lengthens the classical free-wave period in shallow water, while permeability does not.

Introduction—Classical gravity-wave theory as frequently been modified in order to estimate ie viscous dissipation in the boundary layers rigid surfaces such as vertical walls or an npermeable bottom [for example, *Ursell*, 1952; *iesel*, 1949; *Hunt*, 1952]. The effect of propaation over a permeable surface is more difficult determine, since it depends upon the assumed ws of flow in the permeable medium and the oundary conditions at the interface.

Recently *Putnam* [1949] and *Reid* and *Kajiura* 957] have attempted to estimate these losses y showing that Darcy's law is an adequate approximation to unsteady porous flow for this roblem. Their analysis was aimed at determining the dissipation of energy within the ed material due to viscous flow which is actuted by wave-induced pressure fluctuations on ie bottom. In order to simplify the problem, oth papers used the classical irrotational wave olution above a region of viscous porous flow, vith continuity in pressure and vertical velocity t the interface. This leads to a solution in which here is a discontinuity in the horizontal component of velocity at the interface. This does ot represent the real situation very closely, ince in the absence of sand movement along the ed (which would be an additional source of issipation), viscous conditions require the horiontal component of velocity in the water to anish at the bed. In the present paper this ondition, together with continuity of vertical velocity and total vertical stress, leads to a solution for the wave damping which is a function of viscosity, permeability, and porosity. In the case of water waves over a sand bed the porosity is negligible. The method of solution adopted is to expand the wave parameters, which include the damping factor, in powers of two small constants, one proportional to the square root of the kinematic viscosity ν, and the other proportional to the permeability of the sand κ. To the first order in each of these parameters, the damping is found to be the sum of Biesel's solution for zero permeability, and that of Reid and Kajiura for permeability damping where the viscous boundary layer was neglected. To this order of approximation, the wave period is found to be slightly greater than that given by the classical inviscid solution by an amount proportional to $\nu^{1/2}$ but independent of the permeability κ.

The zero order solution in powers of $\nu^{1/2}$ alone indicates that in a situation where neither the permeability nor the porosity is small, there are two possible wave velocities. One is the classical irrotational wave velocity, while the second is somewhat greater by an amount dependent on the porosity of the bed material.

Formulation—We consider a fluid of mean depth h above a porous medium of infinite depth. The fluid is of kinematic viscosity ν, and the porous medium has a permeability κ and porosity θ. Cartesian coordinates are used with the origin at the interface and the y axis vertically upwards.

Small amplitude motions in a viscous fluid may be represented by the velocity components

$$u_1 = -\phi_x - \psi_y \tag{1}$$

$$v_1 = -\phi_y + \psi_x \tag{2}$$

where

$$\nabla^2\phi = 0 \tag{3}$$

$$\nu\nabla^2\psi = \psi_t \tag{4}$$

[*Lamb*, 1945, p. 625].
The pressure, to this order, is given by

$$\frac{p_1}{\rho} = \phi_t - g(y - h) \tag{5}$$

Solutions of (3) and (4) are

$$\phi = (Ae^{Ky} + Be^{-Ky})e^{i(Kx-\sigma t)} \tag{6}$$

$$\psi = (Ce^{my} + D'e^{-my})e^{i(Kx-\sigma t)} \tag{7}$$

corresponding to a wave motion at the free surface of the form

$$\eta = h + A_0e^{i(Kx-\sigma t)} \tag{8}$$

From (4) and (7) we have

$$m^2 = K^2 - \frac{i\sigma}{\nu} \tag{9}$$

so that for real values of σ, (8) represents a progressive wave with a complex wave-number. There is therefore an exponential modulus of decay in the direction of propagation.

If we neglect surface tension, the kinematic and stress conditions at the free surface are

$$\left.\begin{aligned} \eta_t - v_1 &= 0 \\ \frac{\partial v_1}{\partial x} + \frac{\partial u_1}{\partial y} &= 0 \\ -\frac{p_1}{\rho} + 2\nu\frac{\partial v_1}{\partial y} &= 0 \end{aligned}\right\} \quad \text{on} \quad y = \eta \tag{10, 11, 12}$$

For the permeable medium we use equations of motion of the form used by Reid and Kajiura, namely

$$\left.\begin{aligned} \frac{1}{\theta}\frac{\partial u_2}{\partial t} &= -\frac{\nu}{\kappa}u_2 - \frac{1}{\rho}\frac{\partial p_2}{\partial x} \\ \frac{1}{\theta}\frac{\partial v_2}{\partial t} &= -\frac{\nu}{\kappa}v_2 - \frac{1}{\rho}\frac{\partial p_2}{\partial y} \end{aligned}\right\} \tag{13}$$

or

$$\left.\begin{aligned} u_2 &= \frac{1}{Q}\frac{\partial p_2}{\partial x} \\ v_2 &= \frac{1}{Q}\frac{\partial p_2}{\partial y} \end{aligned}\right\} \tag{14}$$

where

$$Q = \rho\left(\frac{i\sigma}{\theta} - \frac{\nu}{\kappa}\right) \tag{15}$$

Continuity requires that $\nabla^2 p_2 = 0$, so we seek a solution of the form

$$p_2 = \text{constant} + (Ee^{Ky} + Fe^{-Ky})e^{i(Kx-\sigma t)} \tag{16}$$

We now stipulate that the real part of K shall be positive, so that waves are propagated in the positive x direction. Thus for the amplitude of the motion to be bounded at great depths we require

$$F = 0 \tag{17}$$

The boundary conditions to be satisfied at the interface $y = 0$ are zero horizontal velocity in the fluid,

$$u_1 = 0, \tag{18}$$

continuity in the vertical component of velocity,

$$v_1 = v_2, \tag{19}$$

and continuity of vertical stress,

$$-\frac{p_1}{\rho} + 2\nu\frac{\partial v_1}{\partial y} = -\frac{p_2}{\rho} + 2\nu\frac{\partial v_2}{\partial y}. \tag{20}$$

We now substitute for p_1, p_2, η, u_i, v_i from equations (6) to (8), (14), (16) in the six boundary conditions (10) to (12) and (18) to (20). Eliminating the unknown constants A, B, C, D', E, A_0 leads to a sixth order determinant from which the wave characteristics are to be found. For the sake of space, this determinant will not be written out in full, but some manipulation and simplification leads to the equation

$$\left(\frac{1}{\rho\nu} - \frac{2K^2}{Q}\right)\{\sigma^2(i\sigma - 2K^2\nu)(K \sinh mh \sinh Kh - m \cosh mh \cosh Kh)$$
$$+ 4i\sigma K^3\nu^2 m(m \sinh mh \sinh Kh - K \cosh mh \cosh Kh + K)$$
$$+ gK(i\sigma - 2K^2\nu)(m \cosh mh \sinh Kh - K \sinh mh \cosh Kh)\}$$
$$+ \frac{m}{Q}\{-4i\sigma K^3\nu^2 m \sinh mh \cosh Kh - gK(i\sigma - 2K^2\nu) \cosh mh \cosh Kh$$
$$+ \sigma^2(i\sigma - 2K^2\nu) \cosh mh \sinh Kh\} = 0 \qquad (21)$$

Zero porosity and permeability—As a particular se, we may take the limit of zero porosity and rmeability; that is, flow over a rigid impermeble bed. In this case boundary conditions (10) (12) still apply at the free surface, together th

$$u_1 = v_1 = 0$$

$y = 0$. The eliminant now consists of a fifth der determinant which reduces to

$$(i\sigma - 2K^2\nu)(K \sinh mh \sinh Kh$$
$$- m \cosh mh \cosh Kh)$$
$$- 4i\sigma K^3\nu^2 m(m \sinh mh \sinh Kh$$
$$- K \cosh mh \cosh Kh + K)$$
$$- gK(i\sigma - 2K^2\nu)(m \cosh mh \sinh Kh$$
$$- K \sinh mh \cosh Kh) = 0 \qquad (22)$$

learly (22) could have been derived from (21) y taking the limit as $Q \to \infty$. We seek a solution of (22) in powers of the kinematic viscosity f the form

$$\left.\begin{aligned} \sigma &= \sigma_0 + \sigma_1\nu^{\frac{1}{2}} + \sigma_2\nu + \cdots \\ K &= k + iD \\ D &= D_1\nu^{\frac{1}{2}} + D_2\nu + \cdots \\ m &= m_0\nu^{-\frac{1}{2}} + m_1 + m_2\nu^{\frac{1}{2}} + \cdots \end{aligned}\right\} \qquad (23)$$

where the σ_n and D_n are real, since we postulate a motion which is strictly periodic in time with a prescribed wave number k. Substituting these expansions in (22), equating powers of $\nu^{1/2}$, and taking real and imaginary parts, we find

$$\sigma_0^2 = gk \tanh kh \qquad (24)$$

$$\sigma_1 = -\frac{gk^2}{(2\sigma_0)^{\frac{1}{2}} \cosh^2 kh} \qquad (25)$$

with

$$m_0 = (1 - i)(\sigma_0/2)^{\frac{1}{2}} \qquad (26)$$

$$m_1 = \frac{(i + 1)k\sigma_0}{4 \sinh 2kh} \qquad (27)$$

and

$$D_1 = \frac{2k^2}{(2\sigma_0)^{\frac{1}{2}}(2kh + \sinh 2kh)} \qquad (28)$$

The attenuation of wave amplitude with distance, in the absence of porosity, is therefore given to this degree of approximation by the factor

$$\exp\left\{-\frac{2k^2\nu^{\frac{1}{2}}x}{(2\sigma_0)^{\frac{1}{2}}(2kh + \sinh 2kh)}\right\} \qquad (29)$$

which agrees with the known result [*Biesel*, 1949; *Hunt*, 1952].

Equation (25) appears to be a new result showing that a strictly periodic wave motion in shallow water is possible only with a period τ which is slightly longer than that given by the classical inviscid solution $\tau_0 = 2\pi/\sigma_0$. To this approximation the wave period is

$$\tau = 2\pi\left\{(gk \tanh kh)^{\frac{1}{2}} - \frac{gk^2\nu^{\frac{1}{2}}}{(4gk \tanh kh)^{\frac{1}{2}} \cosh^2 kh}\right\}^{-1}$$
$$= \frac{2\pi}{\sigma_0 - (\sigma_0\nu/2)^{\frac{1}{2}}k \operatorname{cosech} 2kh} \qquad (30)$$

which differs only slightly from the inviscid solution except in extremely shallow water where the expansions (23) converge so slowly as to render (30) a weak approximation. For example,

$kh = 2\pi$: $\tau \doteq \tau_0(1 + 1.9 \times 10^{-9}\, h^{-\frac{1}{2}})$

$kh = \pi$: $\tau \doteq \tau_0(1 + 6.3 \times 10^{-7}\, h^{-\frac{1}{2}})$

$kh = \pi/2$: $\tau \doteq \tau_0(1 + 9.0 \times 10^{-6}\, h^{-\frac{1}{2}})$

where h is measured in centimeters. The correction may become measureable for values of the wavelength of the order of $10h$ or more, in depths of only a few centimeters. In deep water, however, the effect is certainly negligible.

General solution—We now seek a solution of (21) for non-zero permeability or porosity. Before determining the order of magnitude of Q, and the appropriate method of solution, it is of interest to consider the expansion of (21) in ascending powers of $\nu^{1/2}$, treating Q as an arbitrary constant. The largest terms in (21) are of order $\nu^{-1/2}$ and give

$$\rho\sigma_0(\sigma_0^2 \sinh kh - gk \cosh kh)$$

$$+ iQ(-\sigma_0^2 \cosh kh + gk \sinh kh) = 0 \quad (31)$$

where

$$Q = \rho\left(\frac{i\sigma}{\theta} - \frac{\nu}{\kappa}\right)$$

Equating real and imaginary parts to zero, we find two possible modes of oscillation

$$\sigma_0^2 = gk_0 \tanh k_0h \quad (32)$$

$$\sigma_0^2 = gk_0\left(\frac{\tanh k_0h + \theta}{1 + \theta \tanh k_0h}\right) \quad (33)$$

where k_0 denotes the first approximation as ν approaches zero.

It is clear that in the limit as either the permeability κ or the porosity θ vanishes, then only the first mode (32) can exist, given by the principal term in (31). It would be of interest to know if waves can in fact be propagated according to the second mode (33) when permeability and porosity of the bed material are of the same order of magnitude. For the present application, wave propagation over sand, Reid and Kajiura have shown that since the permeability of ordinary sand is of order 10^{-6}cm^2 and the kinematic viscosity of water is of order 10^{-2}cm^2/sec, then $\nu/\kappa \sim 10^4$sec^{-1}, and the porosity term may be neglected. Thus the acceleration terms are neglected in comparison with the viscous terms, and the equations of motion in the sand reduce to Darcy's law. It follows that in this instance only the first mode of propagation (32) is of importance. The constant Q now reduces to

$$Q = -\rho\nu/\kappa.$$

We now solve (21) for Kh in terms of two small and independent non-dimensional parameters

$$\alpha = \kappa\sigma_0/\nu$$

$$\beta = \frac{1}{h}\left(\frac{\nu}{2\sigma_0}\right)^{\frac{1}{2}}$$

subject to the condition that as α and β appro zero, the solution for Kh shall approach classical irrotational result given by (32). Eq tion (21) also determines mh which has a sin larity at $\nu = 0$. To obtain the wave dampi however, we need only find the first terms the expansion of Kh.

Let us for brevity introduce the notation

$$Kh = Y, \qquad mh = X, \qquad \sigma^2h/g = C,$$

where

$$Y = Y(C, \alpha, \beta)$$

and

$$X = X(C, \alpha, \beta)$$

and assume a Taylor expansion for Y abo $\alpha = \beta = 0$ of the form

$$Y = Y(C, 0, 0) + \alpha Y_\alpha(C, 0, 0)$$

$$+ \beta Y_\beta(C, 0, 0) + \cdot$$

Using such an expansion, we regard σ^2h/g being assigned, and we shall find a correcti term of order $\nu^{1/2}$ to be added to kh. On the oth hand, we could assume k (and $\lambda = 2\pi/k$) to assigned and determine the correction to σ_0 in the expansions (23) above, but it is not nece sary to carry out both procedures, as eith result can be obtained from the other.

The principal terms in (21) are written

$$C(Y \tanh X \tanh Y - X)$$

$$+ Y(X \tanh Y - Y \tanh X$$

$$+ i\alpha X(C \tanh Y - Y) = 0$$

which is to be solved simultaneously with (9 which can be written

$$2\beta^2(X^2 - Y^2) + i = 0$$

The constants Y_α and Y_β are found by differ entiating both equations, first with respect to α and then with respect to β, and setting $\alpha = \beta = 0$. The resulting expressions are

$$Y_\alpha = \frac{2ik_0h}{2k_0h + \sinh 2k_0h}$$

$$Y_\beta = \frac{2(1+i)k_0^2h^2}{2k_0h + \sinh 2k_0h}$$

so that to the first order in α and β we find

$$Kh = kh + iDh$$

where

$$k = k_0 + \left(\frac{\nu}{2\sigma_0}\right)^{\frac{1}{2}} \frac{2k_0^2}{2k_0h + \sinh 2k_0h} \qquad (34)$$

and

$$D = \left(\frac{\kappa\sigma_0}{\nu}\right) \frac{2k_0}{2k_0h + \sinh 2k_0h} + \left(\frac{\nu}{2\sigma_0}\right)^{\frac{1}{2}} \frac{2k_0^2}{2k_0h + \sinh 2k_0h} \qquad (35)$$

It is clear that to this order of approximation the total wave damping is the linear sum of the viscous damping given by (28), where permeability was neglected, and the result obtained by Reid and Kajiura for permeability damping, where the viscous boundary layer was neglected.

Boundary layer approximation—It is of interest to consider further the equations of motion which have been adopted for the solution within the main body of the fluid. In equations (3) and (4) and the free surface conditions (10) to (12) the entire flow is regarded as viscous, a condition which we know exists at small Reynolds numbers. In the present problem this suggests an upper bound on the wave amplitude for the method of solution to be valid. For slightly greater wave amplitudes (still small compared with the wavelength), the effect of viscosity is confined to a region in close proximity to the bed, so that (7) must take the form

$$\psi = D'e^{-my}e^{i(Kx-\sigma t)} \qquad (36)$$

where the real part of m is positive. The free surface conditions are now the inviscid conditions

$$\eta_t - v_1 = 0, \qquad p_1 = 0 \qquad (37)(38)$$

The conditions at $y = 0$ are (18) to (20) as before. The eliminant is now of the fifth order and reduces to

$$i\left(1 - \frac{2K^2\rho\nu}{Q}\right)\{\sigma^2(m\cosh Kh - K\sinh Kh) - gK(m\sinh Kh - K\cosh Kh)\} + \frac{\rho m\sigma}{Q}(gK\cosh Kh - \sigma^2\sinh Kh) = 0 \qquad (39)$$

After substituting expansions (23) in (39), we find it to be identical in terms of order $\nu^{-1/2}$ and order unity with (21) of the full viscous solution. Consequently the solution for Kh agrees to this order with that given by (34) and (35). Thus it is not necessary to include the full viscous boundary conditions at the free surface when proceeding only to terms of order $\nu^{1/2}$ in the solutions for σ and Kh, although the full viscous conditions at the bed must be retained. The solution for D is restricted to wave amplitudes which are small in comparison with the wavelength, and also to depths which are large enough for β to be small, a condition which is almost invariably satisfied.

Comparison with experiment—The loss of amplitude of waves propagated over a permeable surface has been measured by *Savage* [1953]. The measurements were made on waves traveling along a tank of approximately equal width and depth. Viscous damping on the vertical walls was therefore of the same order as that at the bed, and we need to add to equation (35) a term representing this additional dissipation. This term is known [*Hunt*, 1952, equation (22)], so that in a channel of width b equation (35) must be replaced by

$$D = \left(\frac{\nu}{2\sigma_0}\right)^{\frac{1}{2}} \frac{2k_0^2}{2k_0h + \sinh 2k_0h}\left(1 + \frac{\sinh 2k_0h}{bk}\right) + \left(\frac{\kappa\sigma_0}{\nu}\right) \frac{2k_0}{2k_0h + \sinh 2k_0h} \qquad (40)$$

The comparison between (40) and Savage's measurements for both permeable and impermeable smooth beds show surprisingly close agreement. In the case of an impermeable smooth bed, the first two terms of (40) account for 80 per cent of the measured loss in wave height, while in the case of a permeable bed, (40) accounts for 90 per cent of the measured loss in height. It is tempting, therefore, to imagine that the inclusion of higher order terms in the expansions in powers of α and β would account for these small errors. Savage's report, however, also shows the increased loss of wave energy which is caused by a stable rippled sand bed, depending on the height of the ripples, and the even greater loss which occurs when the bed is unstable, that is, under the effect of varying incident wave periods and amplitudes. Such conditions frequently occur in nature and a far

more difficult problem than that treated here is to estimate the energy dissipated in turbulence above a rippled bed, and in moving the bed material.

It appears reasonable to conclude that we have a fairly accurate means of estimating wave damping under rather artificial 'smooth-bed' conditions, as are sometimes present in hydraulic models, but we have only an incomplete picture of the wave dissipation process which occurs in nature.

Acknowledgments—I should like to thank R. O. Reid for his valuable comments on an earlier draft of this paper and for drawing my attention to the *Beach Erosion Board Technical Memorandum 31*.

This paper represents part of an investigation supported by the Engineering Experiment Station of Georgia Institute of Technology.

References

Biesel, F., Calculation of wave damping in a viscous liquid of known depth, *Houille Blanche* **4**, 630–634, 1949.

Hunt, J. N., Viscous damping of waves over an inclined bed in a channel of finite width, *Houille Blanche*, **7**, 836–842, 1952.

Lamb, H., *Hydrodynamics*, Dover Publs., New York, (6th ed.), 738 pp., 1945.

Putnam, J. A., Loss of wave energy due to percolation in a permeable sea bottom, *Trans. Am. Geophys. Union*, **30**, 349–356, 1949.

Reid, R. O., and K. Kajiura, On the damping of gravity waves over a permeable sea bed, *Trans. Am. Geophys. Union*, **38**, 662–666, 1957.

Savage, R. P., Laboratory study of wave energy losses by bottom friction and percolation, *Beach Eros. Bd., Tech. Memo. 31*, 28 pp., 1953.

Ursell, F., Edge waves on a sloping beach, *Proc. Roy. Soc. London, A*, **214**, 79–97, 1952.

(Manuscript received July 28, 1958; revised January 12, 1959.)

Annual Mass and Energy Exchange on the Blue Glacier*

E. LACHAPELLE

University of Washington
Seattle, Washington

Abstract—Field work and techniques of observation at the IGY station at 2010 meters elevation on the Blue Glacier, Mount Olympus, western Washington State, are briefly described. The annual mass exchange on this glacier is large. Only very shallow penetration of subfreezing temperatures occurs, and the winter energy deficit is due almost entirely to increased ice mass. The 1958 ablation season, being long and hot, resulted in a specific mass deficit of 1.7 meters of water and a corresponding specific energy gain of 1.36×10^4 cal/cm^2. During the 1958 melt season the principal sources of heat to the melting snow surface were, in order of importance, solar radiation, eddy conduction, and water vapor condensation. Of this heat, 64.4 per cent was used for ice melt, and the remainder was lost to long-wave radiation cooling and heat of vaporization. Net water vapor transfer at the snow surface was small, but it played a measurable role in the over-all heat balance.

Introduction—The Blue Glacier is situated on the northern flanks of the Mount Olympus massif in the central mountain area of the Olympic Peninsula, western Washington State. From an elevation of 2350 meters at the head of the accumulation zone it descends in two separate ice falls which coalesce to form a valley ice stream with a terminus at 1270 meters elevation. Total area of the Blue Glacier is 4.28×10^6m^2. Morphologically it is a temperate alpine valley glacier with a high annual mass turnover caused by heavy winter snowfall and strong summer ablation. The Blue and adjacent glaciers are the lowest bodies of active glacial ice in the continental United States. These glaciers are nourished by the heaviest annual precipitation in the United States; at higher elevations the precipitation is mostly in the form of snow.

As a part of the USNC-IGY program for glaciology in North America, a research station was established on the Blue Glacier in July of 1957 by the University of Washington. It was manned continuously thereafter for a period of 14 months. The summer of 1957 was spent in constructing the station buildings, installing the power plant and instrumentation, and maintaining routine snow and weather records. By late August this preliminary work was completed, and full-scale observations were initiated. These included standard climatological records, snow melt and accumulation, ice flow, continuous records of wind velocity and air temperature, cloud cover and type, humidity, and types and density of solid precipitation. Automatic recording instruments charted continuous values of incoming and reflected solar radiation, net radiation balance, and total incoming radiation over the snow surface. Daily readings were taken of internal temperatures in the 1958 snow cover and underlying firn. Pits were dug at intervals in the snow cover to give information on snow density, hardness, and stratigraphy; and these data, together with information from a resistance wire settlement gauge, were used to plot a time profile of snow-cover evolution. In addition to these continuous records, an intensive micrometeorological study of energy exchange at a melting snow surface was conducted for approximately six weeks during the summer of 1958. Details of this study are given below in the discussion of the glacier energy budget. At the beginning of the melt season in early May, ablation stakes were planted widely over the glacier. A total of 85 were used at the height of summer melt. These stakes, together with periodic photographs of the snow line position and an extensive accumulation survey in late August of 1958, served as the basis for calculating the annual mass budget.

Mass budget—During the 1957–1958 accumulation season precipitation totaled 301 cm of water in the form of snow at the Snowdome observation station. In addition, 12.3 cm of water

* Contribution no. 42, Department of Meteorology and Climatology, University of Washington.

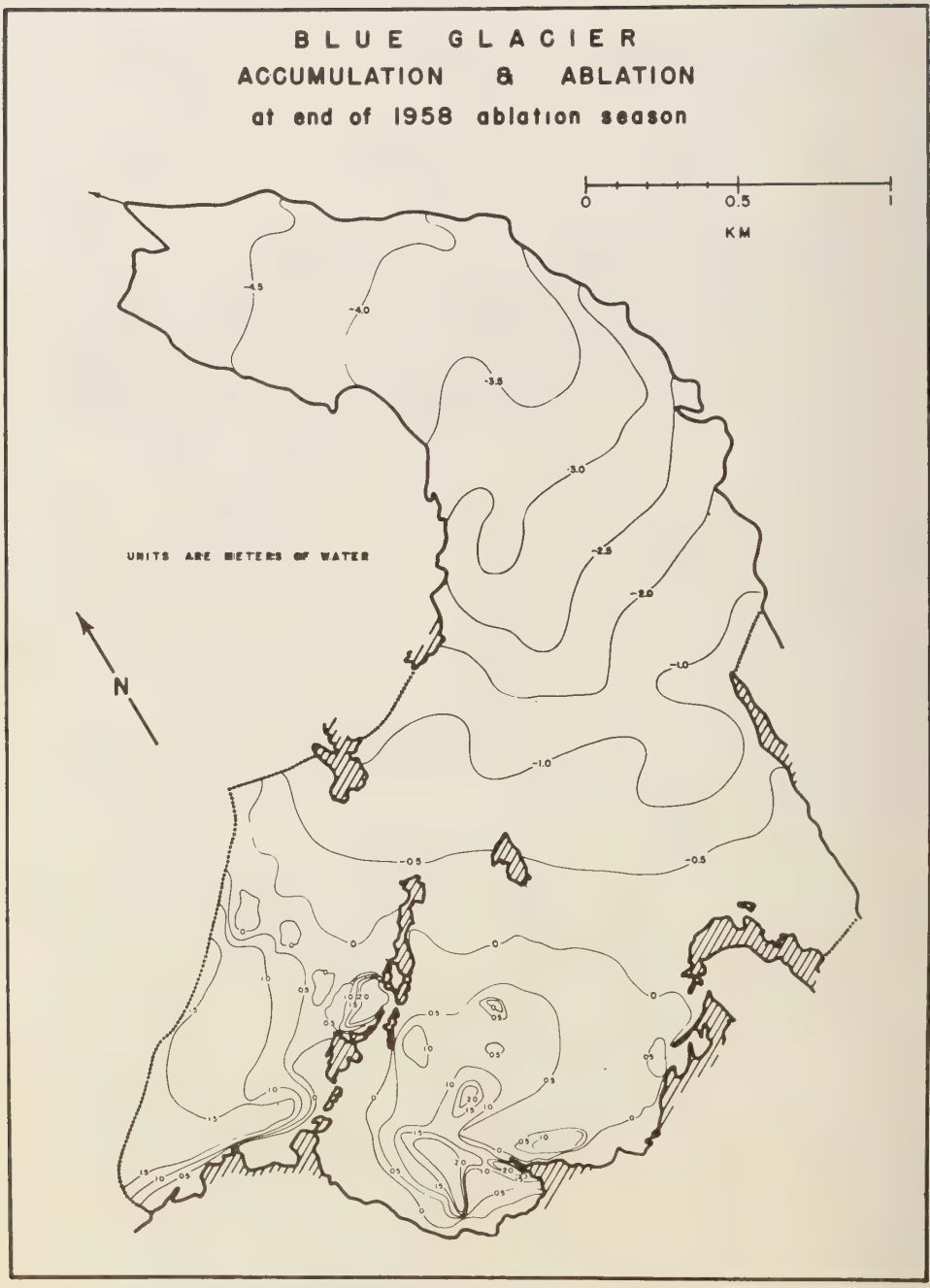

FIG. 1—Blue Glacier accumulation and ablation

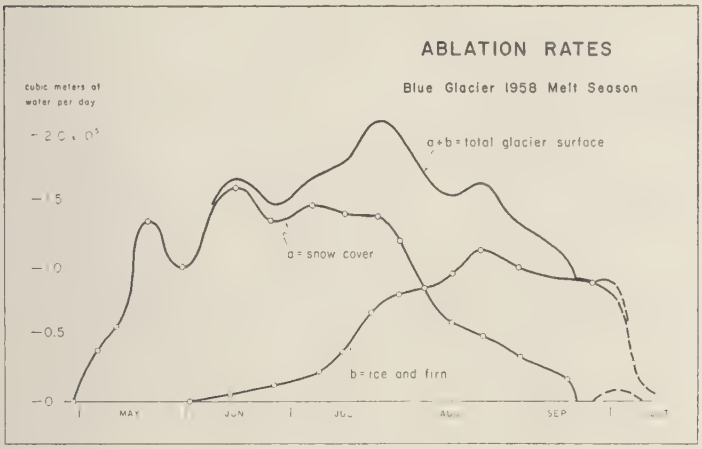

FIG. 2—Ablation rates

ell as rain during the winter and froze within he snow cover to become part of the total ice .ccumulation of 313.3 cm water equivalent. This olid precipitation was in the form of unusually dense snow. The mean density of new snowfalls vas 0.22 g/cm^3, which is over twice the average density of 0.1 usually cited for alpine snowfalls. This high density persisted throughout most of he winter in each new fall of snow, and it appears to be a climatological characteristic of the area. Atmospheric conditions favoring the formation of a large percentage of needle crystals appear to be primarily responsible for this high density.

Snow accumulation on the ground reached a naximum depth of just over 6 meters at the observation station. On the lower part of the glacier this accumulation was 4 to 5 meters, while in the zones of accumulation maxima in he cirque and upper reaches of the Snowdome t reached 10 meters and more. From these accumulation data the maximum total Blue Glacier accumulation (in the solid state) is computed to be 15.0×10^6 cubic meters of water, and the specific accumulation (average depth) s computed to be 3.5 meters of water.

Ablation of this 1958 accumulation began on April 30 and continued, with two short interruptions by cold weather in late May and late June, until late September. The summer of 1958 was long and hot and the snow line recreated up-glacier to an elevation of 2100 meters, some 400 meters higher than the developed firn limit which has marked the annual snow line position in the past several years. Total melt from the 1958 snow cover is computed to be 14.1×10^6 cubic meters of water, a specific loss of 3.3 meters of water.

Following the retreat of the annual snow line, ablation of the exposed ice and firn accounted for an additional loss of 8.0×10^6 cubic meters of water, a specific loss of another 1.9 meters of water. These gains and losses are mapped for the end of the ablation season in Figure 1. The total ablation for the 1958 season for the entire glacier is thus $14.1 \times 10^6 + 8.0 \times 10^6 = 22.1 \times 10^6$ cubic meters of water. This figure exceeded the total annual accumulation by 7.1×10^6 cubic meters of water, the net annual deficit for 1958. This amounts to a specific annual deficit of 1.7 meters of water. The few available records on ice depths in the Blue Glacier suggest that this deficit may be approximately one to two per cent of the total glacier mass.

These budget figures are derived in part from calculation of the ablation rate at selected intervals for both the 1958 snow cover and the exposed area of ice and firn. Figure 2 shows these rates, and their sum, plotted as functions of time. Such curves display the combined effects of weather and glacier topography on the mass budget for any given season. Here the extensive retreat of the 1958 snow line has resulted in strong late-season ablation by uncovering large areas of firn and ice, even though the rate of surface wastage diminished after mid-August.

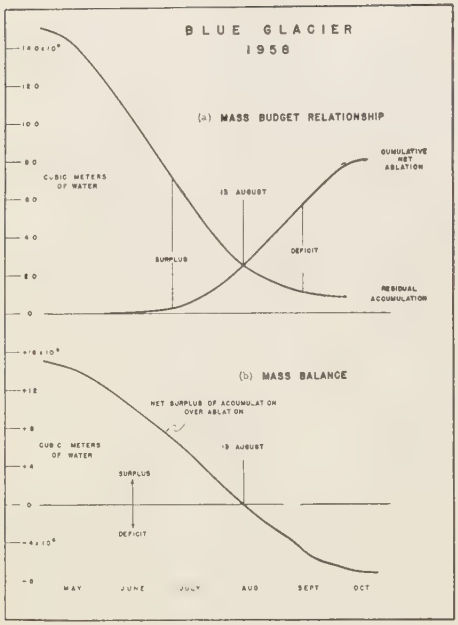

FIG. 3—(a) Mass budget relationship
(b) Mass balance

Examination of the area under the firn and ice melt curve shows that half the total ablation from this part of the glacier (net loss after removal of the winter snow cover) occurred after August 27.

The cumulative net ablation and residual accumulation are plotted in Figure 3a, and the difference between the curves of Figure 3a, the mass balance, is plotted in Figure 3b.

Energy budget—The mass and energy budgets of a thermally temperate glacier are related in the following manner [*Hubley*, 1957a]:

$$\Delta E = -k\Delta M_i \qquad (1)$$

where

ΔE = annual increment of energy
ΔM_i = annual increment of ice mass
k = heat of fusion of ice

During the accumulation season the total mass of ice in the glacier increases, as does its capacity as a heat sink. During the ablation season the glacier gains energy from its environment at the expense of ice mass loss. The ice flow rate is so low that the kinetic energy term in the glacier energy balance is neglected as insignificant compared with the total annual surface heat exchange, as is the heat flow at the ice-earth interface. A loss of potential energy by meltwater runoff also occurs, but this, too, is small compared with the surface exchange of thermal energy. It must be emphasized that the energy gain of a glacier is related to the change of state during the ablation season. This change of state is generally and approximately, but not necessarily, equal to mass *loss* due to liquid runoff. In addition to the energy deficit for the accumulation season explicitly given in (1), an energy deficit is developed by cooling of the firn below freezing and deposition of cold snow. In a thermally temperate glacier this is usually small compared with the deficit due to increased ice mass. In the highly maritime climate experienced by Blue Glacier, this deficit is very small. Figure 4 illustrates the distribution of subfreezing temperatures in snow and firn throughout the winter as observed at the Snowdome station, an area representative of the upper glacier. On the lower glacier the winter cooling is probably even more mild. Two factors are responsible for the shallow penetration of subfreezing temperatures to only 4 meters depth in the firn. One is the recurrence of rainstorms throughout the winter, with rapid snow cover warming by transfer of heat through the medium of percolating water, and the other is the heavy insulation provided by the deep snow cover. On the basis of these snow temperature records, the contribution of winter cooling to the energy deficit is calculated to be 2.5 per cent of the mass energy deficit. Most of this small cooling deficit is eventually converted to a mass energy deficit by the refreezing of percolated rain and melt water. In calculating the 1958 Blue Glacier energy budget, it is thus possible to treat the total ice mass gain as the only significant source of energy deficit.

The specific mass accumulation on the Blue Glacier in 1958 has been shown to be 3.5 meters of water in the form of ice, or 350 g ice/cm^2. The specific energy deficit is found by equation (1) to be 2.80×10^4 cal/cm^2. The total specific ablation of 520 g/cm^2 (5.2 meters of water) corresponds to an energy gain of 4.16×10^4 cal/cm^2. The difference between these two energy figures is 1.36×10^4 cal/cm^2, a specific net energy surplus for the 1958 budget year which can be multiplied by the glacier area to

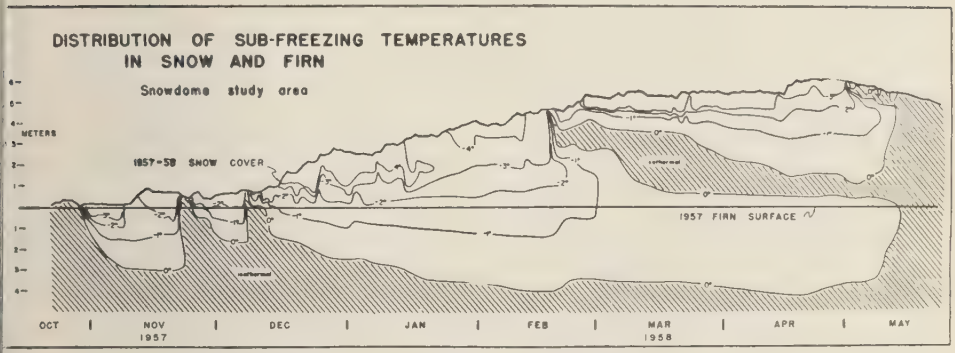

FIG. 4—Distribution of subfreezing temperatures in snow and firn

give a total energy surplus of 5.8×10^{14} cal. Figure 5 displays the annual trend of the Blue Glacier energy balance.

This energy surplus represents energy drawn by the glacier from its environment and absorbed as heat of fusion. Part of the program of observations on the Blue Glacier has been to assess the number and relative importance of factors involved in this energy transfer. Toward this end micrometeorological data were collected on energy transfer at a melting surface for over a month during the height of the 1958 melt season. This was a period of almost continuously calm, clear weather, when it was possible to define quite accurately the fair-weather contributions to snow melt at this latitude and altitude. The investigation did not include observations over a bare ice area, and the following discussion is restricted to energy exchange at the 1958 snow surface.

The energy transfer at a melting snow surface for a given time interval may be expressed by the following relation [*Sverdrup*, 1936; *Hubley*, 1957b]:

$$R_s\downarrow + R_L\downarrow + Q\downarrow + bV\downarrow + c(T_p - T_s)P\downarrow = R_s\uparrow + R_L\uparrow + Q\uparrow + bV\uparrow + kI \qquad (2)$$

where

R_s = short-wave radiation flux, cal/cm²
R_L = long-wave radiation flux, cal/cm²
Q = heat transfer by eddy conduction, cal/cm²
V = water vapor condensation or evaporation, g/cm²
P = precipitation, g/cm²
$(T_p - T_s)$ = temperature difference between liquid precipitation and snow surface, °C
k = heat of fusion of water
b = heat of vaporization of water
I = ice melt, g/cm²
c = specific heat of water

(Arrows indicate heat transfer to or away from the surface.)

The term for heat conduction from below the snow surface is omitted for isothermal snow. In this investigation the terms R_s, V, I, P, T_p, and the net radiation balance $(R_s\downarrow - R_s\uparrow + R_L\downarrow - R_L\uparrow)$ have been measured directly. The value of $(R_L\downarrow - R_L\uparrow)$ is deduced from the latter by subtracting the independently measured incoming and reflected solar radiation. Wind velocity and air temperature distribution near the snow surface were also obtained, but for calculation of the following data, Q has been taken as the residual in equation (2) and assigned a value consistent with energy conservation. All radiation data were recorded continuously, V every two to four hours, I every eight hours, and P every 24 hours. On the basis of these observations, the energy exchange has been computed for 24-hour intervals ending at 2000 hours each day for a total of 37 days of acceptable data. These days all fell within the period between July 12 and August 20, 1958. The heat sources and sinks at the snow surface are shown graphically in Figure 6 for each of these days. For the 37-day period the total energy transfer to the snow surface amounted to 15,600 cal/cm². Of this quantity, 69.3 per cent was contributed by absorbed solar radiation, 24.6 per cent by eddy

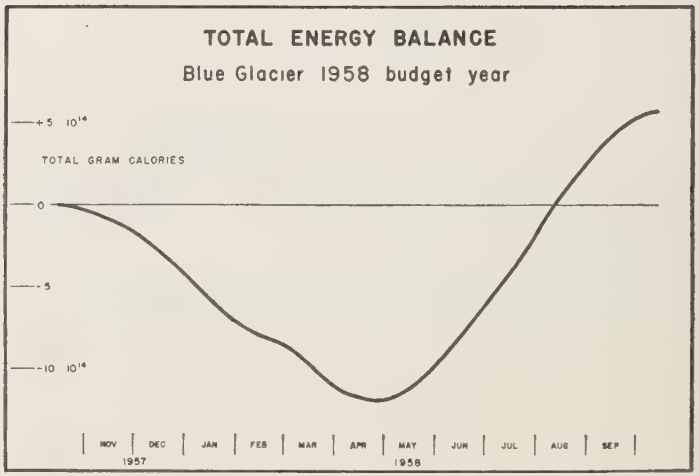

FIG. 5—Total energy balance

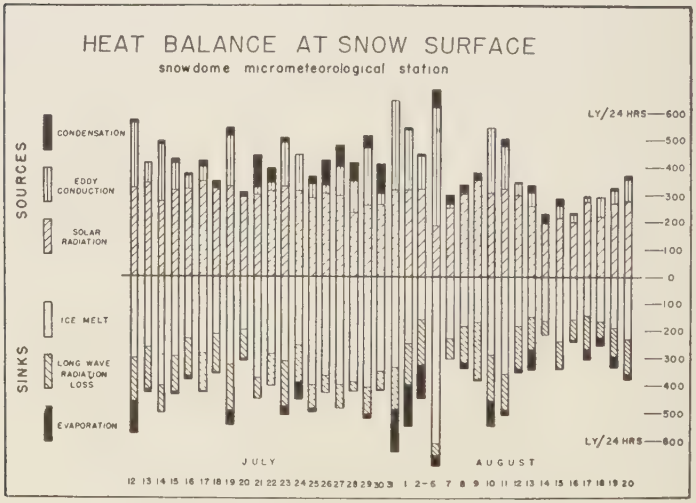

FIG. 6—Heat balance at snow surface

conduction, 6.1 per cent by condensation, and 0.006 per cent by precipitation. From the 15,600 cal/cm² so delivered to the snow surface, 28.0 per cent was lost as net long-wave radiation cooling ($R_L\downarrow - R_L\uparrow$), 7.6 per cent was absorbed as heat of vaporization, and the remaining 64.4 per cent was available for ice melt.

The albedo of the 1958 snow surface during this period of study fluctuated between 0.55 and 0.65 and had a mean value of 0.59. The net positive solar radiation balance averaged 293 langleys per day. Actual radiation heat supply available for ice melt was reduced substantially by a net long-wave radiation balance which was negative throughout the study period except for a few short intervals of overcast sky. This radiation loss from the snow surface amounted to an average of 120 langleys per day. Direct daily measurements showed subsurface ice melt by transmitted solar radiation to be 12 per cent of the total ice melt. Three-fourths of this internal melt occurred within the first 15 cm

elow the surface. Direct, calorimetric measurements showed that only two langleys per day were available for ice melt below the 20-cm evel on a clear day in midsummer.

Total measured condensation during the 37 lays of observation was 1.59 g/cm². This repreented a liquid water contribution at the snow urface equal to 1.2 per cent of the total melt; t exceeded the 0.76 g/cm² of precipitation vhich fell during the same period. The mass gain from condensation was entirely negated by evaporation losses of 1.94 g/cm², which gave a net vapor transfer deficit of 0.35 g/cm². The resulting net energy exchange from vapor transfer was thus 210 cal/cm² for the 37 days. The small masses involved in condensation and evaporation yielded a significant amount of heat transfer, but, for this area in midsummer of 1958, the net heat transfer at the snow surface from this source was small. During fair weather the vapor transfer followed a regular diurnal pattern of condensation in the afternoon and evaporation at night and in the early morning. The daily changeover to condensation was generally accompanied by a rise in the free air dew point, and it often coincided with afternoon cumulus activity over the mountains. A similar diurnal pattern of vapor transfer, though of different time phase, has been noted over snowfields at an elevation of 10,000 ft in the Rocky Mountains of Colorado (M. Martinelli, private communication, 1958).

Independent computation of sensible heat transfer through eddy conduction from the air has been complicated by location of the micrometeorological station on the crest of a sloping snow plateau. The slightly higher snowfields to the south produce during calm, fair weather an irregular and fitful drainage wind which is disturbed by each vagary of the prevailing free wind. Sensitive anemometry has clearly delineated the pattern of this drainage wind and has shown its maximum velocity to vary from one to two meters above the snow surface, but the consequent irregular wind profiles do not readily lend themselves to heat transfer calculations. Sharp discontinuities in both velocity and direction were common in the first 8 meters above the snow surface. Eddy conduction was the dominant source of heat for ice melt on only one day of the observation period, August 6. The weather at this time consisted of a strong west wind, air temperatures around 8°C, low thin clouds and fog, and occasional very light precipitation. It is interesting to note that the single highest 24-hour ice melt of the 1958 season occurred on this day, although air temperatures were well below normal and the net positive radiation heat balance was only half that of a clear day. This is conspicuous evidence of the importance of wind velocity to snowmelt.

Acknowledgments—Particular credit is due to James Hawkins, Yves Eriksson, and Roger Ross of the Blue Glacier Project staff, whose perseverance made the collection of these data possible. Acknowledgment is made of the USNC-IGY grant which basically supported this work, and thanks are also due to the National Park Service, the United States Air Force, and especially to William Fairchild who piloted the project's light ski plane throughout the field operation. Without the support of these agencies and persons, this work could not have been carried out.

References

Hubley, R. C., *Glacier research on Mt. Olympus, Olympic National Park, Washington,* AINA Contract Final Report, 12 pp., 1957a.

Hubley, R. C., An analysis of surface energy exchange during the ablation season on Lemon Creek Glacier, Alaska, *Trans. Am. Geophys. Union,* 38, 68–85, 1957b.

LaChapelle, E., Winter snow observations on Mt. Olympus, *Proc. Ann. Meeting Western Snow Conf.,* 5 pp., 1958 (to be published).

Sverdrup, H. U., The eddy conductivity of the air over a smooth snow field, *Geofys. Publ. Norske Videnskaps-Akad. Oslo,* 11, 69 pp., 1936.

(Manuscript received December 3, 1958; presented at the Pacific Northwest Regional Meeting, November 14, 1958.)

Some Hydrologic Aspects of Alpine Snowfields under Summer Conditions

M. Martinelli, Jr.

Rocky Mountain Forest and Range Experiment Station
U. S. Forest Service
Fort Collins, Colorado

Abstract—Ablation, density, and weather factors were measured at selected snowfields in the Front Range of Colorado during the summers of 1955 and 1956. Water equivalent of ablation and moisture exchange between the atmosphere and the snow surface were computed.

Ablation varied from 1.1 to 2.8 feet per week. It averaged 1.9 feet per week for July, August, and the first half of September. Density of the snow increased during the summers, reached a maximum during August, and then decreased slowly. For each acre of snow existing on August 1, about 11½ acre feet of water were released by ablation during July and August. This amounted to 0.19 acre foot of water per day per acre of snow. Sverdrup's equation indicated that net moisture exchange between the atmosphere and the snow averaged less than two per cent of ablation. Proposals are made to sustain stream flow into the summer by constructing barriers to drift additional snow into natural accumulation areas.

Introduction—The primary objective of this study was to investigate the characteristics of alpine snowfields during summer months and to determine the effect of these snowfields on summer stream flow. Alpine weather records were collected as a secondary and correlated objective.

During the summer of 1955, five alpine snowfields located along the eastern side of the Front Range in central Colorado were studied. A second year's record was taken at two of the snowfields during the summer of 1956.

Matthes [1934], referring to his experience in the Sierra Nevada and on Mount Rainier, said, in part, ". . . the strongly sun-pitted snowfields above 12,000 feet waste away during the summer without contributing a drop of water to the streams in the valley below. . . . It follows that these upper snowfields are in no sense the source of streams and are to be excluded from any estimate of runoff based on snow surveys." As late as 1953, J. E. Church supported these views in a published letter [*Kehrlein* and others, 1953]. However, *Kehrlein* and associates [1953], working near the summit of Mount Whitney (14,496 ft) in July 1951, found that evaporation never exceeded 0.004 ft per day, nor ten per cent of ablation.

Champion [1950], in his study of Scottish snowfields in July 1949, showed that 66.12 acres of snowbeds produced about 49,462 cu ft of melt water per hour. At these snowfields, ablation varied from 0.08 to 0.56 ft/day and showed a linear correlation with average daily air temperature for periods of high relative humidity.

Study areas—The important features of the snowfields selected for study are summarized in Table 1. All were above timber line except the Science Lodge snowfield. Patches of Krummholz extend part of the way up the ridges forming the north and south boundaries of this field. In general, the snowfields had slopes between 12 and 35 per cent. However, in a few places slopes up to 85 per cent were encountered.

Snow surfaces became rippled or slightly pitted at times during both years. Dust and organic material also appeared on the fields in considerable amounts by the middle of the summer.

Instrumentation and methods—Wind travel 6 ft above the ground, precipitation, temperature, and relative humidity (hygrothermograph) were measured adjacent to each snowfield. A grid of poles was established on each snowfield to measure ablation and to facilitate mapping.

Observation of free water on the snowfields during the summer of 1955 prompted snow quality measurements which were started July 18, 1956. The calorimeter technique described by *Bernard* and *Wilson* [1941] was used to determine snow quality in the top foot of the snowfields at weekly intervals. Measurements

TABLE 1—*Summary of important features of the snowfields*

Snowfield	Aspect	Elevation (ft)	Date of first observation	At time of first observation	
				Max. depth (ft)	Area (acres)
Mt. Evans	East	12,500	June 23, 1955	19.5	3.27
			July 3, 1956	16.8	2.28
Science Lodge	South	11,500	July 1, 1955	21.8	8.63
			June 30, 1956	16.8	8.47
Trail Ridge No. 1	Northeast	12,000	July 3, 1955	8.0	0.46
Trail Ridge No. 2	North	11,700	July 4, 1955	21.5[a]	3.81
Corona	North	11,500	July 19, 1955	18.8[a]	2.63

[a] Depth of snow above an ice layer of undetermined thickness

were made betwen 10h 30m and 15h 30m local time.

Snow density was measured with a Mount Rose snow sampler at several places on each snowfield each week. After August 22, 1956 supplemental density determinations were made from pits, using 500-ml cylinders.

Accurate density measurements proved very difficult with the Mount Rose snow sampler. Seldom could it be forced more than two or three feet into the snow before the core had to be emptied to permit deeper sampling. Repeated entry into the hole forced snow into the tube through the slots. As a result, core length exceeded snow depth by 0.4 ft for snow depths from 1.5 to 6 ft. Therefore, densities computed in the usual manner from snow depth were less accurate than those based on core length. In the few cases where a direct comparison could be made, even the Mount Rose densities based on core length averaged 5.7 per cent higher than densities taken in pits nearby. However, for the remainder of this report, all density values not specifically referred to as pit densities will be based on data taken with the Mount Rose sampler and corrected for core length.

Results—Ablation averaged 1.9 ft of snow per week during July, August, and the first half of September (Table 2). Weekly ablation varied from 1.1 to 2.8 ft of snow. Short-term ablation measurements showed a range of 0.06 ft /hr to 0.003 ft/hr. The short-term data also indicated the following diurnal trend of ablation: mornings averaged 0.035 ft/hr; afternoons, 0.025 ft/hr; and overnight, 0.010 ft/hr.

The ratio of water equivalent of ablation (in feet) to degree days above 32°F for the Mount Evans and Science Lodge snowfields averaged 0.013 for 1955 and 0.015 for 1956. These values fall on either side of the ratio given by *Weiss* and *Wilson* [1958] for nontimbered sites in early June in California and Montana.

Density of the snow in the alpine fields was essentially the same as that mentioned by *Seligman* [1936] for thawed firn snow (0.6 to 0.7g/cm^3) and very wet snow (0.8 g/cm^3).

The sharp increase in density shown in Figure 1 during late July 1955 is thought to be the result of heavy and frequent rains. During the four weeks that followed July 20, 1955, the longest rain-free period at the Trail Ridge No. 2 field was four days; at the Mount Evans field it was two days.

TABLE 2—*Ablation in feet of snow per week for the summers of 1955 and 1956*

Snowfield	July		August		September[a]	
	1955	1956	1955	1956	1955	1956
Mt. Evans	1.8	1.5	1.7	1.4	1.4	1.4
Science Lodge	2.3	2.0	2.4	2.1	···	1.9
Corona	2.4[b]	···	2.0	···	1.5	···
Trail Ridge No. 2	2.2	···	2.0	···	1.3	···
Trail Ridge No. 1	2.4	···				

[a] September data are for the first two weeks only.
[b] Reading started on July 19, 1955.

TABLE 3—*Water equivalent of ablation (in feet)*

Period of observation		Locations and years						
		Corona	Mt. Evans		Science Lodge		Trail Ridge No. 2	Trail Ridge No. 1
From	To	1955	1955	1956	1955	1956	1955	1955
July 4	July 18	...	2.15	2.35	2.56	3.38	2.61	2.53
July 18	July 31	2.63	2.20	1.94	3.09	2.46	2.63	...
July 31	Aug. 31	6.50	5.85	4.89	8.06	6.98	6.73	...
Totals:								
July 4	Aug. 31	...	10.20	9.18	13.71	12.82	11.97	...

Another factor which contributed to high densities, especially during rainy periods, was the poor internal drainage of the fields resulting from numerous ice layers. On several occasions water was seen flowing over the snow surface for a short distance before it disappeared into the snow. Inspection of these over-the-surface streams usually revealed an ice layer on which the water was flowing. On other occasions, water was seen draining into density sample holes from slush that had formed just above buried ice layers.

A trend toward an increase in snow density with depth was noted both years from data obtained with the Mount Rose sampler. The 1956 pit densities from the Mount Evans snowfield also showed an increase in density with depth. However, pit studies at the Science Lodge snowfield the same year were less conclusive.

Snow quality in the upper foot of the Mount Evans field varied from 91 to 95 per cent for the period July 18 to August 29, 1956. This indicates between 5 and 9 per cent free water in the snow. At Science Lodge, snow quality in the top foot of the field varied from 85 to 91 per cent; however, for very hard and icy parts of the field it was usually in the middle eighties. The one sample taken from a slush layer at the lower edge of the Mount Evans field showed a snow quality of 63 per cent. In this case, water could be seen draining into the hole as the sample was removed.

Table 3 permits a direct comparison of the water equivalent of ablation for four fields for the same summer. In addition, two fields can be compared for two successive summers. An average of 11.5 ft of water was released during July and August. It is significant that more than half of this was released in August, when there are few other sources of stream flow.

Evaporation and condensation at the snow surface were computed from local weather data and Sverdrup's equation [*Light*, 1941] after it had been adjusted for elevation. Atmospheric moisture exchange exceeded 5 per cent of the water equivalent of ablation only twice and averaged 1.8 per cent for 33 observation periods in 1955. The next year it exceeded 2 per cent of the water equivalent of ablation once and averaged 1.1 per cent for nine periods of observation.

Precipitation and temperatures for the study sites are summarized in Table 4. The lack of alpine weather records precludes any comparison of weather during the study periods with 'normal' conditions. However, in the high val-

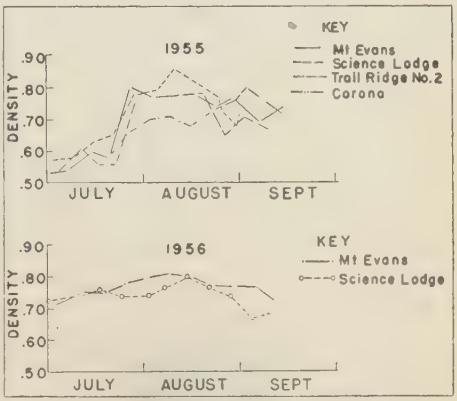

FIG. 1—Average density of alpine snowfields as measured with a Mount Rose snow sampler

TABLE 4(a)—*Summary of precipitation (in feet) for the summers of 1955-1956*

Snowfield	1955			1956		
	July	August	September	July	August	September
Mt. Evans	0.35	0.62	0.04	0.22[b]	0.18	0.01[c]
Science Lodge	0.22	0.35	0.04	0.24	0.18	0.01[d]
Corona	···	0.27	0.07	···	···	···
Trail Ridge No. 2	0.14[a]	0.32	0.05	···	···	···

[a] Record started July 5, 1955.
[b] Record started July 2, 1956.
[c] Record ended September 19, 1956.
[d] Record ended September 27, 1956.

TABLE 4(b)—*Summary of average temperatures* (°F) *for the summers of 1955-1956*

Snowfield	1955			1956		
	July	August	September[a]	July	August	September[b]
Mt. Evans						
Daily mean	45.8	43.8	43.0	43.6	41.2	···
Daily maximum	54.5	51.1	52.4	52.2	50.0	···
Daily minimum	37.8	37.2	35.8	35.7	34.4	···
Science Lodge						
Daily mean	50.3	49.5	48.5	47.7	45.4	45.9
Daily maximum	60.9	58.2	58.9	57.7	55.2	56.6
Daily minimum	43.8	43.6	41.4	40.5	38.9	37.3
Corona						
Daily mean	···	48.3	47.3	···	···	···
Daily maximum	···	57.7	57.4	···	···	···
Daily minimum	···	41.2	39.4	···	···	···
Trail Ridge No. 2						
Daily mean	···	46.8	45.5	···	···	···
Daily maximum	···	55.8	54.8	···	···	···
Daily minimum	···	40.7	37.6	···	···	···

[a] Only first 18 days of September 1955 were recorded.
[b] Only first 9 days of September 1956 were recorded.

leys 10 to 12 miles distant and 4000 to 5000 ft below the snowfields, the weather deviated from normal in only one important respect during the period [*U. S. Weather Bureau*, 1955, 1956]. Precipitation for August 1955 was much greater than usual, especially in the vicinity of Mount Evans.

Precipitation fell as rain, hail, graupel, or as a mixture. Periods of intensive precipitation were usually associated with thunderstorms. Intensities as high as 0.14 to 0.16 ft/hr were recorded for 5- to 10-minute intervals during August 1955.

Wind speeds, based on weekly wind travel, averaged four to eight miles per hour during July and August of both summers. Winds increased about 50 per cent during September. Maximum wind speed at the Science Lodge snowfield during the summer of 1956 was 31 mph for a one-hour period. It was not possible to determine maximum speeds for the other sites.

These relatively light winds appear contradictory to the general impression of alpine conditions. However, the weather instruments for this study were located adjacent to snow ac-

cumulation areas. The fact that snow drifts into these spots indicates that they are protected from strong winds. It was not practical to record gust velocities, which are usually about twice the average velocity.

Conclusions and recommendations—Alpine snowfields are an important source of summer stream flow in central Colorado. Each acre of snow present during July and August releases an average of 60,000 gal (0.19 ac ft) of water per day for stream flow. In order to estimate the total contribution of alpine snowfields to summer stream flow, it is necessary to know the amount of snow present. Studies now in progress are expected to yield such information for a selected portion of the Colorado Rockies.

Field observations suggest that the size and depth of drifts are a function of the size and shape of the barrier behind which they accumulate. Observations also indicate that many of the natural barriers in the alpine regions are inadequate to hold the snow which falls during the accumulation period. If these impressions are true, artificial barriers erected on sites where drifting occurs naturally should induce additional drifting. Such barriers could be used to increase the size of the snowfields that usually persist until late summer. They could also be used to increase the depth and the size of snowfields that normally disappear by early July. In this way, both the amount and the duration of melt water released to the streams during the summer would be increased.

Acknowledgments—This study was carried out through the cooperation of the State University of New York, College of Forestry, at Syracuse, New York; the Rocky Mountain Forest and Range Experiment Station, Forest Service, U. S. Department of Agriculture; and the Colorado State University. The following organizations provided accommodations during the field seasons or granted permission to carry out field work in areas under their jurisdiction, or both: Rocky Mountain National Park, Institute of Arctic and Alpine Ecology at the University of Colorado, the City of Boulder, Colorado, and the Inter-University High Altitude Laboratories at the University of Denver.

References

Bernard, M., and W. T. Wilson, A new technique for the determination of heat necessary to melt snow, *Trans. Am. Geophys. Union,* 22, Pt. 1, 178–181, 1941.

Champion, D. L., Ablation in the Scottish Highlands, *Meteorol. Mag.,* 79, 292–295, 1950.

Kehrlein, O., E. Serr, Sr., R. D. Tarble, and W. T. Wilson, High Sierra snow ablation observations, *Proc. Ann. Meeting Western Snow Conf.,* pp. 47–50, 1953.

Light, P., Analysis of high rates of snow-melting, *Trans. Am. Geophys. Union,* 22, pt. 1, 195–205, 1941.

Matthes, F. E., Ablation of snow-fields at high altitudes by radiant solar heat, *Trans. Am. Geophys. Union,* 15, pt. 2, 380–385, 1934.

Seligman, G., *Snow structure and ski fields,* Macmillan Co., London, 554 pp., 1936.

U. S. Weather Bureau, *Climatological data, Colorado,* 60 (6), 81–100; 60 (7), 101–116; 60 (8), 117–132, 1955.

U. S. Weather Bureau, *Climatological data, Colorado,* 61 (6), 81–98; 61 (7), 99–114; 61 (8), 115–130, 1956.

Weiss, L. L., and W. T. Wilson, Snow-melt degree-day ratios determined from snow-lab data, *Trans. Am. Geophys. Union,* 39, 681–688, 1958.

(Manuscript received June 2, 1958; revised January 22, 1959; presented at the Thirty-ninth Annual meeting, Washington, D. C., May 1958.)

The Pattern of Fresh-Water Flow in a Coastal Aquifer

R. E. GLOVER

U. S. Geological Survey
Denver, Colorado

Abstract—Formulas are developed for the flow pattern followed by the seaward-moving fresh ground water as it nears a beach. It is found that, under steady flow conditions, a sharply defined interface is formed between the fresh and salt water. Along the interface the pressure of the static salt water, owing to its greater density, is counterbalanced by the pressures which drive the fresh water seaward. The fresh water escapes through a gap between this interface and the shore line. An increase in the flow of fresh water widens the gap. Tidal action causes a diffusion of salt water across the interface. This salt is carried back to sea with the fresh-water flow.

Introduction—Where permeable beds underlie a land area near the sea and extend some distance seaward from the shore line, the infiltration from rainfall causes a continuous flow of fresh water toward the sea. It has been found that under these conditions an extensive body of fresh water is commonly present beneath the land. This body of fresh water is often a valuable source of water supply. Because the flow of fresh water toward the sea must come into balance with the supply from rainfall infiltration, a seaward gradient must be present. The water table under the land, therefore, has the form of a mound. The density difference between sea water and fresh water is only about one-fortieth of the density of fresh water, and for this reason the fresh-water body has a thickness below sea level of about 40 ft for each foot of elevation of the water table above sea level [*Badon Ghyben*, 1889; *Herzberg*, 1901]. Near the seashore, however, dynamic factors become important. If static conditions alone were to prevail here the fresh-water body would taper to a knife edge at the beach and there would be no way for the fresh water to escape. When the dynamic factors are considered it is found that the fresh water flows through a narrow gap between a fresh water - salt water interface and the water-table outcrop at the beach [*Hubbert*, 1940]. In the analyses that follow, however, the flow through the seepage surface above sea level is assumed to be negligible. A short distance back from the beach the static conditions are closely met. Under steady-flow conditions the fresh water - salt water interface would be sharply defined, but tidal action and the rise and fall of the water table maintain a zone of diffusion between the fresh and salt water.

Flow net—A close representation of the flow conditions near a beach can be obtained by modifying a solution previously obtained for the flow of ground water under gravity forces [*Kozeny*, 1953]. The flow net for the present case can be obtained from the relationship

$$x + iy = \frac{K}{2\gamma Q}(\phi + i\psi)^2 \qquad (1)$$

where

x represents a distance measured horizontally landward from the shore line (ft)

y is a distance measured vertically downward from sea level (ft)

$i = \sqrt{-1}$

If Q represents the fresh-water flow per unit length of shore line (ft²/sec)

K the permeability of the strata carrying the fresh-water flow (ft/sec)

and γ the excess of the specific gravity of sea water over fresh water (dimensionless)

then

$$\phi = (\gamma Q/K)^{\frac{1}{2}}[x + (x^2 + y^2)^{\frac{1}{2}}]^{\frac{1}{2}} \qquad (2)$$

$$\psi = (\gamma Q/K)^{\frac{1}{2}}[-x + (x^2 + y^2)^{\frac{1}{2}}]^{\frac{1}{2}} \qquad (3)$$

The interface between the fresh water and sea water can be plotted from the expression

$$y^2 - \frac{2Q}{\gamma K}x - \frac{Q^2}{\gamma^2 K^2} = 0 \qquad (4)$$

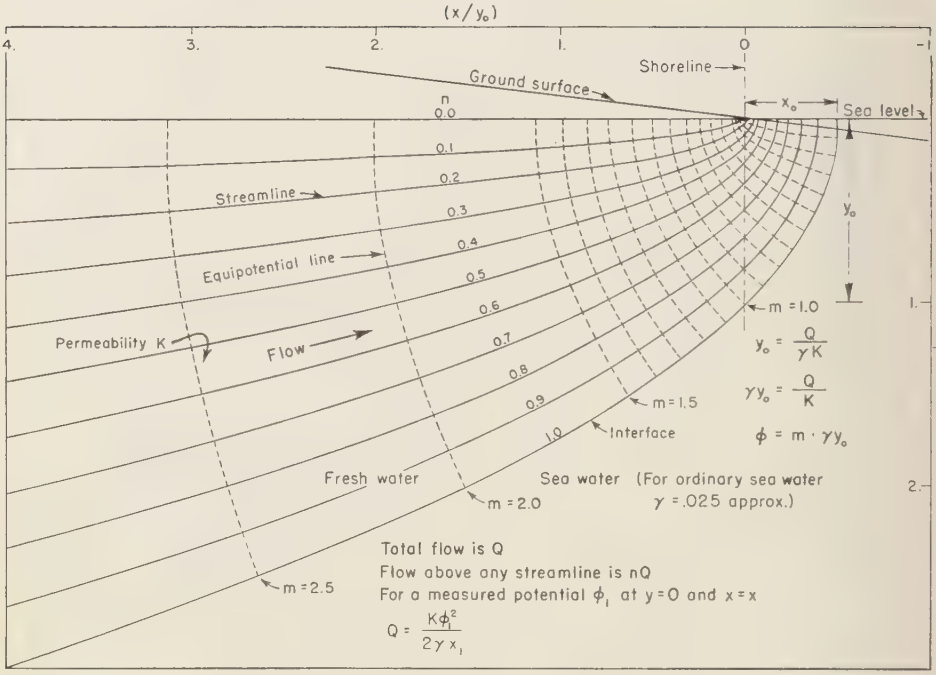

FIG. 1—Flow pattern near a beach

The width of the gap through which the fresh water escapes to the sea is

$$x_0 = -\frac{Q}{2\gamma K} \tag{5}$$

In the present case the potential, ϕ, can be identified with the pressure which drives the fresh water. It is expressed in feet of fresh water. The flow function, ψ, also is expressed in feet of water. The product $K\psi$ then has the same dimensions as Q. The stream function has the property that for a selected value $\psi = \psi_1$, the product $K\psi_1$, substituted in expression (3) yields a streamline. The fresh-water flow above this streamline is nQ.

The potential along the line $y = 0$ is

$$\phi_0 = (2\gamma Q x/K)^{\frac{1}{2}} \tag{6}$$

This is the height of the water table at the distance x back from the shore line. A plot of this flow net is shown in Figure 1.

Some features of this solution deserve comment. If the supply of fresh water to the aquifer decreases so that Q decreases, then the width of the gap through which the fresh water can escape also decreases. The seaward flow of fresh water is proportional to the square of the potential ϕ_0 measured at a selected distance $x = x_1$ from the shore line. In times of drought the seaward flow is diminished, and this acts to conserve the fresh-water body. Thus, once established, the fresh water does not quickly waste away.

The pattern of flow described in this paper is based on the assumption that the salt water is essentially static. It has been hypothesized by H. H. Cooper of the U. S. Geological Survey [Cooper, 1959] that where a zone of diffusion exists between the salt water and the fresh water, the salt water is not static but flows in a cycle from the floor of the sea to the zone of diffusion and back to the sea. Cooper reasons that this flow is induced by the dispersion of salt produced by a reciprocative motion of the salt-water front. Such a circulation would alter the balance between the two fluids to an extent depending on the magnitude of the circulation.

References

Badon Ghyben, W., Nota in verband met de voorgenomen put boring nabij Amsterdam [Notes on the probable results of the proposed well drilling near Amsterdam], *Koninkl. Inst. Ing. Tijdschr.*, 1888–89, The Hague, pp. 8–22, 1889.

Cooper, H. H., A hypothesis concerning the dynamic balance of fresh water and salt water in a coastal aquifer, *J. Geophys. Res.*, 64, 461-467, 1959.

Herzberg, Alexander, Die Wasserversorgung einiger Nordseebäder [The water supply on parts of the North Sea coast], *J. Gasbeleucht. u. Wasserversorg.*, Jahrg. 44, Munich, 1901.

Hubbert, M. K., The theory of ground-water motion, *J. Geol.*, 48, 785–944, 1940.

Kozeny, Josef, *Hydraulik*, Springer Verlag, Vienna, 1953.

(Manuscript received December 5, 1958.)

A Hypothesis Concerning the Dynamic Balance of Fresh Water and Salt Water in a Coastal Aquifer

H. H. COOPER, JR.

U. S. Geological Survey
Tallahassee, Florida

Abstract—The dispersion of salts produced by reciprocative motion of the salt-water front in a coastal aquifer induces a flow of salt water from the floor of the sea into the zone of diffusion and back to the sea. The head losses that accompany the landward flow tend to lesson the extent to which the salt water occupies the aquifer.

Introduction—Published explanations of the steady-state balance between salt water and fresh water in a coastal aquifer, beginning with *Badon Ghyben* [1889] and *Herzberg* [1901], commonly assume that the salt water is static. Under this assumption the balance would be as shown in Figure 1. The depth below sea level to a point on the interface would be [*Hubbert*, 1940, p. 872]

$$z = \frac{\rho_f}{\rho_s - \rho_f} h$$

where ρ_f is the density of the fresh water, ρ_s is the density of the sea water, and h is the head of fresh water above sea level at the point on the interface. An equation for determining the shape and position of the interface with a known rate of discharge of fresh water under one set of boundary conditions has recently been devised by *Glover* [1959] through an adaptation of a solution by *Kozeny* [1953] for an analogous problem of free-surface gravity flow. Equations for the interface under several sets of boundary conditions have been derived by H. R. Henry (in preparation).

It is the thesis of the present paper that where a zone of diffusion exists, the salt water is not static but flows perpetually in a cycle from the floor of the sea into the zone of diffusion and back to the sea, and that this flow tends to lessen the extent to which the salt water occupies the aquifer.

That this cycle must exist in some degree becomes evident if one considers that there is a continuous discharge of salty water from the zone of diffusion into the sea (Fig. 2). For if

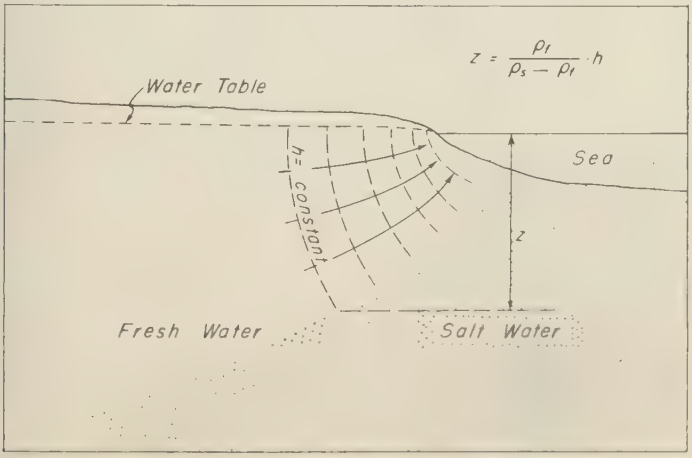

FIG. 1—Balance between fresh water and salt water in a coastal aquifer, with the salt water static

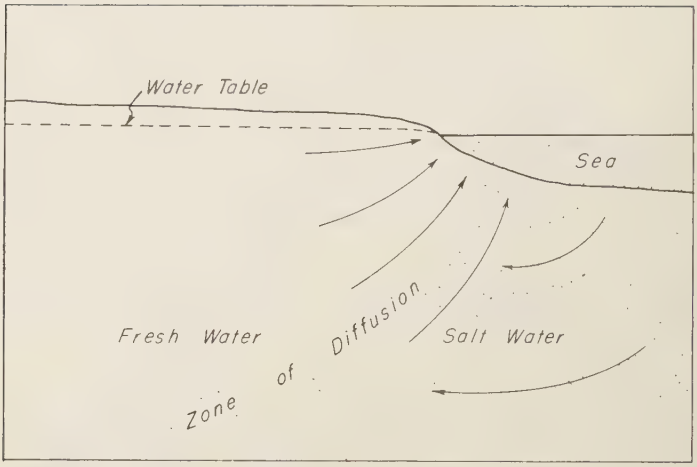

FIG. 2—Circulation of salt water from the sea to the zone of diffusion and back to the sea

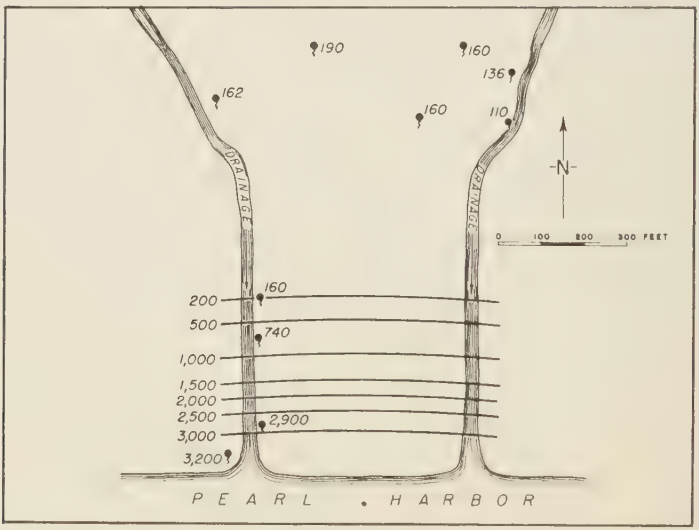

FIG. 3—Map of Waimano Springs, Oahu, Hawaii, showing the chloride content of water from orifices, 1957; lines and figures represent the chloride content in parts per million

there is such a discharge, the sea itself must be the source of the salts that are carried back to the sea, and hence the salts must by some means be transported from the floor of the sea through the aquifer into the zone of diffusion. We may rule out any form of dispersion or diffusion as the principal mode of transportation of the salts from the sea to the zone of diffusion on the grounds that these processes occur only when there is a concentration gradient, and the concentration gradient that exists across the zone of diffusion will not in general extend in sufficient magnitude all the way back to the sea floor. Therefore, we may conclude that the salts are transported largely by a hydraulic flow of the salt water, as indicated in Figure 2, with a consequent loss of head in the salt-water environment.

One example of a discharge of salty water from the zone of diffusion is the flow of springs

around Pearl Harbor, Hawaii. Ordinarily, most of the seaward discharge of water from a coastal aquifer occurs at the floor of the sea, but around Pearl Harbor a sizable quantity of water issues from terrestrial springs as the result of the presence of the 'caprock,' a relatively impervious blanket of weathered volcanic debris that underlies and rims the harbor and forces some of the ground water from the basaltic aquifer to discharge in springs along its inland perimeter. Typical of these is Waimano Springs (Fig. 3), consisting of several orifices that yield water of different salinities. The total flow of the several orifices of Waimano Springs ranges from 15 to 20 million gallons per day. The water from these orifices increases in salinity toward the sea, and chloride content ranges from less than 200 ppm at the orifices farthest inland to as much as 3200 ppm at the one nearest the shore. The chloride content of sea water at most places is about 19,000 ppm.

The great thickness of the zone of diffusion beneath the Pearl Harbor area is indicated by Figure 4, which shows the chloride content of water at various depths as determined from the drilling of a deep test well. The zone begins at about 200 ft and ends at perhaps 1200 ft, thus having a thickness of 1000 ft or more.

Another place at which there is evidence of discharge from the zone of diffusion is the Cutler area, near Miami, Florida. The zone of diffusion in the Biscayne aquifer of this area, which consists predominantly of cavernous limestone, is represented by the isochlors in Figure 5. The control points for the isochlors are shown by the black dots, which represent the bottoms of fully cased wells. These wells were drilled for the purpose of extracting water samples and measuring pressure heads at isolated depths, as a part of an investigation by the U. S. Geological Survey of the various factors relating to the hypothesis described in this paper. The thickness of the zone of diffusion is limited by the thickness of the aquifer, but its horizontal breadth at the base of the aquifer, as reckoned from the isochlors, is probably about 2000 ft. The zone extends several hundred feet beyond the shore line. The distribution of salts is doubtless influenced by the presence of beds of low permeability in the aquifer.

As most of the seaward discharge from the Biscayne aquifer occurs at the floor of the sea,

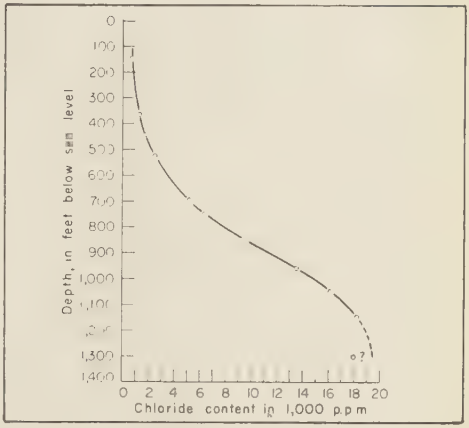

FIG. 4—Chloride content of water from test well at Pearl Harbor, 1958

there is no opportunity to obtain representative samples of the water being discharged to determine its salinity. We may infer, nevertheless, that salty water is being discharged from the fact that the shallow wells that end in the zone of diffusion beneath the floor of the sea tap salty water under sufficient head to rise above sea level.

Mechanics of the cyclic flow—But what causes the sea water to move in its cycle through the aquifer? Since the water has the same fluid potential when it re-enters the sea as when it leaves, one might reason that there can be no hydraulic gradient and hence no flow. To understand how a flow may exist under these circumstances, let us consider the processes that operate in the zone of diffusion. Sea water and fresh water become intimately mixed in the zone of diffusion by the mechanism that creates this zone. The effect of this is the same as if some of the salt ions were extracted from the sea water and injected into the flowing fresh water. The diluted sea water, having become less dense than native sea water, rises along a seaward path. The resulting circulation is analogous to the circulation in thermal convection, differing from it only in that changes in density are produced by changes in concentration rather than by changes in temperature. Meanwhile, the salts that are introduced into the fresh-water environment are carried back to the sea by the flow of the fresh-water system. (It is convenient to consider the salt-water environment as includ-

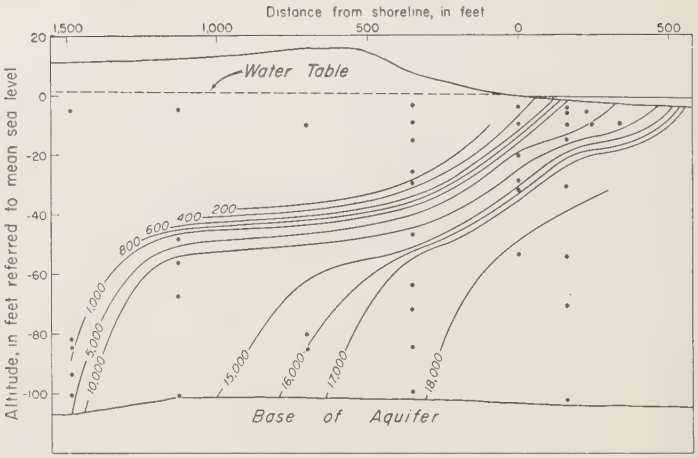

FIG. 5—Section through Cutler area, near Miami, Florida, showing the zone of diffusion, 1958; lines represent the chloride content in parts per million

ing that part of the zone of diffusion from which there is an efflux of salts by dispersion, and the fresh-water environment as including the part into which there is an influx of salts by dispersion. The boundary between the two will then be the point of inflection of the concentration curve.)

Apparently, then, the circulation is induced by the transfer of salts out of the salt-water environment. The forces that effect this transfer must be powerful enough to recreate the zone of diffusion continuously as it is dissipated by the flow of mixed water to the sea. As molecular diffusion is much too feeble for this, we must look for something more potent.

Dispersion—A mechanism that appears to be powerful enough to cause sufficient mixing is the reciprocative motion of the salt-water front that occurs as the result of ocean tides and of the rise and fall of the water table due to variations in recharge and other forces, including pumping. It has been theorized by *Palmer* [1927, pp. 51–52] and *Wentworth* [1948] that it is this to-and-fro motion that creates the zone of diffusion. The process by which two miscible liquids interfuse about their boundary when the boundary is caused to move by hydraulic flow is known as dispersion. In laminar flow through permeable porous media, dispersion is produced by the combined effects of convection (transfer of a fluid into the region of another due to variations in velocities within the interstices) and molecular diffusion [*Taylor*, 1953, p. 187]. During a movement of the salt-water front in either direction, the convection component of dispersion causes elements of each fluid to be transferred into the opposite environment, wherein to a large extent they become inseparably blended with the other fluid by mixing and molecular diffusion. Were the displaced elements not to become blended, but were they to remain discrete during and after the transfer, the potential gradients acting upon them in the foreign environments would drive each back to its original environment. Furthermore, the dispersion would be largely negated at each reversal of motion if the elements were to retain their identity in continuous filaments and retrace their path. Thus, both convection and molecular diffusion are important parts of the dispersion process, convection in producing large transfers and molecular diffusion in completing the blending.

From the results of their experiments with Ottawa and Monterey sands, *Rifai* and others [1956] concluded that the coefficients of longitudinal dispersion (dispersion in the direction of flow) with unidirectional flow in granular permeable media is practically proportional to the mean velocity of flow, so that $D = Mv^n$, where D is the coefficient of dispersion, M is a constant whose magnitude depends on the properties of the medium, v is the mean interstitial velocity, and the exponent n is approximately

nity. They found the values of M to be 0.063 or Ottawa sand and 0.13 (computed from neir Table V; the value of 0.013 given in their ig. 18 appears to be incorrect) for Monterey and. Recent experiments by *Orlob* and *Radakrishna* [1958] indicate that the medium dispersion constant M increases with the uniformity oefficient of the medium and becomes as high s 2.79 for a sand having a uniformity coefficient of 3.88.

If the coefficient of longitudinal dispersion is ractically proportional to the first power of the nean interstitial velocity, it may, in the case of dispersion due to ocean tides, be expressed

$$D = 4MA/t_0 \qquad (1)$$

where A is the amplitude and t_0 is the period of he displacement of water in the aquifer caused by ocean tides.

The amplitude of the tide-produced displacement of water may be related approximately to he amplitude of the tide and the distance from he shore line as follows. The tide-produced change in the artesian head with reference to its nean in a semi-infinite artesian aquifer is found o be [*Jacob*, 1949, p. 365; *Ferris*, 1951, p. 149]

$$h = h_0 \exp(-x\sqrt{\pi S/t_0 T}) \cdot \sin(2\pi t/t_0 - x\sqrt{\pi S/t_0 T})$$

where

h_0 = amplitude of the tide
x = distance from the shoreline
t = time referred to the beginning of a tidal cycle
t_0 = period of the tide cycle
S = coefficient of storage
T = coefficient of transmissibility.

The gradient producing the displacement will herefore be

$$\frac{\partial h}{\partial x} = -h_0\sqrt{\pi S/t_0 T}\exp(-x\sqrt{\pi S/t_0 T}) \cdot [\sin(2\pi t/t_0 - x\sqrt{\pi S/t_0 T}) + \cos(2\pi t/t_0 - x\sqrt{\pi S/t_0 T})].$$

The displacement will be zero at a time t_1 when $\partial h/\partial x$ is a maximum, or when the quantity n parentheses is $\pi/4 + n\pi$. It will be extreme at a time t_2 when $\partial h/\partial x = 0$, or when the quantity in parentheses is $3\pi/4 + n\pi$. Thus, with the substitutions

$$u = 2\pi t/t_0 - x\sqrt{\pi S/t_0 T}$$
$$du = 2\pi\, dt/t_0,$$

the amplitude of the displacement will be

$$A = K/\theta \int_{t_1}^{t_2} (\partial h/\partial x)\, dt$$
$$= (Kh_0/\theta)\sqrt{t_0 S/4\pi T}\exp(-x\sqrt{\pi S/t_0 T}) \cdot \int_{\pi/4}^{3\pi/4} (\sin u + \cos u)\, du$$
$$= (Kh_0/\theta)\sqrt{t_0 S/2\pi T}\exp(-x\sqrt{\pi S/t_0 T}), \qquad (2)$$

where K is the permeability and θ is the effective porosity of the aquifer.

With (1) and (2) one may estimate the coefficients of tide-produced dispersion at given distances from the shore line in a typical coastal aquifer, if it is assumed that the medium dispersion constants obtained from experiments with unidirectional flow are applicable, and that the displacements of the interface will be the same as the displacements that would occur if the water in the aquifer were all of one density. The latter assumption appears to be reasonable when we consider that in most aquifers the interface will move very slowly in response to changes in head and that its maximum displacement will be only a fraction of that which would be required for it to adjust completely to the extremes of the tide. Equation (2) was derived for artesian aquifers but probably will give a fair approximation of the amplitude of the displacement in a nonartesian aquifer if an appropriate value for the coefficient of storage is used.

The amplitude of the oscillation of water at various distances from the shore line in a hypothetical nonartesian aquifer of sand is illustrated in Figure 6. If the medium dispersion constant of the sand were 1.0, the coefficient of dispersion would be 100 cm²/day at about 300 ft from the shore line, and 10 cm²/day at about 900 ft from the shore line. Beyond 1500 ft it would not be significantly larger than 1 cm²/day, which is approximately the coefficient of molecular diffusion of sodium chloride [*Hodgeman*, 1945, p. 1695].

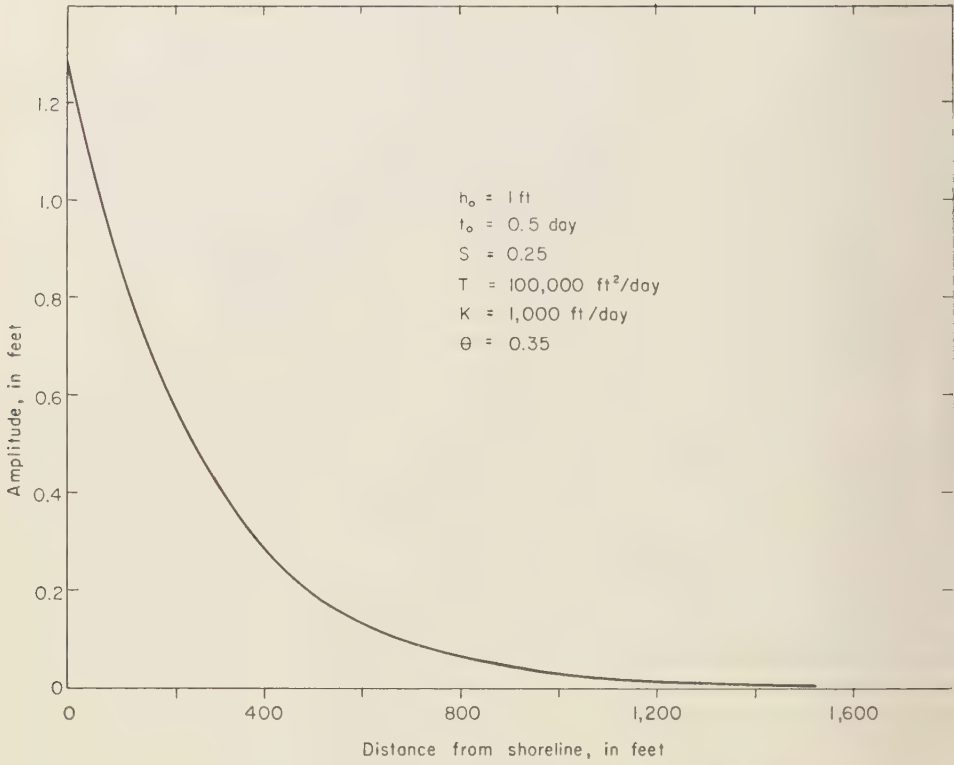

FIG. 6. Amplitude of tide-produced motion of water in a coastal aquifer

It appears likely, however, that in aquifers that consist of alternating beds of high and low permeabilities, as practically all aquifers do, there is a mixing mechanism that will produce rates of dispersion considerably larger than those indicated by laboratory experiments on unidirectional flow through homogeneous sand. Suppose, for example, that we have an aquifer made up of alternating beds having permeabilities in the ratio of ten to one, and that initially there is a sharp interface lying diagonally across the beds. If, with a rise of the tide, the interface were to move landward a distance of x units in a bed of high permeability, it would move only about $0.1x$ units in an adjacent bed of low permeability. Consider, now, what would happen if the fresh water were then to begin flowing in a direction diagonally across the beds in an upward path toward the sea. Apparently, the water in the various beds would become fairly well mixed, so that there would result a zone nearly x units wide in which the concentration of salts would be some fraction of that of sea water, this fraction being dependent on the relative thicknesses and porosities of the beds. With each additional tidal cycle the zone would widen further until ultimately the distribution of salts would come to a steady state wherein the average rate at which the salts were carried into an element of the aquifer by dispersion would be in balance with the rate at which they were carried out of it by hydraulic flow. The rate of dispersion produced by this process would doubtless be greater in an aquifer of cavernous limestone or basalt than in one of laminated sand.

The reader will understand that the hydraulics is somewhat more complicated than postulated here. The example given is merely a device to illustrate the idea of dispersion by differential displacement and cross-bed mixing. The displacements and mixings will not, of course

ccur as separate, alternate events but will op-
rate simultaneously much of the time, each
laying a more prominent part at one phase in
ne tidal cycle than at another.

Summary—It appears to be reasonably cer-
ain that wherever a zone of diffusion exists in a
oastal aquifer a flow of sea water from the floor
f the sea into the zone of diffusion will occur.
he flow may be interrupted or reversed during
w stages of the tide or high stages of the water
able, but on the average it will persist in a
ndward direction. Apparently, the only ques-
on in a given case is one of magnitude. The
agnitude of the flow evidently will be gov-
rned chiefly by that of the dispersing mechan-
m that induces it, and it may in some places
e large enough to produce head losses in the
alt-water environment that would lessen ap-
reciably the extent to which the salt water oc-
upies the aquifer.

Acknowledgments—The author is grateful to
). A. Davis, F. N. Visher, and J. F. Mink, all of
ne U. S. Geological Survey at Honolulu, for their
enerous permission to publish Figures 3 and 4
rior to their own publication of their findings.
Ie is indebted to F. A. Kohout, of the U. S.
eological Survey at Miami, for the collection
nd compilation of the data shown in Figure 5,
nd to R. E. Glover, of the U. S. Geological Sur-
ery at Denver, for suggesting the equation for
ne tide-produced displacement of water in a
oastal aquifer. Richard Skalak of Columbia Uni-
ersity reviewed the manuscript and made help-
il suggestions.

References

ADON GHYBEN, W., Nota in verband met de voorgenomen put boring nabij Amsterdam, *Koninkl. Inst. Ing. Tijdschr.*, 1888–89, The Hague, p. 21, 1889.

FERRIS, J. G., Cyclic fluctuations of water level as a basis for determining aquifer transmissibility, *UGGI, Assoc. Intern. Hydrol. Sci., Assemb. gen., Bruxelles,* 2, 148–155, 1951.

GLOVER, R. E., The pattern of fresh-water flow in a coastal aquifer, *J. Geophys. Research,* 64, 457–459, 1959.

HERZBERG, ALEXANDER, Die Wasserversorgung einiger Nordseebader, *J. Gasbeleucht. u. Wasserversorg.*, Jahrg. 44, Munich, 1901.

HODGEMAN, C. D., *Handbook of Chemistry and Physics,* Chemical Rubber Publishing Company, Cleveland, 2640 pp., 1945.

HUBBERT, M. K., The theory of ground-water motion, *J. Geol.* 47, 785–944, 1940.

JACOB, C. E., Flow of ground water, *Eng. Hydraulics,* chap. 5, Proc. Fourth Hydraulics Conf. Iowa Inst. Hydr. Research, John Wiley and Sons, New York, 1039 pp., 1949.

KOZENY, JOSEF, *Hydraulik,* Springer Verlag, Vienna, 588 pp., 1953.

ORLOB, G. T., AND G. N. RADHAKRISHNA, The effect of entrapped gages on the hydraulic characteristics of porous media, *Trans. Am. Geophys. Union,* 39, 648–659, 1958.

PALMER, H. S., The geology of the Honolulu artesian system, *Suppl., Honolulu Sewer and Water Comm. Rept.*, 1927.

RIFAI, M. N. E., W. J. KAUFMAN, AND D. K. TODD, Dispersion phenomena in laminar flow through porous media, *Progr. Rept. 2, Canal Seepage Research,* University of California, Berkeley, 157 pp., 1956.

TAYLOR, G. I., Dispersion of soluble matter in solvent flowing slowly through a tube, *Proc. Roy. Soc. London, A,* 219, 186–203, 1953.

WENTWORTH, C. K., Growth of the Ghyben-Herzberg transition zone under a rinsing hypothesis, *Trans. Am. Geophys. Union,* 29, 97–98, 1948.

(Manuscript received December 29, 1958; presented at the Thirty-Ninth Annual Meeting, Washington, D. C., May 6, 1958.)

The Role of Hysteresis in Reducing Evaporation from Soils in Contact with a Water Table

RICHARD A. SCHLEUSENER AND A. T. COREY

Department of Civil Engineering
Colorado State University
Fort Collins, Colorado

Abstract—Evaporation studies were conducted on three soil types in contact with a water table. For conditions of high evaporativity or increased depth to the water table, it was found that evaporation from the soils was not always in proportion to the rate of evaporation from a free-water surface. Under some conditions there was an inverse relation between evaporation from the soils and that from the free-water surface.

Analysis of upward movement of water from a water table in the absence of hysteresis effects does not provide a satisfactory explanation for this inverse relation.

A capillary tube model is used to explain qualitatively these results on the basis of reversals of changes in pressure in the soil water. This hysteresis phenomenon is believed to be responsible for reducing evaporation from soils in contact with a water table.

Introduction—Research has been conducted on evaporation from soils in contact with a water table. A fine sand, a loam, and a clay loam were placed in 3½-inch i.d. lucite containers and were subjected to varying conditions of temperature, humidity, infra-red radiation, wind motion, and depth to the water table in a chamber where a controlled atmosphere could be maintained. The evaporativity of the atmosphere was measured by the rate of evaporation from a fourth column of sand wherein the water table was maintained at the surface. This fourth column is termed a "free-water surface" in this discussion. All of the evaporating samples were placed on a rotating table at equal radii to insure uniform exposure of each sample. Water was supplied to the base of each column at a constant pressure from a Mariotte-siphon bottle. Rates of evaporation were determined by periodic weighing of the supply bottles. The runs were continued until a steady rate of evaporation was attained. Runs varied in length from several days to about one week. The columns were fitted with thermocouples to permit measurements of vertical temperature gradients. Insulation was provided to minimize radial temperature gradients.

The water-table depths investigated were 6, 12, 18, and 23.5 inches, and with the water table at each of these depths, a series of nine runs was conducted. Each successive run in the series produced a higher evaporativity than the preceding run. Evaporation rates from the free-water surface were averaged for each of the runs for the four water-table depths, and are shown in Figure 1. Depths to the water table of more than 23.5 inches were simulated by supplying water to the bases of the soil columns at pressures less than atmospheric. While this system did not duplicate exactly a longer column of soil, the difference was considered to

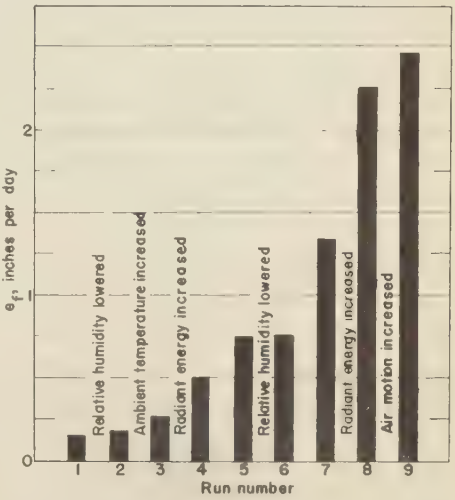

FIG. 1—Average evaporation rates from free-water surface (e_f) for various evaporating conditions

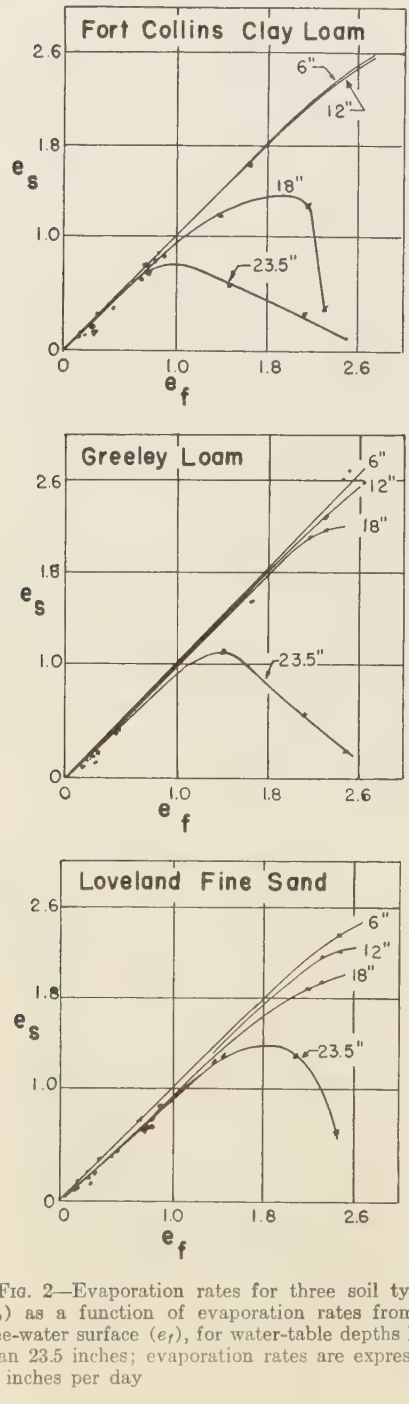

FIG. 2—Evaporation rates for three soil types (e_s) as a function of evaporation rates from a free-water surface (e_f), for water-table depths less than 23.5 inches; evaporation rates are expressed in inches per day

be small, since most of the resistance to flow occurs in the surface layer.

Experimental results—This discussion is confined to the results of the combined effects of soil and ambient factors on evaporation. Results of independent variation of ambient parameters are presented by *Schleusener* [1958] elsewhere. Figure 2 shows the evaporation rate for the three soil types plotted as a function of the evaporation rate from a free-water surface. Figure 2 shows that each soil type exhibits similar characteristics. For low evaporativity or small water-table depths, evaporation from the soils (e_s) is approximately the same as from the free-water surface (e_f). For greater depths to the water table and higher evaporativity each soil exhibited a maximum value of evaporation rate, so that increased evaporativity produced a *decreased* evaporation rate in the soils.

This phenomenon is considered to be significant because it has not been explained by existing theory.

Definitions of basic terms and symbols:

C Hydraulic conductivity, the ratio of the volume flux to the hydraulic gradient normal to a specified plane within a porous solid; the term is used in reference to a saturated system; dimensions: L/T

e Rate of evaporation; dimensions: L/T

Evaporativity The potential rate of evaporation produced by ambient conditions, measured by the rate of evaporation from a free-water surface; dimensions: L/T

k Unsaturated conductivity, the hydraulic conductivity for saturations less than unity

n a dimensionless exponent greater than unity dependent on soil type

P Pressure in the liquid phase (water)

P_c Capillary pressure, the difference in pressure ($P_{air} - P$) caused by interfacial forces in the soil pores

P_e Entry pressure, the capillary pressure required to initiate desaturation of a saturated porous solid

P_d A capillary pressure, approximately equal to P_e, determined by the intersection of the straight-line portion of the $P_c - K_{rw}$ curve with the value of $K_{rw} = 1$

S Saturation, the fraction of the pore volume that is occupied by water

w Specific weight of water
z Elevation above the water table

Definitions of derived dimensionless quantities:

$q = e/C$, dimensionless evaporation rate
$K_{rw} = k/C$, relative permeability, the ratio of the unsaturated conductivity at a particular degree of saturation to the hydraulic conductivity at a saturation of unity
$Y = P_c/P_d$, dimensionless capillary pressure
$Z = z/(P_d/w)$, dimensionless elevation above the water table

Upward movement of water from a water table in the absence of hysteresis effects—An analysis of the upward movement of water from a water table in the absence of hysteresis effects may be made using a modification of the familiar Darcy equation

$$e = -k\frac{\partial h}{\partial z} \tag{1}$$

where $\partial h/\partial z$ is the gradient of hydraulic head upward from the water table, and other symbols are defined previously. The hydraulic head of the liquid phase may be written as

$$h = \frac{V^2}{2g} + \frac{P}{w} + z$$

and since the velocity of flow in the soil is very small, the hydraulic head may be written as

$$h = \frac{P}{w} + z \tag{2}$$

The vertical gradient of hydraulic head may be obtained by differentiation of (2) with respect to z, thus

$$\frac{\partial h}{\partial z} = \frac{\partial\left(\frac{P}{w}\right)}{\partial z} + 1 \tag{3}$$

By definition,

$$P_c = P_{air} - P$$

and if the pressure of the air is considered to be zero

$$P_c = -P \tag{4}$$

Substitution of (4) into (3) and substituting the result into (1) yields

$$\frac{\partial \frac{(P_c)}{w}}{\partial z} = \frac{e}{k} + 1 \tag{5}$$

In order to evaluate (5), the relation of the unsaturated conductivity k to capillary pressure, P_c must be known. Reference to Figure 3 shows that over a wide range of capillary pressures this relation may be approximated by

$$k \approx C\left(\frac{P_d}{P_c}\right)^n \tag{6}$$

Work done by *Corey* [1954], based on both theory and experimental observation, indicated that for a large class of oil-bearing materials, the value of n was approximately eight. Appropriate measurements of capillary pressure and unsaturated conductivity were made to determine the n value of (6) for the soil types used in these experiments. The technique used for measuring capillary pressure was described by *Staley* [1957], and measurements of unsaturated conductivity were made using equipment and procedure similar to those described by *Corey* [1957]. The results of the measurements are given in Figure 3. From the measured slopes of the lines on Figure 3 it may be determined that the n values were 13, 14, and 25 for the Fort Collins clay loam, Greeley loam, and Loveland fine sand, respectively.

Substitution of (6) into (5) yields

$$\frac{\partial \frac{P_c}{w}}{\partial z} \approx \frac{e}{C}\left(\frac{P_c}{P_d}\right)^n + 1 \tag{7}$$

Dividing both numerator and denominator of the left-hand side of (7) by P_d/w gives

$$\frac{\partial \frac{P_c}{P_d}}{\partial \frac{z}{\frac{P_d}{w}}} \approx \frac{e}{C}\left(\frac{P_c}{P_d}\right)^n + 1 \tag{8}$$

The significance of the term P_d/w may be seen by noting that when $P_d = P_c$, the term P_d/w represents the thickness of the zone of complete saturation. At the top of this zone, the value of $z/(P_c/w)$ is unity. At the water table, the value of $z/(P_c/w)$ is zero.

Eq. (8) may be written in terms of dimensionless quantities as

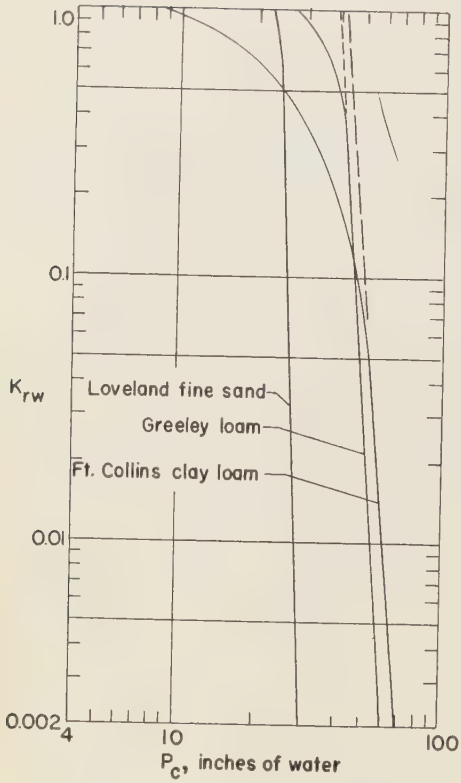

FIG. 3—Relation between capillary pressure (P_c) and relative permeability (K_{rw}) for three soil types

$$\frac{\partial Y}{\partial Z} \approx q Y^n + 1 \tag{9}$$

Eq. (9) is the differential equation describing upward flow of water from a water table for the assumed conditions. It will be noted that (9) applies for the following conditions: $q > 0$, $Z > 1$, $n > 1$, and when $Z = 1$, $Y = 1$.

Analysis of (9) will show that the evaporation rate q reaches a finite limit as the capillary pressure Y becomes infinite at a particular $Z = Z_1$ at the surface of the soil.

For large values of Y and any steady state $q > 0$

$$q Y^n \gg 1 \tag{10}$$

For steady state conditions q is no longer a function of Y or Z and under the conditions of (10) we may write (9) as

$$\frac{dY}{dZ} \approx q Y^n \tag{11}$$

It will be noted that (11) is an exact equation for the case where gravity effects may be neglected, that is, for a horizontal column. A solution of (11) is

$$\frac{Y^{(1-n)}}{1-n} \approx qZ + \text{Constant} \tag{12}$$

We now apply the boundary condition $Y = 1$ at $Z = 1$ to (12) and obtain

$$\text{Constant} \approx \frac{1}{1-n} - q \tag{13}$$

Substitution of (13) into (12) yields

$$\frac{1}{y^{(n-1)}} = (1-n)\left(qZ + \frac{1}{1-n} - q\right) \tag{14}$$

Evaluating (14) in the limit as $Y \to \infty$ at $Z = Z_1$ we obtain

$$q = \frac{1}{(n-1)(Z_1 - 1)} \tag{15}$$

Eq. (15) indicates that for all $n > 1$ and $Z_1 > 1$, q has a finite limit as Y becomes infinite at $Z = Z_1$. In other words, this analysis shows that a limiting rate of evaporation from soils should be reached as evaporativity increases.

A graphical solution of (8) by *Staley* [1957] using an n value of eight showed a limiting value of evaporation rate with increased capillary pressure. An analytic solution by *Gardner* [1958] of an equation comparable to (8), using n values of $\frac{3}{2}$, 2, 3, and 4, also predicts a limiting rate of evaporation. It is significant that their analyses are at variance with the experimental observations presented in Figure 2.

Departure of observations from theory—Several reasons might be advanced for the departure of observations from the theory outlined above. Drying of the surface layer of soil provides a satisfactory explanation for these effects, since when the surface layer of soil is dry, the relation between capillary pressure and unsaturated conductivity will no doubt change drastically from that given by (6).

Philip [1957] has suggested a negative correlation between evaporation from a dry and a saturated soil based on consideration of the effects of a downward heat flux in the soil. This

possibility was recognized, and the effect of downward temperature gradients on evaporation rates was measured when the water table was deeper than 23.5 inches. Results from the tests indicated that elimination of a radiant energy source did not restore evaporation rates to the original rate that existed prior to the application of radiant energy. From these results it was concluded that a downward temperature gradient does not provide a complete explanation for the inverse relation between evaporativity and evaporation from soils in contact with a water table.

Neither of the above hypotheses answers the question of what happens to the flux of water as the soil dries from a saturated state to a moisture content less than that at field capacity. Experimental observations and theory may be reconciled through the hysteresis hypothesis which follows.

Hysteresis effects—A capillary tube model for the explanation of hysteresis effects in soils is presented in Figure 4. Figure 5 shows a schematic representation of the change in capillary pressure at a point such as *c* in the model as desaturation progresses. In the following discussion reference is made to these figures to show that a reversal in the direction of pressure change can take place without a corresponding reversal in the desaturation process.

If no evaporation takes place from the soil during the time from *e* to *f* (Fig. 5), the capillary pressure will remain constant at a point such as *c* (Fig. 4) in the capillary model. If evaporation begins at the time *f*, the capillary pressure at *c* will increase because of head loss through the tube. At some capillary pressure *g* the interface will still be at the position *a*, and will remain there until a critical capillary pressure is reached, at which time the interface will move to a new position *b*. At this position further air entry is prevented by the smaller diameter of the tube. The effect of desaturation in this particular pore is to change the position of the interface from *a* to *b* and to decrease the capillary pressure. The water originally stored between *a* and *b* is transferred to other connected pores such as the pore *d*. With the interface established at the position *b*, water transfer from *b* to *a* takes place by vapor movement at a much slower rate than the previous rate of transfer in the liquid phase. The total flow

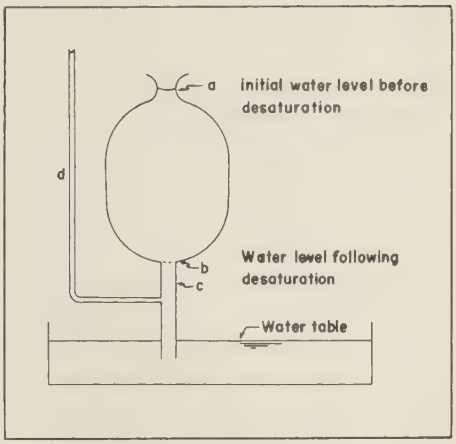

FIG. 4—Model for capillary tube analogy of hysteresis effects during desaturation of a soil in contact with a water table

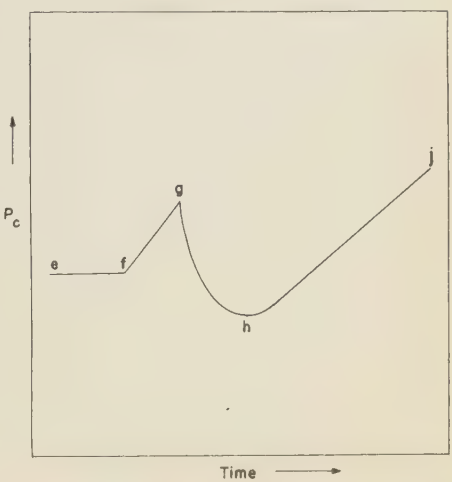

FIG. 5—Schematic representation of the change in capillary pressure (P_c) with time during desaturation at a point in the capillary model corresponding to the point *c* in Figure 4

through the model will be less than when the pore was completely saturated. The resulting reduction in head loss through the tube below *c* contributes to a lowering of the capillary pressure at *c*, as does the initial release of the water held between *a* and *b*, so that the capillary pressure reaches a value *h*. At this point the capillary pressure is lower than the initial

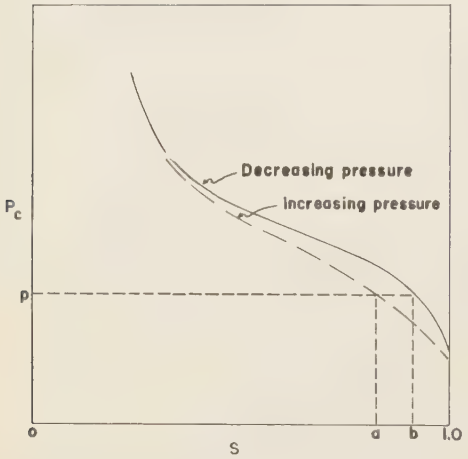

FIG. 6—A relation between capillary pressure (P_c) and saturation (S), (hypothetical data)

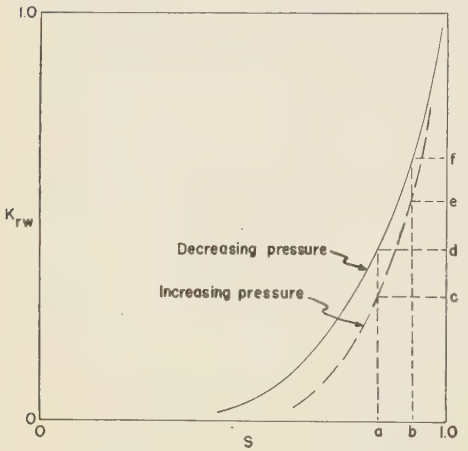

FIG. 7—A relation between relative permeability (K_{rw}) and saturation (S), (hypothetical data)

value e. Despite this lower value, water cannot rise in the tube above b because of the larger diameter of the tube. Thus a reversal in the direction of pressure change can take place in the model without a corresponding reversal in the desaturation process.

As evaporation continues the capillary pressure will increase to a higher value j until at some higher capillary pressure another set of smaller pores will be emptied and the process will be repeated. The net result of this process is that initial desaturation begins an irreversible reduction in the rate of water transfer to the surface; this occurs despite increase in evaporativity. This process could explain the observed inverse relation between evaporativity and evaporation from soils which cannot be explained satisfactorily by the standard capillary flow analysis.

The preceding analysis of the effects of hysteresis in producing reversals of direction of pressure change may be extended from the model to explain similar hysteresis effects in the soil. It should be noted that such effects are possible in the model and presumably in the soil only because part of the capillary pressure at any elevation is produced by resistance to flow. It is likely that the relative importance of hysteresis in the *soil* at a point such as c will depend on the relative magnitude of the capillary pressure produced by this resistance compared with the capillary pressure that would exist at that point, if there were no flow. Hence, such a phenomenon could not exist if the capillary pressure was increased by lowering the water table in a system in which no evaporation was permitted.

The effect of hysteresis on the relationship between capillary pressure and permeability can best be illustrated by an example. Figure 6 shows a relation between saturation and capillary pressure. Figure 7 shows a hypothetical relation between saturation and relative permeability. The existence of a double-valued relation between capillary pressure and saturation is well known and is shown in Figure 6. The existence of a similar double-valued relation between relative permeability and saturation is postulated and is shown in Figure 7. From examination of these two figures, it will be seen that a reversal of direction of pressure change at a given capillary pressure p will produce a reduction of relative permeability. The amount of the reduction will be from f to d if the double-value relation postulated in Figure 7 is not valid; it will be a greater amount from f to c if the relation is valid. In either case, a reduction of considerable magnitude in permeability will be effected.

The preceding analysis shows that the functional relationship between permeability and capillary pressure is probably altered by a reversal in the direction of pressure change in the soil water. Moreover, once desaturation begins,

an irreversible process begins which can proceed only in the direction of further reduction of rate of water transmission to the surface. Consequently, a maximum rather than a limiting rate of evaporation from soils results under these conditions.

The hysteresis effects described above provide a basis for a qualitative explanation of the inverse relation between evaporation from soils and evaporativity under the conditions of the experiment.

Resume—Experimental evidence is presented which shows that when evaporativity exceeds the flow of water to the soil surface, the flow to the surface from a water table at a fixed depth is reduced. A theory is presented which predicts that as soon as evaporation from a bare soil exceeds the rate of transfer of water to the surface, the mechanism of transfer is thereafter a process of imbibition by the drier surface soil. Because of hysteresis in the relation between conductivity and soil water content, water transfer by the imbibition process is slower than that occurring at a smaller evaporativity. The implications are these:

(1) Under certain conditions there will be an inverse relation between evaporativity and evaporation from bare soils. This fact makes the measurements from evaporation pans entirely unreliable as an estimate of the evaporation from bare soils.

(2) Treatments which cause rapid initial drying of the soil surface should conserve soil moisture under most conditions.

References

Corey, A. T., The interrelation between gas and oil relative permeabilities, *Producers Monthly*, 19, 38–41, 1954.

Corey, A. T., Measurements of water and air permeability in unsaturated soil, *Soil Sci. Soc. Am. Proc.*, 21, 7–10, 1957.

Gardner, W. R., Some steady-state solutions of the unsaturated moisture flow equation with application to evaporation from a water table, *Soil Sci.*, 85, 228–232, 1958.

Philip, J. R., Evaporation and moisture and heat field in the soil, *J. Meteorol.*, 14, 354–366, 1957.

Schleusener, R. A., Factors affecting evaporation from soils in contact with a water table, Ph.D. dissertation, Colorado State University, 144 pp., 1958.

Staley, R. W., Effect of depth of water table on evaporation from fine sand, M.S. thesis, Colorado State University, 101 pp., 1957.

(Manuscript received August 19, 1958; revised January 22, 1959.)

The Determination of Soil Moisture under a Permanent Grass Cover

G. W. SMITH

Regional Research Centre
Imperial College of Tropical Agriculture
Trinidad, West Indies

Abstract—Using climatological, soil, and plant data, an attempt has been made to calculate the moisture status of a soil under a permanent grass cover. It has been shown that it is insufficient to use formulas which estimate potential evapotranspiration only, such as those of Thornthwaite, Blaney and Criddle, or Penman. When these methods were modified to account for decreasing evapotranspiration with decreasing soil moisture, better results were obtained. The ratio of actual to potential evapotranspiration has been denoted by the symbol F. Three different possibilities for the dependence of F on soil moisture have been examined. The theoretical figures have been compared with figures obtained by augering over a period of about 22 months.

It is shown, both graphically and statistically, that Thornthwaite's F factor theory is more satisfactory than Penman's or Veihmeyer's. When Thornthwaite's method is used, there is no statistically significant difference between moisture deficits based on the Penman, Blaney and Criddle, or Thornthwaite equations for potential transpiration.

Introduction—Considerable interest exists in the estimation of the amount of water contained in the soil at any time. *Eastwell* [1953] has made an extensive survey of those methods which involve measurement of some physical property of the soil dependent on its moisture content. These methods do not allow moisture estimations to be made in retrospect. The purpose of this paper is to examine the 'climatological' method. If weather data are available (as is often the case) it is possible by this approach to estimate the moisture status of the soil at any time.

In this method, climatological data are used to estimate the amount of water which is withdrawn from the soil by the plant cover (that is, by evapotranspiration). The difference between this amount and the rainfall gives the quantity of water remaining in the soil.

The first step is to calculate the potential evapotranspiration (the amount of water used by a crop which completely covers the surface of the soil when the water supply is non-limiting). It will be shown later that actual evapotranspiration is not, in general, identical with potential evapotranspiration, but that the ratio, actual to potential, varies with the soil moisture status. The exact nature of this variation has been the subject of considerable discussion.

An attempt has been made in this paper to answer the question: "Which method of potential evapotranspiration estimation, combined with which theory of the variation of actual evapotranspiration with soil moisture, gives results which are closest to those obtained by observation?"

Methods of estimating potential transpiration—Blaney and *Criddle* [1950], in an attempt to assess water requirements of various crops, recognized the role played by some of the factors controlling transpiration. They realised that in many places, records of solar radiation, wind speed, and humidity were difficult or impossible to obtain. They therefore ignored the effect of wind and humidity altogether, but attempted to include the effect of solar radiation by introducing a term in their formula which represented the theoretical day length on the particular date under investigation. Mean air temperature was introduced directly. To make some allowance for the effect of soil and plant type, depth of rooting, etc., they introduced a 'consumptive use (evapotranspiration) factor,' developed empirically from experimental values.

Thornthwaite [1948] proposed a formula which relates potential transpiration to mean air temperature and latitude. His method has been used extensively, particularly in the United States. Like the Blaney-Criddle formula, it is largely empirical. Modifications to the original

equation have been suggested both by Thornthwaite and his associates [*Thornthwaite* and *Mather*, 1955a] and by other workers such as *Garnier* [1956] in Nigeria.

Penman [1948] has elaborated a theory which consists of a combination of energy balance and aerodynamic theories. The final equation is somewhat complex. It gives values of open-water surface evaporation, rather than of potential evapotranspiration. However, it is claimed that the two quantities are closely related. If E_o = open-water evaporation and E_T = potential transpiration, Penman showed experimentally that

$$E_T = fE_o$$

where f has values (in England) of 0.8 for the period May-August, 0.7 for September, October, March, and April, and 0.6 for the remainder of the year.

The Blaney-Criddle formula appears to have been used almost exclusively by irrigation engineers. It does not seem to have been used to estimate actual values of soil moisture. Thornthwaite's method has been used widely for this purpose, as has Penman's. While the underlying theory of the latter is considerably more satisfactory than that of Thornthwaite, it has the disadvantage that four climatological parameters are involved. Thornthwaite's method uses values of mean air temperature, latitude, and date only.

The dependence of evapotranspiration on soil moisture status—The variation in transpiration with soil moisture is not yet thoroughly understood. Veihmeyer and his associates take the view that soil moisture has virtually no influence on transpiration provided that it fluctuates only between field capacity and wilting point [*Veihmeyer* and *Hendrickson*, 1955]. Logically, it would appear unlikely that this is so. Since, by definition, transpiration proceeds at the potential rate when the soil is at field capacity, and since, by implied definition, transpiration ceases completely at wilting point, it seems unlikely that there should be an abrupt transition at wilting point from the potential rate to zero. Veihmeyer's views are supported, in part, by the work of *Hagan* and others [1957].

Thornthwaite and *Mather* [1955b] consider that the ratio of potential to actual evapotranspiration varies linearly with the amount of 'available' water in the rooting zone of the crop considered. Thus, when the soil moisture is at field capacity, potential transpiration is equal to actual transpiration. At the wilting point, the ratio is small or zero; that is, actual evapotranspiration is either a very small fraction of potential evapotranspiration or zero. These two workers have published results of soil moisture calculations using this theory, and satisfactory agreement between calculated and measured figures was obtained. Thornthwaite's views are supported by *Makkink* and *Van Heemst* [1956], *Slatyer* [1956], *West* and *Perkman* [1953], and *Taylor* [1952.] The ingenious method of *Bloodworth* and others [1955] also provides evidence of decreasing evapotranspiration with decreasing soil moisture.

Penman [1956] holds a view which is intermediate between those of Veihmeyer and Thornthwaite. With soils sufficiently deep for the rooting habit of plants to be unchecked, he considers that evapotranspiration continues at the potential rate from field capacity until "the readily available water around the roots is used." Thereafter, the actual transpiration decreases fairly sharply. Water is still removed from the soil, but at a much lower rate than the potential, and significantly greater than zero.

These three theories are summarized in Figure 1, in which the ratio of actual to potential transpiration has been called the F factor. The 'Penman' curve is an adaptation of a figure given by *Penman* [1949].

Experimental—The experimental area, described more fully in *Smith* [1954], was a site in the immediate vicinity of the meteorological station at Imperial College in Trinidad. It had a permanent, long established cover of savanna grass (*Axonopus Compressus*). Auger samples were taken weekly for a total period of 22 months. Twelve samples were obtained on each occasion, half at a depth of 0 to 6 inches and the remainder between 6 and twelve inches. The mean of these determinations was taken as the soil-moisture content in the rooting zone.

The necessary constants were found to be as follows: rooting zone, 18 inches (457 mm); apparent specific gravity (volume weight), 1.44; field capacity, 31.7 pct; wilting point, 9.0 pct; and Blaney-Criddle factor, 0.75 (mean value given for pasture). In order to convert moisture

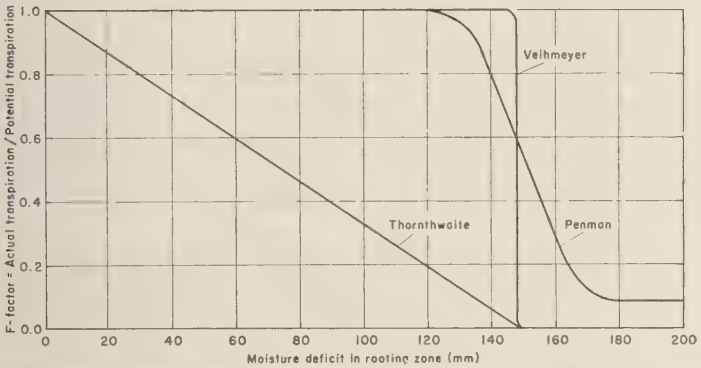

FIG. 1—Relation between F factor and soil moisture deficit according to Penman, Thornthwaite, and Veihmeyer

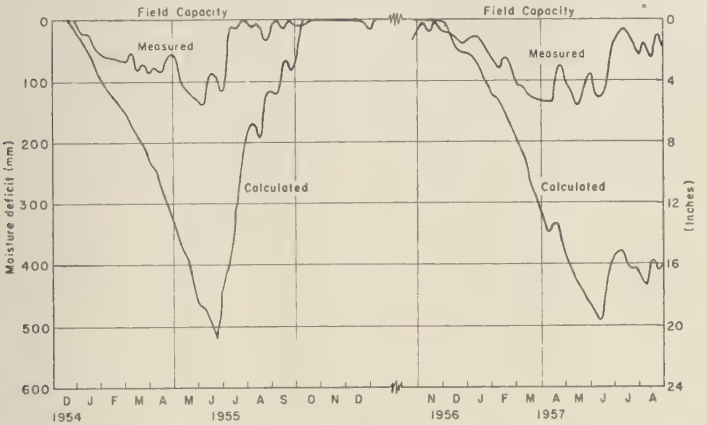

FIG. 2—Relation between measured and calculated soil-moisture deficit (Thornwaite, uncorrected)

measurements to 'deficits,' the following equation was used [*Smith*, 1956]:

$$D = 208.6 - 6.581S$$

where D is the moisture deficit, mm

S is the measured soil moisture, pct of dry weight

The effect of considering potential evapotranspiration alone—In order to show that it is necessary to consider the effect of decreasing transpiration with decreasing moisture content, it was assumed that $F = 1$, over the entire range of soil moisture. Figure 2 shows the result of doing this, using the method of Thornthwaite to calculate potential transpiration. Comparison with the measured values shows that the method gives results which are very seriously in error. In June 1955 the moisture deficit was apparently 520 mm. This could not possibly be correct, since an 18 inch (457 mm) depth of soil could only contain 457 mm of water even if no solid matter whatever were present.

Curves showing moisture deficits calculated by the Blaney-Criddle and Penman methods give similar results.

The effect of using various types of F factor correction—In Figures 3, 4, and 5 the results are shown using Penman, Blaney-Criddle, and Thornthwaite estimates of potential evapotranspiration, each being modified by using Penman, Thornthwaite, and Veihmeyer F factors. From these, it is fairly clear that the Thornthwaite F factor gives the closest ap-

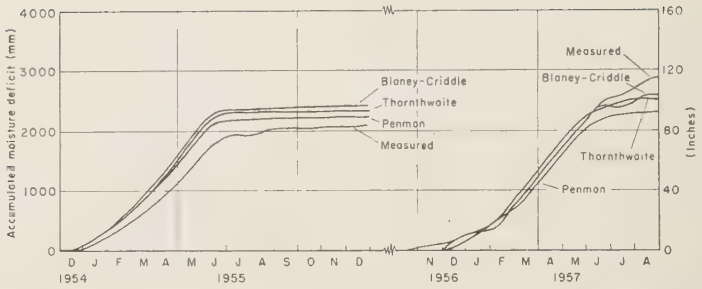

FIG. 3.—Relation between measured and calculated accumulated moisture deficits (Thornthwaite *F* factors)

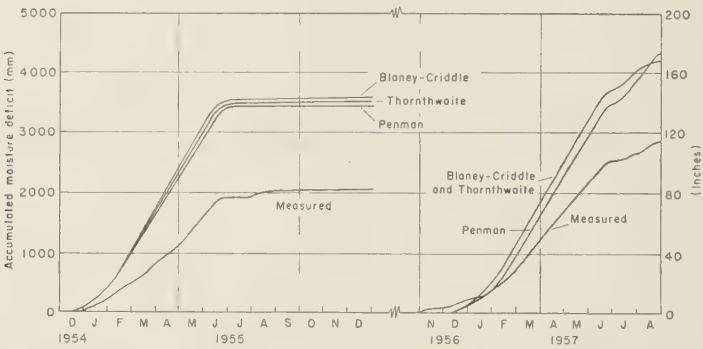

FIG. 4—Relation between measured and calculated accumulated moisture deficits (Penman *F* factors)

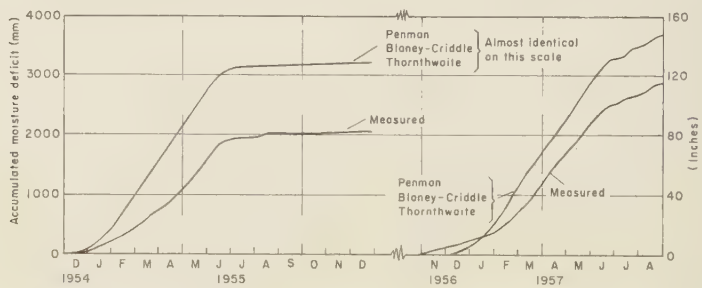

FIG. 5 Relation between measured and calculated accumulated moisture deficits (Veihmeyer *F* factors)

proach to the measured values of moisture deficit. In order to show up the differences in the most effective way, accumulated deficits have been plotted. In Figure 6, two of the most promising methods have been used to plot moisture deficit curves. They are those using the Thornthwaite and Penman methods for potential transpiration, each modified by Thornthwaite *F* factors.

It is at once evident that a considerable improvement has been effected by using the *F* factors. It is now no longer possible for absurdly high values of moisture deficit to be obtained during long periods of dry weather, as was the case when *F* factors were always unity.

Statistical analysis of results—To summarize the results, a statistical analysis was performed. The moisture deficit obtained by calculation

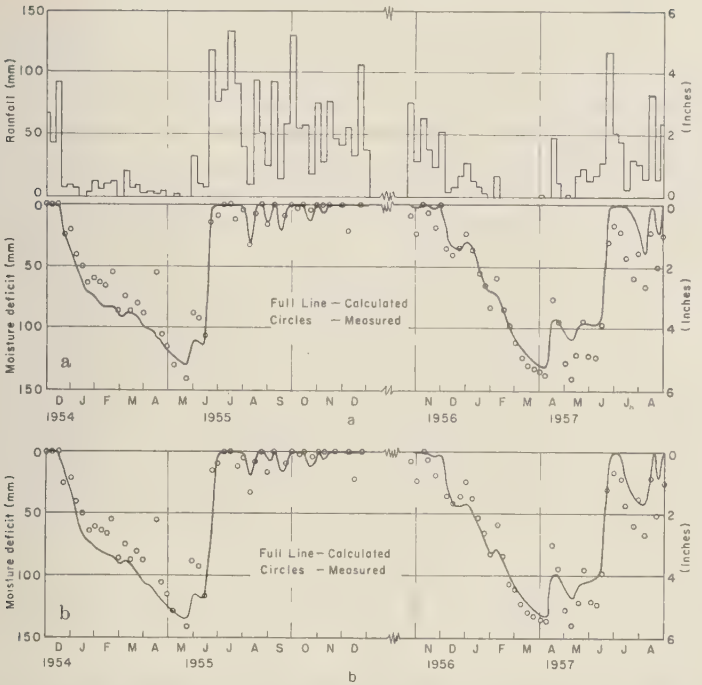

FIG. 6—Relation between measured and calculated soil-moisture deficits (a) (Penman, with Thornthwaite F factors) (b) (Thornthwaite, with Thornthwaite F factors)

was considered to be the independent factor x, and the deficit actually measured by augering, the dependent factor y. Linear regression equations were calculated for each of nine possibilities. In the ideal case, when the calculated and measured values agree exactly, the regression equations will take the form

$$y = x$$

Where perfect agreement does not exist, the form will be

$$y = mx + c$$

Thus one criterion of reliability of estimation will be the closeness of m to one and of c to zero.

Another criterion will be the size of the variance of the deviations of the calculated points from the linear regression line. The smaller this is, the less will be the scatter of the points from the regression line. Table 1 shows the analysis.

While this table is not intended to be a summary of a complete and detailed statistical treatment, it does help to show the main trends more clearly than do the graphs. It will be observed that the estimates based on Penman and Veihmeyer F factors are generally of a lower order of reliability than those based on Thornthwaite F factors. The table shows, rather surprisingly, that no greater reliability is obtained by using the complicated Penman formula for potential evapotranspiration rather than the simpler Thornthwaite method.

The difference between any two variances is not statistically significant unless their ratio is greater than about 1.65 ($P = 0.01$). There are no significant differences between the last three methods of Table 1.

Conclusions—It has been demonstrated that the moisture status of the soil cannot be estimated on the basis of using figures of potential evapotranspiration alone. It is necessary to account for the fact that actual evapotranspiration is not always equal to potential evapotranspiration. The theory that most closely fits the observed facts is that of Thornthwaite.

TABLE 1—*Statistical summary of results*

Method used[a]	Variance[b,c]	Regression equation[d]
Thornthwaite-Penman	558	$y = 0.55x + 6$
Blaney-Criddle-Veihmeyer	319	$y = 0.65x + 5$
Penman-Penman	315	$y = 0.60x + 2$
Penman-Veihmeyer	310	$y = 0.67x + 3$
Thornthwaite-Veihmeyer	294	$y = 0.67x + 3$
Blaney-Criddle-Penman	269	$y = 0.58x + 4$
Blaney-Criddle-Thornthwaite	222	$y = 0.87x + 7$
Penman-Thornthwaite	216	$y = 0.92x + 8$
Thornthwaite-Thornthwaite	189	$y = 0.90x + 6$

[a] The first name mentioned refers to the method used to calculate potential evapotranspiration, the second to the type of F factor correction.

[b] Degrees of freedom: one because of regression; 86 because of deviations from regression line; the total number of 'calculated' values was 95, but on a few occasions measured figures were not available; this reduced the number of complete pairs of observations.

[c] The table has been arranged in decreasing order of the variances of the deviations from the linear regression equation.

[d] y = measured moisture deficit, x = calculated moisture deficit.

An unexpected result was the relatively poor agreement obtained using the Penman method of estimating potential evapotranspiration. It is believed that this may be due to uncertainty in the value to be used for f. A value of 0.8 was used for all months (Penman, private communication), but this figure is not wholly supported by experimental evidence obtained in Trinidad. Since there was some doubt about the validity of this evidence, it was considered preferable to use Penman's recommended figure.

Note that the results obtained in this paper need not necessarily be true for all soils and crops. For instance, with a crop having a very deep rooting habit it is possible that the moisture stored in the rooting zone might be sufficient at all times for potential transpiration to be substantially equal to actual transpiration. The curves shown in Figure 1 would then be applicable only in a narrow range close to the region in which $F = 1$. In this case, it is likely that the use of the F factors would be of little practical importance.

Acknowledgments—It is a pleasure to acknowledge the help that has been received in the preparation of this paper by my colleagues in Trinidad. I should particularly like to mention T. A. Jones, G. E. Hodnett, and I. Pothecary, with all of whom I have had helpful discussions.

REFERENCES

BLANEY, H. F., AND W. D. CRIDDLE, Determining water requirements in irrigated areas from climatological and irrigation data, *U. S. Dept. Agr., Soil Conserv. Serv., SCS-TP-96,* 48 pp., 1950.

BLOODWORTH, M. E., J. B. PAGE, AND W. R. COWLEY, A thermoelectric method for determining the rate of water movement in plants, *Soil. Sci. Soc. Am. Proc.,* 19, 411–414, 1955.

EASTWELL, B. A., In situ methods of measuring soil-moisture content—a critical resume, *Tech. Rept. Brit. Elec. Research Assoc. W/T27,* 19 pp., 1953.

GARNIER, B. J., A method of computing potential evapotranspiration in West Africa, *Bull. Inst. Franc. Noire, A,* 18, 665–676, 1956.

HAGAN, R. M., M. L. PETERSON, R. P. UPCHURCH, AND L. G. JONES, Relationships of soil-moisture stress to different aspects of growth in Ladino clover, *Soil Sci. Soc. Am. Proc.,* 21, 360–365, 1957.

MAKKINK, G. F., AND H. D. J. VAN HEEMST, The actual evapotranspiration as a function of potential evapotranspiration and the soil moisture tension, *Neth. J. Agr. Sci.,* 4, 67–72, 1956.

PENMAN, H. L., Natural evaporation from open water, bare soil, and grass, *Proc. Roy. Soc. London, A,* 193, 120–146, 1948.

PENMAN, H. L., The dependence of transpiration on weather and soil conditions, *J. Soil Sci.,* 1, 74–89, 1949.

PENMAN, H. L., Evaporation, an introductory survey, *Neth. J. Agr. Sci.,* 4, 9–29, 1956.

Slatyer, R. O., Evapotranspiration in relation to soil moisture, *Neth. J. Agr. Sci.*, 4, 73–76, 1956.

Smith, G. W., Evapotranspiration in Trinidad, B.W.I., *Publs. Climatol.*, 7, 125–139, Johns Hopkins Univ., Lab. of Climatol., 1954.

Smith, G. W., The estimation of soil moisture, with particular reference to tropical conditions, unpubl. thesis, London Univ., 116 pp., 1956.

Taylor, S. A., The use of mean soil-moisture tension to evaluate the effect of soil moisture on crop yields, *Soil Sci.*, 74, 217–226, 1952.

Thornthwaite, C. W., An approach towards a rational classification of climate, *Geograph. Rev.*, 38, 55–94, 1948.

Thornthwaite, C. W., and J. R. Mather, The water balance, *Publs. Climatol.*, 8, 104 pp., Johns Hopkins Univ., Lab. of Climatol., 1955a.

Thornthwaite, C. W., and J. R. Mather, The water budget and its use in irrigation, *Yearbook Agr., U. S. Dept. Agr.*, 346–357, 1955b.

Veihmeyer, F. J., and A. H. Hendrickson, Does transpiration decrease as the soil moisture decreases?, *Trans. Am. Geophys. Union*, 36, 425–448, 1955.

West, E. S., and O. Perkman, The effect of soil moisture on transpiration, *Australian J. Agr. Research*, 4, 326–333, 1953.

(Manuscript received May 12, 1958; revised January 14, 1959.)

Letters to the Editor

DISCUSSION OF PAPER BY S. IRMAY, 'ON THE THEORETICAL DERIVATIONS OF DARCY AND FORCHHEIMER FORMULAS'

JOHN HAPPEL

Department of Chemical Engineering
New York University, New York, N. Y.

Without wishing to multiply treatments which involve a derivation of the well-known Darcy formula for flow through porous media, I believe it worth calling attention to a recent treatment which for the case of regular particles not only arrives at the basic equation but numerical values for the permeability constant itself [*Happel*, 1958a]. *Irmay's* [1958] paper applies to both the Darcy and Forchheimer formulas, but as far as the Darcy equation is concerned it still requires the employment of an experimentally determined permeability constant.

A new mathematical approach has been developed on the basis that two concentric spheres can serve as the model for a random assemblage of solid spheres through which fluid is moving. The inner sphere comprises one of the particles in the assemblage and the outer sphere consists of a fluid envelope with a 'free surface.' The appropriate boundary conditions resulting from these assumptions enable closed solutions to be obtained for the Navier-Stokes equations omitting inertia terms.

Perhaps the most striking confirmation of the theory is the case of flow through packed beds. A correlation very widely used at present for resistance to flow is that due to Kozeny and is referred to in Irmay's paper. This equation enables the effect of solids concentration to be estimated on a semitheoretical basis, but it still requires the employment of an experimentally determined constant to characterize the medium involved. Thus,

$$V = \left[\frac{(1 - \phi)^3 a^2}{9\phi^2 k}\right] \times \frac{\Delta p}{\mu L} \qquad (1)$$

where ϕ is the fractional volume solids concentration, a is the particle radius, μ is the fluid viscosity, k is the experimentally determined Kozeny constant, Δp is the pressure drop, L is the length of bed, and V is the superficial fluid velocity through a porous bed. The Darcy constant is the item in brackets in (1). Irmay's paper, insofar as it refers to Darcy's equation, is a theoretical development of this formula in a more general form, since he does not require a bed of regular shaped particles.

For the case of uniform granular particles, extensive investigations by *Carman* [1956] indicate that the constant $k \simeq 5$. For absolutely uniform spheres the value of $k = 4.8$ is recommended, but the experimental accuracy of the data is probably no better than $\pm$ 10 to 15 per cent. The present theory enables a value to be predicted for this constant,

$$k = \frac{(1 - \phi)^3(3 + 2\phi^{5/3})}{6\phi - 9\phi^{4/3} + 9\phi^{8/3} - 6\phi^3} \qquad (2)$$

In the range of solids concentration $\phi = 0.3$ to 0.8 (that is, porosity $\eta = 20$ to 70 per cent in Irmay's terminology) the relationship given in (2) agrees on the average to within 8 per cent with the Carman-Kozeny equation employing $k = 5$ and considerably better in the middle of the range. Since the resistance to flow in a bed corresponding to $\phi = 0.75$ is approximately 400 times as great as if the particles were suspended in a very dilute medium (Stokes' Law), this can be considered very good validation. Furthermore in the range of ϕ less than 0.3 the Carman-Kozeny relationship does not hold, but the relationship given by (2) gives satisfactory results to the extreme of dilution.

Other interesting studies, using the same 'free surface' model [*Happel*, 1958b] involve rate of sedimentation of particles and estimation of viscosity of particle suspensions without resort to any experimental constants. These studies also show good agreement with available experimental data.

References

Carman, P. C., *Flow of gases through porous media*, Academic Press, New York, 182 pp., 1956.

Happel, J., Viscous flow in multiparticle systems: slow motion of fluids relative to beds of spherical particles, *A.I.Ch.E. Journal*, 4, 197–201, 1958a.

Happel, J., Fluid flow in multiparticle systems, *Trans. N. Y. Acad. Sci.*, 20, 404–410, 1958b.

Irmay, S., On the theoretical derivations of Darcy and Forchheimer formulas, *Trans. Am. Geophys. Union*, 39, 702–707, 1958.

(Received November 10, 1958.)

Author's Reply to Preceding Discussion

S. Irmay

Israel Institute of Technology, Haifa, Israel, and Institute of Mathematical Sciences, New York University, New York, N. Y.

Happel's [1958] interesting paper shows an ingenious way of finding the Darcy formula on the basis of the creeping flow theory, if it is assumed that a spherical solid particle is moving through a concentric viscous liquid sphere with a free surface. His results appear to agree with the Kozeny-Carman relationship $n^3/(1-n)^2$ for a wide range of porosities n. He also finds the value of the numerical coefficient, which is usually not determined by other theories. His method is analogous to statistical averaging over a volume of the porous medium, which is essentially the method used by the author.

The Kozeny-Carman relationship with a numerical coefficient can be found in several other ways. One way [*Irmay*, 1951] is to assume the capillary-tube analogy and use the Poiseuille formula in the form

$$q = KJ \tag{1}$$

where q is a specific discharge (that is, discharge per unit area), J is hydraulic gradient, K is hydraulic conductivity, and D is tube diameter. We have

$$K = (1/32)\, D^2 g/\nu \tag{2}$$

Introducing the hydraulic radius R, defined as the ratio of the volume of liquid to the total surface of the wall, and whose value for a circular tube is R = D/4, we get

$$K = (\tfrac{1}{2})R^2 g/\nu \tag{3}$$

Following the practice accepted by hydraulic engineers, we extend the validity of (3) to porous media. The volume of liquid in a unit of soil volume is the porosity n, the volume of soil grains (assumed spherical and of diameter d) is $(1-n)$, and the specific surface is $d/6$. Hence

$$R = \frac{dn}{6(1-n)} \tag{4}$$

Combining (3) and (4) we get

$$K = \frac{g}{\nu}\left[\frac{d^2 n^3}{72(1-n)^2}\right] \tag{5}$$

Another method of finding this relationship has been proposed by the author [*Irmay*, 1955]. The model employed is that of a solid rock fissured along three systems of parallel and mutually-inclined planes. The Poiseuille formula applied to each fissure results in the Darcy formula. The hydraulic conductivity K is then a symmetrical second rank tensor with its components given as functions of the geometry of the fissured medium. Only in the case of mutually orthogonal fissures of identical size and spacing does K become the usual scalar coefficient. The dependence of K on the porosity is given to first approximation by

$$K = \frac{g}{\nu}\left[\frac{d^2 n^3}{81(1-n)^2}\right] \tag{6}$$

where d is the side length of each cube. The agreement with (5) is excellent in view of the very different models assumed. A more refined theory replaces $n^3/(1-n)^2$ by

$$[1 + (1-n)^{\frac{1}{3}}][1 - (1-n)^{\frac{1}{3}}]^3/(1-n)$$

with an appropriate (well-defined) numerical coefficient. The two expressions are proportional

for $n<0.65$. A full presentation of this method will be the subject of another paper.

This similarity of results obtained by such widely divergent methods is probably due to the fact that flow through porous media is a very complex phenomenon. Thus, averaging on the basis of any plausible model gives agreeable results; though this agreement does not necessarily prove the validity of the models assumed.

The method developed by the author in this paper has two advantages. First, it is not based on any analogies or models, but only on statistical averaging. The same method, when applied to unsaturated media, gives the generalized diffusion equation and the cubical dependence of K on the degree of saturation [*Irmay*, 1954, 1956]. This method will be fully developed in another paper. Secondly, to the author's knowledge, this is the only method for deriving the Forchheimer formula.

References

Happel, J., Viscous flow in multiparticle systems; slow motion of fluids relative to beds of spherical particles, *A.I.Ch.E. Journal*, 4, 197–201, 1958.

Irmay, S., On the motion of capillary moisture in soils, *Hebrew Inst. Tech., Haifa, Sci. Publ. 4*, pp. 43–90, 1951 (in Hebrew with English abstr.).

Irmay, S., On the hydraulic conductivity of unsaturated soils, *Trans. Am. Geophys. Union.*, 35, 463–467, 1954.

Irmay, S., Flow of liquids through cracked media (abstr.), *Bull. Research Council Israel, Sect. A*, 5, p. 84, 1955.

Irmay, S., Extension of Darcy law to unsteady unsaturated flow through porous media, *Publ. 41, Symposia Darcy*, Assoc. Intern. Hydrol., UGGI, pp. 57–66, 1956.

Discussion of Paper by Hsin Kuan Liu, 'A Note on the Differential Equation of Steady, Gradually Non-Uniform Flow in Open Channels'

Ven Te Chow

University of Illinois
Urbana, Illinois

It is believed that the confusion involved in the derivation of the gradually-varied-flow equation is due to a disagreement between the mathematical and the physical rules of sign convention: a descending slope is considered as negative in analytic geometry, but as positive in physical hydraulics.

In the author's note [*Liu*, 1958] a compromise for the disagreement is made by equating a positive quantity in the mathematical sense to a negative quantity in the physical sense; that is, $x = -l$.

In traditional hydraulics, however, the compromise is simply made by assuming that the (physical) slope or gradient is opposite in sign to the (mathematical) change with respect to x. This rule is represented by (8).

There is another rule of sign convention [*Mitchell*, 1954, p. 19; *Chow*, 1955, p. 2] by which only the mathematical sign convention is observed. As flow always involves a loss of energy, this rule dictates that the loss in head is equal to the initial value minus the final value. Hence, the friction loss dE is positive in the direction of flow; that is, $dE/dx = S_e$.

Similarly, the difference in elevation is made equal to the initial value minus the final value. Hence, the difference in elevation dz is positive in the direction of a descending slope; that is, $dz/dx = S_0$.

Thus, (2) should be

$$\frac{dE}{dx} = \frac{d}{dx}\left(\frac{V^2}{2g}\right) + \frac{dy}{dx} + \frac{dz}{dx} \tag{13}$$

From (13),

$$\frac{dy}{dx} = -\frac{S_0 - S_e}{1 + \frac{d}{dy}\left(\frac{V^2}{2g}\right)} \tag{14}$$

It should be noted that the use of the above-mentioned rule of sign convention has resulted in a negative sign preceding the right side of (14). This negative sign, however, would not be shown in a traditional derivation of the equation. In analytic geometry, the negative sign

simply explains that dy/dx is negative (or positive) if the slope of the water surface is descending (or ascending) downstream.

References

Chow, V. T., Integrating the equation of gradually varied flow, *Proc. Am. Soc. Civil Engrs.*, 81, Paper 838, 1–32, 1955.

Liu, H. K., A note on the differential equation of steady, gradually non-uniform flow in open channels, *Trans. Am. Geophys. Union*, 39, 939–940, 1958.

Mitchell, W. D., Stage-fall-discharge relations for steady flow in prismatic channels, *U. S. Geol. Survey Water Supply Paper 1164*, 159 pp., 1954.

(Received January 7, 1959.)

Airborne Gravity Meter Test

Lloyd G. D. Thompson

Air Force Cambridge Research Center
Bedford, Massachusetts

Airborne tests made with a LaCoste and Romberg gravity meter have shown that gravity measurements in a flying aircraft are feasible. The flight tests were made on a USAF KC-135 over Edwards Air Force Base, California, on November 6 and 7, 1958.

Precise flight and position data were obtained by a Doppler Navigation System on board the aircraft and by a ground tracking range using an Askania Camera Positioning System. With the aircraft flying on automatic pilot, several traverses over the tracking range were made flying north, south, and west at 20,000 feet and 30,000 feet with different airspeeds. In all of these runs the gravity meter performed much better than it would have performed on a surface ship, for which it was designed. Direct in-flight evidence that the instrument was affected by gravitational changes was obtained when the meter recorded roughly a 100-milligal increase over the Tehachapi Mountains. While the final results are not yet available, it is believed from the nature of the gravity meter records and the precision of the flight data that the results are accurate to about 10 milligals. These gravity measurements are the first ever known to have been made in a flying aircraft. It now seems possible to develop an airborne gravity survey system which will provide data over the entire world in a few years.

Acknowledgments—Lucien LaCoste provided and operated the gravity meter. The tests, a part of the Air Force Cambridge Research Center Gravity Project, were conducted in cooperation with the Flight Test Center at Edwards Air Force Base.

(Received December 7, 1958)

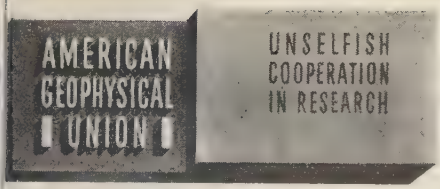

AMERICAN GEOPHYSICAL UNION

1515 Massachusetts Avenue, N.W., Washington 5, D. C.

Established by the National Research Council in 1919 for the development of the science of geophysics through scientific publication and the advancement of professional ideals.

APPLICATION FOR MEMBERSHIP

Please refer to qualifications on reverse side and designate below type of membership desired:

Member ($10) ☐ Associate ($10) ☐ Student ($3) ☐

Application forms for Corporation Membership are available upon request.

1. _____
Surname *First Name* *Middle Name*

2. _____
Preferred mailing address for publications

_____
Permanent address

3. _____ 4. _____
Place *Month* *Day* *Year of Birth* *Country of citizenship/naturalization*

5. _____
Nature of work and title and/or military rank; name and address of organization with which you are associated.

6. Check section or sections with which affiliation is desired.

☐ Geodesy
☐ Seismology
☐ Meteorology
☐ Geomagnetism and Aeronomy
☐ Oceanography
☐ Volcanology, Geochemistry, and Petrology
☐ Hydrology
☐ Tectonophysics

7. **EXPERIENCE (List below)**

Dates: From To Name and address of organization Title, duties, nature of work

8. **EDUCATION (List below)**

Dates: From To School Address Major Subject Degree, if any

*9. References: Please list below names and addresses of two or three references; include members of the AGU or others who know you well.

*10. Titles of technical contributions or publications, particularly those in the geophysical sciences, and where published.

*11. Brief statement of any special interests or qualifications in the geophysical sciences.

Date _____ _____
Written Signature

* Applicants for student membership may omit Questions 9, 10, and 11, but must fill in Question 12. Please return form with check or money order payable to American Geophysical Union, 1515 Massachusetts Ave., N.W., Washington 5, D. C.

(over)

12. (STUDENT MEMBERS ONLY) The person whose signature appears on the reverse side is known to me and is a student majoring in_____(subject) at_____ (Name of college or university) expected to graduate in_____(year) with the degree of_____

☐ He is a full-time student, or ☐ a teaching or research assistant enrolled in more than half of a full-time academic program.

_____
(Signature of faculty sponsor)

☐ Check here if faculty sponsor is a member of AGU and willing to act as a regular sponsor for associate membership as well.

_____
(Typed or printed name of sponsor)

_____
(Title)

QUALIFICATIONS FOR MEMBERSHIP IN THE AMERICAN GEOPHYSICAL UNION

The membership of the AGU shall consist of Members, Associate Members, Student Members, and Corporation Members.

Those eligible as candidates for election to the grade of MEMBER shall be:

MEMBER (a) Persons who have made an active contribution to geophysical research through observation, publication, teaching, or administration. Definite evidence should be presented to the Membership Committee. "Publications" may include books, articles, unpublished manuscripts, inventions, or development of geophysical instruments.

(b) Persons who have made active practical application of geophysical research. It should be shown that the nominee's work has not been purely routine, but that it has tended to create new knowledge of, or to broaden or strengthen the application of, geophysical research. In general, the minimum qualifications for membership will be not less than three years of professional experience in some phase of geophysics.

Those eligible as candidates for election to the grade of ASSOCIATE MEMBER shall be:

ASSOCIATE MEMBER Persons who have an active interest in physical processes of the Earth or technical assistance in the application of geophysics. In general, the minimum qualification for associate membership will be acceptable training or experience in some field of geophysics or allied science.

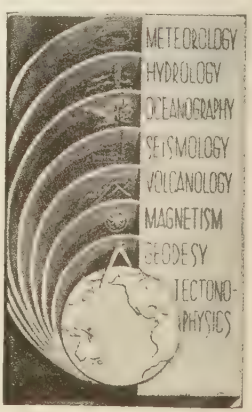

CORPORATION MEMBER Corporations and other interested organizations shall be eligible as candidates for election to CORPORATION MEMBERSHIP. They shall have the privilege of designating a representative who has the rights and privileges of Members (use special form).

STUDENT MEMBER Those eligible as candidates for election to the grade of STUDENT MEMBER shall be persons who are graduate or undergraduate students in residence at least half-time and who are specializing in the geophysical sciences. Teaching or research assistants enrolled in more than half of a full-time academic program may also be eligible for Student Membership. Student Members shall have all the privileges of Members except that they shall not vote or hold office.

American Geophysical Union

PROPOSAL FOR CORPORATION MEMBERSHIP

To the Executive Committee, American Geophysical Union
1515 Massachusetts Ave., N.W., Washington 5, D. C.

Gentlemen:

As an indication of our interest in the aims and activities of the American Geophysical Union, and to assist in maintaining and extending its program of publication and other work in the development of the geophysical sciences, the undersigned applies for Corporation Membership in the AGU and, until further notice, agrees to pay annual dues, currently at the rate of $100 per unit of corporation membership, in accordance with the information set forth on the back of this sheet.

Company or Organization _____

By _____ Title _____
(Signature)

Address _____

City _____ State _____

General fields of activity _____

_____

_____

_____

The following person is designated as our representative in this membership _____

_____ Title _____

Number of units of membership desired (this will be taken as one unless otherwise indicated) _____

Place _____

Date _____

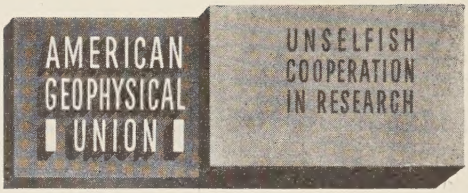

INFORMATION CONCERNING CORPORATION MEMBERSHIP

The American Geophysical Union is a non-profit scientific organization established by the National Research Council. It is the American National Committee of the International Union of Geodesy and Geophysics, and its Executive Committee is the Committee on Geophysics of the National Research Council.

Extracts from the Statutes:

Article 3. Membership—The membership of the American Geophysical Union shall be as follows:

(e) *Corporation Members*—Corporations and other organizations interested in geophysics elected by the Executive Committee of the Union. The designated representative of each such organization shall enjoy the privileges of a Member.

Extracts from the By-Laws:

(2) . . . Members of class (e) shall pay dues of $100 for each calendar year; . . .

(21) One copy of each issue of (a) the *Transactions*, (b) *Journal of Geophysical Research*, (c) any published *List of Members and Officers*, and (d) any other publication which may be approved for *free distribution* to the membership by the Executive Committee of the Union, shall be sent to each . . . Corporation Member. . . . Each . . . organization in good standing may purchase any available publication of the Union at a discount from printed price list to non-members. The General Secretary is authorized to establish discounts for sales of publications.

Action of the Executive Committee, November 29, 1946:

(1) A list of corporation members shall be published on one or more pages immediately after the final page of text in each issue of the *Transactions*.

(2) A list of corporation members shall be included in the Membership Directory as a distinct unit.

AMERICAN GEOPHYSICAL UNION

1515 Massachusetts Ave., N.W.
Washington 5, D. C.

Information for Contributors to the *Journal of Geophysical Research*

Manuscripts—Send manuscripts to J. A. Peoples, Jr., Department of Geology, University of Kansas, Lawrence, Kansas. Manuscripts, including proof copies of figures, should be submitted in triplicate to expedite review and publication. Manuscripts should be in English, typewritten on heavy paper on one side of page only, double spaced (including abstracts and references), with generous margins.

Ample space should be allowed for mathematical expressions, which should be typed or very plainly written by hand. Particular attention should be given to legibility of subscripts and superscripts and to differentiation between capital and lower case letters. Unusual symbols and cumbersome notations should be avoided. Fractional exponents should be used in preference to root signs, and the solidus (/) should be used for fractions wherever its use will save vertical space.

Authors are urged to have their papers critically reviewed by their associates for scientific validity, manner of presentation, and use of English before submitting them for publication.

Abstracts—An abstract must accompany each manuscript. It should be a concise but comprehensive condensation of the essential parts of the paper, suitable for separate publication, and adequate for the preparation of general indexes to geophysical literature.

References and footnotes—References should be indicated in the text by the insertion in brackets of the author's name and the year of publication, thus: [*Trelease*, 1951]. If the author's name is part of the text, only the year is bracketed. If there are two or more references citing different papers published in the same year by the same author, distinguish them by the letters a, b, c after the year. At the end of the paper, list all references alphabetically by the authors' names. Include in each entry the following: name of senior author, followed by his initials; names of junior authors, each preceded by his initials; title of paper (or book); title of publication or journal; volume number; inclusive page numbers; year of publication. Abbreviations of journals follow the style used in *Chemical Abstracts*. If in doubt, give the full title of the publication or journal. When a book is cited, add the publisher's name, the city of publication, and the total number of pages. Reference to specific pages may be made in the text if appropriate. Acknowledge unpublished reports and private communications in the text, not as references. Avoid footnotes to the text; use parenthetic sentences instead of footnotes if possible.

Tables and figures—Material suitable to tabular form should be arranged as a table and may be typewritten on a separate page. Tables must be numbered according to their sequence in the text, and each table should have a title. Column headings should be short and self-explanatory; more complete explanation may be given in footnotes to the table. Authors should avoid repeating in the text material which is given in tables or figures.

Figures should be prepared with the column width of this Journal in mind (a scale of two to four times that of the published figure is usually adequate). Lettering and symbols should be large enough to stand reduction and remain legible. Captions should be typed on a separate page, not lettered in the figures. Necessary legends or lettering in the figures should be executed to meet competent drafting standards, not typewritten. If the author cannot arrange for suitable lettering, he may send the drawings with the lettering lightly penciled in or shown on a proof copy, and the lettering will be done at the editorial office.

Line drawings should be in India ink on white paper or tracing cloth. Coordinate paper should be avoided, but, if used, it must be blue-lined and the coordinate lines which are to show must be inked.

Photographs are acceptable only if they have good intensity and contrast. They should be unmounted, glossy prints.

Figures should be identified by numbering lightly in pencil, and 'top' of each figure should be indicated.

Acknowledgments—Acknowledgments should be made only for significant contributions by the author's professional associates. A brief closing statement will usually suffice.

References

American Chemical Society, *List of periodicals abstracted by Chemical Abstracts*, Chemical Abstracts Service, Ohio State Univ., Columbus, 314 pp., 1956.

American Institute of Physics, *Style Manual*, American Institute of Physics, New York, 28 pp., 1951.

American Mathematical Society, A manual for authors of mathematical papers, *Bull. Am. Math. Soc.*, 49, no. 3, pt. 2, 1–16, 1943.

Emberger, M. R., and M. R. Hall, *Scientific writing*, Harcourt, Brace and Co., New York, 468 pp., 1955.

Taft, K. B., J. F. McDermott, and D. O. Jensen, *The technique of composition*, 3rd ed., Farrar and Rinehart, New York, 628 pp., 1941.

Trelease, S. F., *The Scientific paper—how to prepare it, how to write it*, Williams and Wilkins Co., Baltimore, 175 pp., 1951.

U. S. Geological Survey, *Suggestions to authors of the reports of the United States Geological Survey*, 5th ed., U. S. Govt. Printing Office, Washington, 255 pp., 1958.

William Byrd Press, *Mathematics in type*, Richmond, 58 pp., 1954.

(Journal of Geophysical Research, Vol. 64, No. 4, April, 1959)

Contents